THE ROLE OF THE SEROTONIN REUPTAKE TRANSPORTER ON CYTOSKELETAL DREBRIN A EXPRESSION IN DENDRITIC SPINES:

IMPLICATIONS FOR NEUROPSYCHIATRIC DISORDERS

BY

DANIEL CHAJI

VICTORIA UNIVERSITY OF WELLINGTON

2020

A thesis submitted in fulfilment of the requirements for the degree of Master of Science in Cognitive and Behavioural Neuroscience

ABSTRACT

Knockout of the serotonin reuptake transporter (SERT) in murine animals has been shown to model various neuropsychiatric disorders such as major depressive disorder, autism spectrum disorder, and substance use disorder. Moreover, evidence suggests that abnormalities in glutamatergic synapses at the level of dendritic spines may be involved in the aetiology of these disorders. This thesis investigated the extent to which the SERT knockout model adequately parallels dendritic spine abnormalities associated with these disorders. This investigation focused on an oft-neglected F-actin binding protein highly-localised to dendritic spines, drebrin A, because any changes to dendritic spines would result in changes to drebrin expression, alongside more common markers for assessing synaptic activity, PSD95 and synaptophysin. The frontal cortex was assessed across the three SERT knockout genotypes at a pre-weaning timepoint and at early adulthood. Results indicated a pattern towards reduced expression for drebrin, PSD95 and synaptophysin at the mRNA level, as well as reduced synaptophysin expression at the protein level, at the pre-weaning stage among SERT knockout animals. No synaptic abnormalities were observed at early adulthood. These abnormalities during development were mirrored by a substantial reduction in dendritic spine density on SERT knockout mature cortical neurons *in vitro*. The recently developed and highly-sensitive *in situ* hybridization method for assessing mRNA expression in tissue, RNAscope®, was also optimised for drebrin mRNA. Altogether, the results suggested that serotonergic activity influences dendritic spine density and synaptic marker expression insofar as the serotonin system acts as a neuromodulator of the glutamate system, which coincides with the peri- and post- natal development period. These effects seemed to result in aberrations to glutamatergic neurotransmission and dendritic spine activity, which may be contribute to the mechanisms involved in neuropsychiatric disorder pathophysiology. Finally, a model involving activation of the 5-HT_{2A} receptor to partly explain the findings in this thesis, is proposed.

ACKNOWLEDGEMENTS

Just as it takes a village to raise a child, so too does it take a whole department (or two) to raise a thesis. First and foremost, thank you to my supervisors, Professor Bart Ellenbroek and Dr Darren Day, for allowing me to undertake this research. Bart, thank you for supporting me continuously since 2017 when I first worked in your lab until now. Your unwavering support, knowledge, advice, and humour was much appreciated. Thank you for trusting me to conduct more molecular-based research, as without that trust this project would not have been possible. Darren, I consider you as much my primary supervisor as Bart was. Your scientific rigour and passion are unmatched. Thank you endlessly for welcoming me into your lab group and allowing me to conduct this research in your lab space, with all the resources, time, and space that this meant.

To Jess, my partner in crime. I did not expect my master's year to give me a best friend for life, yet here we are; I couldn't have imagined a better person to share this experience with. There is too much to say here, but just know that the love and friendship you have shown towards me throughout this time is something I will cherish forever. To Dr Jen Soundy, the alpha, for the thesis formatting help, reminders to take a chill pill, endless cakes, and the friendship. You have helped me experience more than I thought I would these last twelve months, and for that I thank you immensely. To all other DJD lab members, thank you for putting up with lab sheriff, and I wish you every success in your research and lab work.

To the BK lab: Kendra, Dr Kelly Paton, and Amy. Thank you for befriending me and making me feel so at home in the SBS department. Kendra, for always lifting my spirits when they were down and knowing how to make me laugh when I needed it the most. Kelly, for the good talks and the amazing hugs. Thank you for helping me with the dendritic spine analysis methodology. Amy, for all the inside jokes, for allowing me to annoy you 24/7 just because I enjoyed it so much, and for helping me with tissue collection and the ICC experiments. A

whole week of buying you coffee is not enough to thank you for readily agreeing to help me out at the drop of a hat.

To the Pitman lab, especially Matire and Aanchal. Matire, my ninth best friend, for being my confidante during my time here. You truly have a heart of gold and I appreciate so much the love and support you have given me. I couldn't have asked for a better 339 demonstrating partner. Aanchal, thank you for the endless laughs and inside jokes and for suffering together with me as we finished our respective master's theses.

To the SBS and psychology staff members: thank you for providing me with all the assistance I needed. To Mary, you truly are a ray of sunshine. Aimee, for working so hard with me day in, day out to organise the breeding and animal numbers. Jenny, for being (another) ray of sunshine, and for always being willing to help with tissue collection regardless of how full your plate was. Sushila, for all the training and the help on the new confocal. Nev, for helping with the 3D-printed brain blocks and sorting all revisions to their dimensions so quickly.

To my mum and dad, brother and sisters. It will take me a lifetime to repay you for the support and love you have given me throughout my time studying here. I could not have asked for a more loving family, even if you (still) don't understand what my research is about.

Last but not least, to Dr Varun Venkatesh, my mentor. Words will not be able to adequately describe what your mentorship has done for me. Thank you, from the bottom of my heart, for trusting me back in 2018 to pursue the research in this thesis with me. All the skills and techniques I have conducted in this thesis would not have been possible without your excellent teaching, mentorship and expertise. You saw skills and talents in me which I failed to see in myself and took the plunge. I hope this plunge has paid off, and I hope this thesis makes you proud - it is as much your thesis as it is mine. You have changed my life and my career prospects, and for that I will forever be in your debt. I am so glad to call you one of my greatest friends. I hope you and I will be able to conduct research together again.

TABLE OF CONTENTS

LIST OF FIGURES

LIST OF TABLES

LIST OF ABBREVIATIONS

5-HT	Serotonin
AD	Alzheimer's Disease
AMPA	α-amino-3-hydroxy-5-methyl-4-isoxazolepropionic acid
ANOVA	Analysis of variance
ASD	Autism spectrum disorder
BCA	Bicinchoninic acid
BDNF	Brain-derived neurotrophic factor
BSA	Bovine serum albumin
CaMKII	Ca^{2+}/calmodulin-dependent protein kinase II
CNS	Central nervous system
CPP	Conditioned place preference
CRF	Corticotrophin releasing factor
DA	Dopamine
DA-actin	Drebrin A-bound F-actin
DapB	4-hydroxy-tetrahydrodipicolinate reductase
DAKO	Drebrin A knockout
DAPI	4′,6-diamidino-2-phenylindole
DAT	Dopamine transporter
dNTP	Deoxyribonucleotide triphosphate
DSM-V	Diagnostic and Statistical Manual for the Treatment of Mental Disorders, 5th Edition
EDTA	Ethylenediaminetetraacetic acid
ENU	N-ethyl-N-nitrosourea
F-actin	Filamentous actin
FC	Frontal cortex
FFPE	Formalin-fixed paraffin-embedded
GluN1	Glutamate receptor subunit zeta-1
GR	Glucocorticoid receptor
HET	Heterozygous
HOM	Homozygous
HPA Axis	Hypothalamic-pituitary-adrenal axis

ICC	Immunocytochemistry
IHC	Immunohistochemistry
ISH	*In situ* hybridization
KO	Knockout
LB	Laemmli Buffer
L allele	Long allele of the 5-HTTLPR
LTD	Long-term depression
(c)LTP	Chemically-induced long-term potentiation
M	Molar
mM	Millimolar
µM	Micromolar
MAP2	Microtubule-associated protein 2
MCI	Mild cognitive impairment
MDD	Major depressive disorder
MDMA	3,4-methylenedioxymethamphetamine; ecstasy
NAcc	Nucleus accumbens
NMDA	*N*-methyl-D-aspartate
NRT	Non-reverse transcribed control
NTC	No template control
PBS	Phosphate-buffered saline
(q)PCR	(Quantitative) Polymerase chain reaction
(m)PFC	(Medial) Prefrontal cortex
PI	Protease inhibitor
PFA	Paraformaldehyde
PND	Postnatal day
PNS	Peripheral nervous system
PSD	Postsynaptic density
PSD95	Postsynaptic density-95
PVDF	Polyvinylidene difluoride
PVN	Paraventricular nucleus of the hypothalamus
Q-Q plot	Quantile-quantile plot
RFU	Relative fluorescent units

RIPA	Radioimmunoprecipitation assay
RNA-seq	RNA-sequencing
RT	Room temperature
S allele	Short allele of the 5-HTTLPR
SDS	Sodium dodecyl sulphate
SDS-PAGE	Sodium dodecyl sulphate polyacrylamide gel electrophoresis
SEM	Standard error of the mean
SERT	Serotonin reuptake transporter
SSRI	Selective serotonin reuptake inhibitor
SUD	Substance abuse disorder
SYP	Synaptophysin
TE	Tris-EDTA
TAE	Tris-acetate-EDTA
TBS(T)	Tris-buffered saline (with Tween-20)
TCA	Tricyclic antidepressant
WT	Wildtype

CHAPTER 1. GENERAL INTRODUCTION

1.1. General Background

The societal burden of neuropsychiatric disorders is one of the leading threats on human health today, particularly in the developed world [1, 2]. Psychiatric disorders such as major depressive disorder (MDD) and substance abuse disorders (SUDs), as well as neurodevelopmental disorders such as autism spectrum disorder (ASD), have substantially increased the occurrence of human morbidity, suicide, and economic cost [1, 3]. Moreover, the aetiology of these neuropsychiatric disorders are yet to be fully elucidated [4], which in turn makes managing symptoms and developing effective treatments more difficult. While diagnostic criteria for many neuropsychiatric disorders have been established, of which those in the *Diagnostic and Statistical Manual for the Treatment of Mental Disorders* (DSM-V) are the most widely used [5], these criteria focus on symptoms and lack explanations on the biological or aetiological underpinnings causing such symptoms [6]. Investigating the neurobiological bases of these disorders is therefore warranted, as this may provide novel avenues for treatment and may dictate how they should be managed and diagnosed at the clinical level.

While comprehensive aetiologies delineating the neurological bases of these disorders have not been established, empirical evidence has highlighted the brain abnormalities and biomarkers that are associated with these disorders [1], both in humans and their respective animal models. Such evidence has demonstrated that across all neuropsychiatric disorders, abnormalities exist at both the systems level, and at the molecular and cellular levels, and that these changes in brain activity underly their respective symptomology. In particular, the serotonin (5-hydroxytryptamine; 5-HT) system has been heavily implicated in the pathogenesis and pathology of various neuropsychiatric disorders, including MDD, SUDs, and ASD [7, 8].

1.1.1. Serotonin and Major Depressive Disorder (MDD)

Many of the behavioural alterations in major depressive disorder (MDD), such as a persistent depressed mood, anhedonia and alterations in appetite, sleep, energy and weight [5], have been linked to abnormal serotonergic neurotransmission [9, 10]. One of the main reasons supporting this relationship between MDD and 5-HT is that treatment with selective serotonin reuptake inhibitors (SSRIs) reduces depressive symptomology. SSRIs fulfil this function by increasing 5-HT activity in the synapse via the inhibition of the serotonin reuptake transporter (SERT) [11]. Other antidepressant classes, including tricyclic antidepressants (TCAs), also inhibit SERT activity and therefore prolong 5-HT activity in the synapse [12]. This chronic increase in 5-HT synaptic presence is linked to an increase in hippocampal neurogenesis, which is theorised as a factor necessary for the alleviation of depressant symptoms at the behavioural level [13]. Specifically, chronic antidepressant treatment restores brain-derived neurotrophic factor (BDNF) levels, a neurotrophic factor central to adult hippocampal neurogenesis and plasticity, which is reduced in the brains of MDD patients [13, 14]. The pharmacodynamics of TCAs and SSRIs therefore demonstrate that 5-HT is involved in the pathology of MDD, such that enhancing 5-HT activity by blocking reuptake can alleviate depressive symptomology via indirect mechanisms on BDNF and neurogenesis.

Not only is synaptic 5-HT activity involved in the pathology of MDD, at the genetic level, the SERT gene has also been implicated in enhanced susceptibility to developing this disorder [13, 15]. A polymorphism found on the promoter region (5-HTTLPR) of the SERT gene (*SLC6A4*) in humans (Figure 1.1.1) has been associated with an increased risk of developing MDD [13]. Those carrying the long (L) 5-HTTLPR allele, containing 16 repeats, have normal SERT levels, while carriers of the short (S) 5-HTTLPR allele, containing 14 repeats, have reduced SERT mRNA expression [13, 16]. As a result, short allele carriers have reduced transcriptional SERT efficiency and therefore decreased 5-HT reuptake activity [17].

The relationship between the 5-HTTLPR polymorphism and depression is driven by the finding that individuals with one or two copies of the short allele coding for the SERT are more likely to be influenced by stressful life events, and therefore more likely to develop depression and exhibit suicidality than carriers of the long allele [18]. Therefore, rather than a direct relationship between the SERT gene and depression, this finding identifies the short allele polymorphism as a moderator of serotonergic response to stress [18]. However, a recent study which was comparatively well-powered compared to previous studies (n = 60,000-400,000) failed to show that the SERT polymorphism is involved in MDD susceptibility or that possessing the short allele moderates the relationship between stress response and MDD [19]. Therefore, while previous research has identified a SERT-MDD association, it is important to consider that this association lacks consistent replicability.

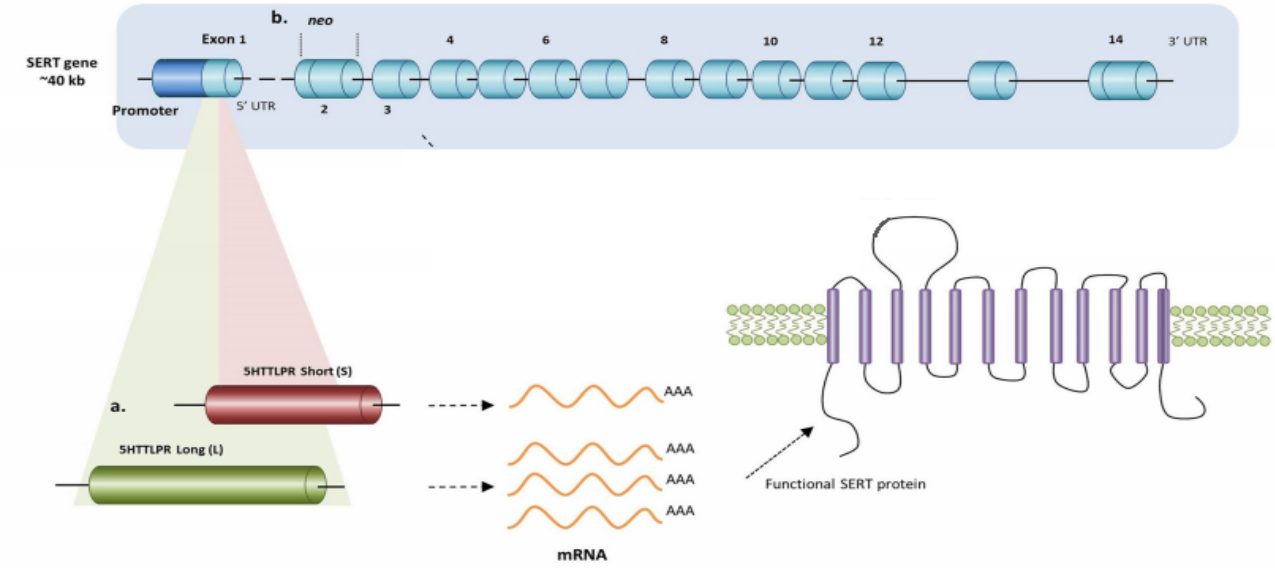

Figure 1.1.1 Allelic variance for the *SLC6A4* (SERT) gene in humans at the promoter region. This variance results in differential transcription for functional SERT levels in the brain. Figure modified and adapted from [20] under Attribution 4.0 International (CC BY 4.0) License (https://creativecommons.org/licenses/by/4.0/).

1.1.2. Serotonin and Substance Abuse Disorders (SUDs)

While the motivation garnered towards, and reinforcement from, drugs of abuse characteristic of SUDs is primarily influenced by an abnormal increase in dopaminergic activity [21], some drugs have also been shown to influence serotonergic activity via both direct and indirect mechanisms [22]. For example, long-term use of 3,4-methylenedioxymethamphetamine (MDMA; ecstasy), which inhibits SERT activity and induces reverse transport, reduces cerebral 5-HT activity via the reduction of 5-HT axon terminals and loss of SERT expression, a finding demonstrated in positron emission tomography studies in humans and rhesus monkeys [23, 24, 25]. Moreover, methamphetamine-dependent individuals showed greater craving for and use of methamphetamine across an 8-week trial of SSRI treatment in a placebo-controlled experiment, demonstrating that increased serotonergic presence in the synapse via SERT inhibition is involved in craving among methamphetamine addicts [26], although the main pharmacodynamic target of this drug is the dopamine (DA) transporter (DAT) [23]. In another placebo-controlled study, SSRIs reduced alcohol craving among alcohol-dependent individuals [27]. These results taken together suggest that alterations in extracellular 5-HT activity are central to the dependence on various drugs of abuse, even those drugs that do not have strong affinity for, or directly target, the serotonergic system.

Given the pattern of findings implicating the SERT in SUDs across various abusive drugs, it is unsurprising then, that the 5-HTTLPR polymorphism implicated in MDD susceptibility has also been implicated in SUDs [22]. For example, in an African American sample the short 5-HTTLPR allele predicted cocaine and heroin dependence [28]. However, this relationship was not found in a sample of Spanish individuals [29], demonstrating that the effect of the 5-HTTLPR polymorphism on cocaine dependence may be moderated by ethnicity, or that sufficient power is required for any effects to be detected [22]. The relationship between

drugs of abuse and the 5-HTTLPR polymorphism in humans has also been demonstrated in methamphetamine [30], heroin [31], alcohol [28] and nicotine [32]. Across these findings, it is evident that the 5-HTTLPR polymorphism, particularly the short allele, confers greater risk for drug dependence. However, the lack of replicability of these findings indicates that other factors (e.g. ethnicity, sex, age of onset) may also be involved and may interact with the 5-HTTLPR polymorphism to confer this risk [22].

1.1.3. Serotonin and Autism Spectrum Disorder (ASD)

Along with MDD and SUDs, the 5-HT system has been implicated in autism spectrum disorder (ASD). This relationship is unsurprising given that ASD is characterised by social and emotional learning deficits, aggression, repetitive behaviours and stereotypy [5, 33], which are domains that converge on the serotonergic system [17]. One of the main indicators of serotonergic abnormality in ASD is the increased 5-HT platelet levels observed in autistic individuals, known as hyperserotonaemia [34, 35]. This hyperserotonaemia in the peripheral nervous system (PNS) contrasts the hyposerotonaemia in the central nervous system (CNS). Studies demonstrate there is reduced 5-HT presence in the brains of autistic children, as indicated by diminished cortisol response following 5-hydroxytryptophan exposure, the immediate precursor to 5-HT, compared to non-autistic controls [36]. Therefore, ASD is characterised by major serotonergic imbalances across both the PNS and the CNS. Because 5-HT alterations during development have long-term effects at the cellular and behavioural levels [34], these imbalances likely underly the behavioural abnormalities associated with this neurodevelopmental disorder, highlighting the importance of normal 5-HT activity during development.

However, several factors, such as genetic polymorphism, can alter this serotonergic activity during development, in turn influencing long-term phenotypic changes, such as those

related to ASD [37]. Once again, just as the 5-HTTLPR polymorphism is implicated in the aetiology of MDD and SUDs, it has also been implicated in ASD. Although there are mixed findings, evidence suggests a relationship between the short allele on the 5-HTTLPR and autism risk. For example, in a study by Gebril and colleagues [35], genomic DNA was purified from the blood of Egyptian autistic children, with the 5-HTTLPR gene amplified using polymerase chain reaction (PCR) and the presence of the short and long alleles for this promoter region detected using agarose gel electrophoresis. The results demonstrated a significantly higher presence of the short allele in the autistic group, while the short allele was absent from all samples in the control group. However, employing these same methods in an Indian sample of autistic children showed no significant difference in the presence of short and long alleles of the 5-HTTLPR polymorphism [38]. In another study, the authors demonstrated that the short allele of the 5-HTTLPR polymorphism was associated only with specific subdomains of ASD diagnostic criteria, such as nonverbal IQ, rather than ASD as a whole [33]. However, in a subsequent meta-analysis which included this dataset, no association between the 5-HTTLPR short allele and ASD was found [39].

Overall, evidence exists to support a role of this polymorphism in the promoter region of the SERT gene and ASD, but it is also clear that there is evidence contradicting these findings. These disparities are also seen with SUDs and MDD and may be due in part by the heterogeneity of these neuropsychiatric disorders. Because of this heterogeneity, cofactors such as ethnicity, sex, and even experimental methodology, may moderate the relationship between this polymorphism and MDD, SUDs, and ASD, thus influencing whether such a relationship will be identified. These issues highlight the limitations of analysing and comparing empirical data at the human level. In contrast, experimental approaches that utilise genetic animal models of disease are one of the most common methods to elucidate how genes of interest are related to these diseases without the presence of confounding factors.

1.2. The Serotonin Transporter (SERT) Knockout Model

Because the 5-HTTLPR polymorphism is a commonly recurring susceptibility gene linked to multiple neuropsychiatric disorders, the serotonin transporter (SERT) knockout (KO) model was established to identify the neurobiological and behavioural consequences of altered SERT function [40]. The SERT KO model was first created in the mouse using homologous recombination [41, 42]. It was later established in the rat using N-ethyl-N-nitrosourea (ENU) mutagenesis, resulting in a premature STOP codon (a C>A conversion from TGC to TGA) on exon 3 of the *SLC6A4* (SERT) gene [40]. This genetic targeting results in offspring homozygous (HOM; SERT-/-) or heterozygous (HET; SERT+/-) for the SERT, along with unaffected wildtypes (WT; SERT+/+). SERT HOM animals produce no SERT mRNA nor express functional SERT at the protein level, thereby resulting in a nine-fold increase in extracellular 5-HT, whereas SERT HET express half the SERT levels observed in WTs [40, 42, 43]. SERT HET animals therefore have reduced SERT mRNA expression and SERT binding efficacy, which mimics the phenotypes observed in short allele carriers of the 5-HTTLPR polymorphism in humans [15, 16, 44, 45]. Indeed, these parallels indicate that SERT HET animals are useful for modelling the neurobiological and behavioural changes associated with the short allele in the human condition, and by extension, how this short allele may confer risk or susceptibility for developing neuropsychiatric disorders.

1.2.1. The SERT KO Model and MDD

Behavioural assays in the SERT KO model demonstrate that these animals exhibit greater anxiety- and depression- like behaviours compared to SERT WT animals [46]. SERT HOM mice displayed longer immobility in the tail suspension test than WTs and reduced locomotor activity in a novel environment, indicating greater levels of learned helplessness and reduced interest in exploratory behaviour [47]. Holmes and colleagues also showed reduced light-dark transitions in the light-dark exploration test and reduced open-arm entries in the

elevated plus maze in SERT HOM and HET mice compared to WT mice [46]. Studies in SERT HOM rats showed similar findings, with reduced open-arm entries in the elevated plus maze, less time spent in the centre of an open field test, and less sucrose preference in SERT HOM rats compared to WT [48]. These results are characteristic of an anxiety- and depression- like phenotype in the SERT KO model at the behavioural level.

The finding that SERT KO models have altered neuroendocrine responses to stress may be underlying these anxiety-related behavioural phenotypes. In response to stress, SERT HOM mice show a 10-fold higher increase in plasma epinephrine levels compared to SERT WT [49]. The authors suggest the exaggerated adrenomedullary response to stress contributes to the anxious-phenotype in these HOM mice. A recent study also demonstrated that in female SERT HET rats, early life stress results in reduced anhedonia during adulthood. This anhedonic response was coupled with a reduction in nerve growth factor mRNA expression in the basolateral amygdala and hypothalamic paraventricular nucleus (PVN), which are two brain regions involved in stress response [44]. This altered stress response in SERT HET rats exposed to early life stress is important given the theory that in humans, MDD develops among short allele carriers especially when this genetic vulnerability interacts with stressful life events [44, 50].

These data are consistent with previous reports that both corticotrophin releasing factor (CRF) mRNA expression in the PVN, and glucocorticoid receptor (GR) mRNA expression in the pituitary gland, hypothalamus, and adrenal cortex, were reduced in SERT HOM and HET mice compared to WT mice under basal conditions [51]. HOM mice also demonstrated increased CRF receptor binding and reduced GR mRNA after pharmacologically-induced stress. Thus, the SERT KO model results in a functional impairment in the regulation of the hypothalamic-pituitary-adrenal (HPA) axis. Further, BDNF mRNA expression, known to be reduced after chronic and acute stress [52], is also reduced in both the hippocampus and

prefrontal cortex (PFC) in SERT HOM and HET rats [53, 54]. Because MDD in humans is associated with altered HPA axis regulation and reduced BDNF expression, and in turn heightened reactivity to stress, the SERT KO model is indeed reflective of the neurobiological changes associated with MDD. Therefore, the murine SERT KO model parallels both the neurobiological phenotypes as well as the behavioural phenotypes of MDD, highlighting its usefulness in studying the underlying mechanisms associated with this disorder.

1.2.2. The SERT KO model and ASD

While SERT KO models have been used to study ASD, the relevance of this model for mimicking ASD-like phenotypes is unclear [55]. Kalueff and colleagues conducted a behavioural battery in SERT HOM, HET, and WT mice [56]. They demonstrated that SERT KO mice approached novel objects less, spent less time interacting with conspecifics, and fewer attempts to remove sticky labels from their tails, compared to SERT WT. In an open-field test, KO mice displayed hypolocomotion and reduced number of visits, and time spent, in the centre of the field. KO animals also produced more stereotypic tics compared to WT animals. The altered social behaviour in this study is consistent with other findings that SERT KO (HOM and HET) animals show less preference for stranger conspecifics in the social approach-avoidance test [57] and in other social interaction tests involving novel conspecifics [55]. Therefore, the reduced sociability, as well as the hypolocomotion and stereotypy is consistent with ASD-like behaviour in the human condition. These parallels highlight that the SERT KO model is a representative model for examining the ASD-like phenotypes in humans, at least at the behavioural level [57]. However the representativeness of the SERT KO model for mimicking ASD has been recently challenged, because the deficits in this murine model are considered too broad and not specific to ASD-like characteristics [55]. Related to this, there is a dearth of studies linking neurobiological changes in the SERT KO model to neurobiological alterations in ASD, likely due to the heterogeneity of this disorder. Nonetheless, genetic SERT

ablation as a model for the behavioural phenotypes of ASD may still be utilised, despite the heterogeneity and broad range of these phenotypes observed in ASD at the human level.

1.2.3. The SERT KO Model and SUDs

Given the involvement of the short 5-HTTLPR allele in the susceptibility to developing SUD, the SERT KO model has been studied in relation to motivation towards drug seeking and enhanced drug reinforcement. SERT KO rats self-administer more cocaine in both a controlled (short access to cocaine) and compulsive (long access to cocaine) drug-seeking environment compared to SERT WTs under both fixed and progressive ratios [58]. These data replicate previous reports [59] and complements the finding that the SERT KO model in both rats and mice exhibit greater preference for environmental stimuli associated with the subjective experience of cocaine in the conditioned place preference (CPP) paradigm [59, 60]. These findings suggest that the nine-fold increase of extracellular 5-HT observed in the SERT HOMs facilitates the rewarding properties of, and subjective experience associated with, cocaine.

In contrast to cocaine, which is considered a standard 'drug of abuse', the relationship between MDMA and the SERT KO model is less clear. For example, MDMA self-administration was not maintained in SERT KO mice exposed to 2 hr daily sessions, compared to WT [61]. Comparatively, research from our lab showed that SERT HOM rats acquired MDMA self-administration faster than SERT WT animals, under similar experimental conditions [62]. All SERT HOMs reached MDMA self-administration within 25 days, while only half of the WTs did so within this timeframe. SERT HOMs also had higher breakpoints than WT rats. These findings indicate that SERT KO rats are more sensitive to the rewarding properties of MDMA, in part due to the ratio of extracellular dopamine and 5-HT, and that in the absence of the SERT, MDMA can only act on the DAT. This may result in greater MDMA-induced DA neurotransmission over 5-HT neurotransmission, in a way similar

to other drugs of abuse such as cocaine. The difference in these murine SERT KO models acquiring MDMA self-administration can be explained by the differential pharmacodynamic effects of MDMA in rats and mice, given that the pharmacodynamics of MDMA in humans and non-human primates is akin to that in rats but not mice [62].

As an extension to the study of MDMA self-administration in the SERT KO rat, our lab conducted an RNA-sequencing (RNA-seq) experiment to determine the differential regulation of genes in the frontal cortex among clean SERT HOM, HET and WT rats compared to MDMA-exposed SERT HOM, HET and WT rats (unpublished data). One of the most prominent findings from this study demonstrated that markers of synaptic plasticity were heavily upregulated after MDMA self-administration and were also differentially regulated in non-drug exposed SERT HOM and HET rats compared to WT rats. Many of these synaptic markers upregulated by MDMA are localised at the dendritic spines of glutamatergic synapses and their presynaptic terminals. These synaptic compartments linking dendritic spines to presynaptic terminals are essential for synaptic plasticity and contribute to the neurobiological basis of learning and memory in health and in neuropsychiatric disease [63]. For example, the dendritic actin cytoskeleton protein drebrin (*Dbn1*), the postsynaptic density protein Postsynaptic Density-95 (PSD95; *Dlg4*) and the presynaptic vesicular transport protein synaptophysin (*Syp*) are all involved in regulating plasticity and were all significantly upregulated after MDMA self-administration (Figure 1.2.1). Of additional interest was that the mRNA expression of many synaptic proteins among clean SERT HOM, HET, and WT animals also showed trends towards differential regulation. However, because of the low sample size within each group (n = 4), significant differences could not be identified in these preliminary findings. Given that many neuropsychiatric disorders are characterised by changes in synaptic plasticity [63], the aim of this thesis was to extend on these preliminary data by further elucidating the role and implications of synaptic plasticity regulation in the SERT KO model.

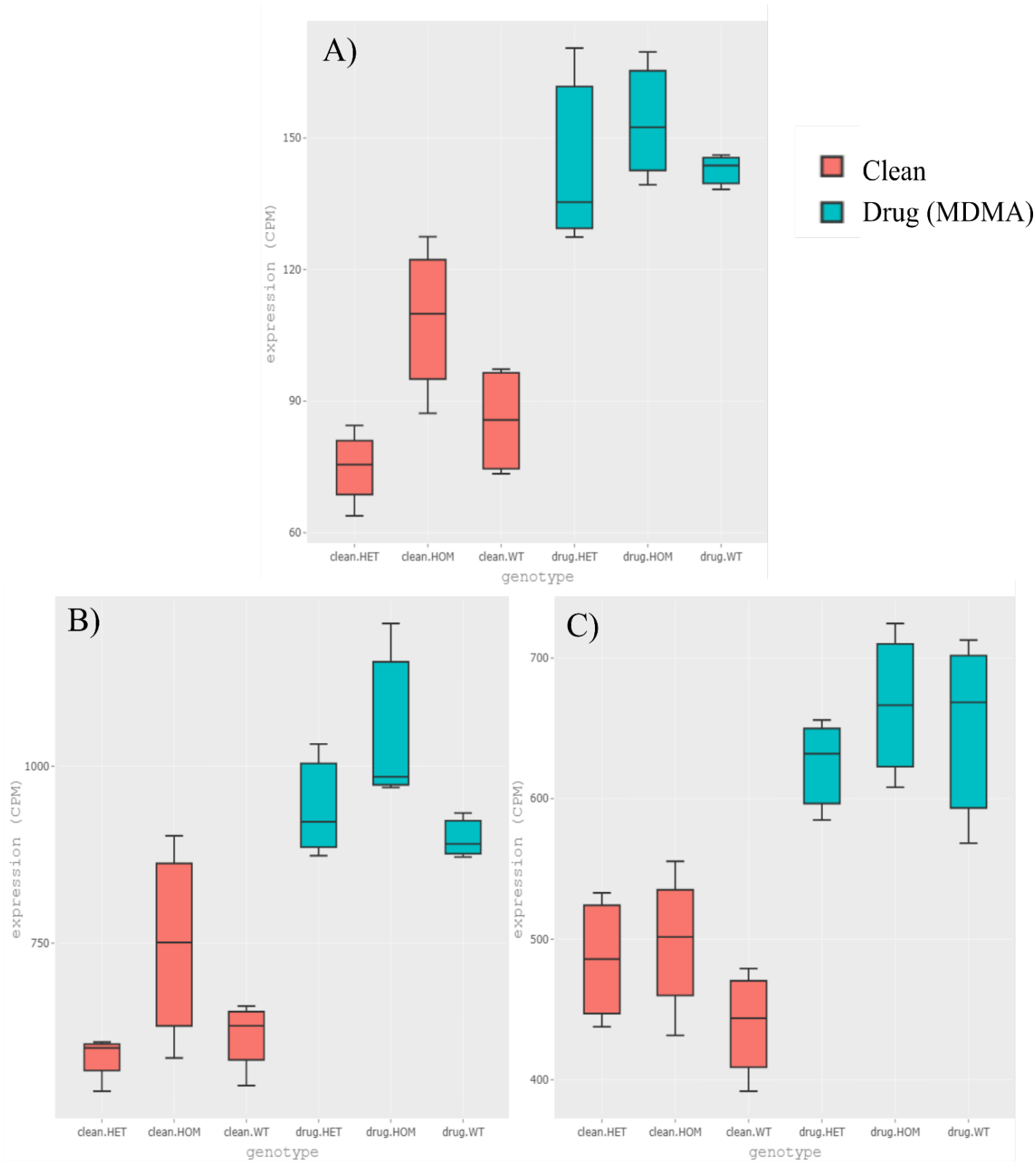

Figure 1.2.1 RNA-seq data displaying differential regulation of A) drebrin (*Dbn1*), B) PSD95 (*Dlg4*) and C) Synaptophysin (*Syp*) RNA expression (in counts per million) across SERT genotype with or without exposure to MDMA self-administration (unpublished data). Upregulation of *Dbn1*, *Dlg4*, and *Syp* in MDMA self-administering compared to clean animals are all significant: *Dbn1*, $p = 7.8 \times 10^{-8}$; *Dlg4*, $p = 6.3 \times 10^{-8}$; *Syp*, $p = 2.5 \times 10^{-8}$.

1.3. Synaptic Plasticity

Synaptic plasticity refers to the formation, maturation and alteration of synaptic connections between presynaptic and postsynaptic neurons at the synaptic cleft. For the glutamatergic system, synaptic plasticity governs the regulation of excitatory neurotransmission in the CNS [63, 65]. Almost all excitatory synapses reside at presynaptic terminals and their adjacent dendritic spines, which are 1 μm protrusions along neuronal dendrites consisting of a spine head and a spine neck or shaft (Figure 1.3.1) [66]. Because spines are excitatory in nature, they express the glutamatergic α-amino-3-hydroxy-5-methyl-4-isoxazolepropionic acid (AMPA) receptor and *N*-methyl-D-aspartate (NMDA) receptor. The AMPA and NMDA receptors are major regulators of plasticity. For example, spine size is directly correlated with the number of active AMPA receptors on spines [67, 68]. Moreover, dynamic changes in synaptic plasticity via the electrophysiological and neurochemical processes of long-term potentiation (LTP) and depression (LTD) will influence the expression of these receptors and therefore the morphology and functional activity of these dendritic spines [65, 66, 67].

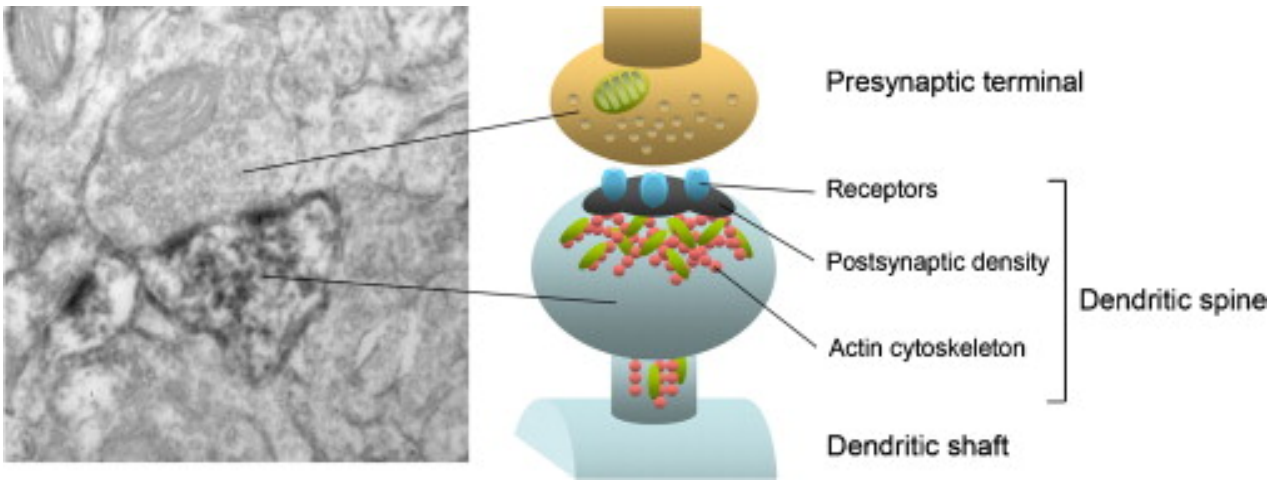

Figure 1.3.1 Ultrastructure of excitatory synapses using electron microscopy depicting the presynaptic terminal and dendritic spine. A schematic diagram of these structures is also depicted. AMPA and NMDA receptors are abundant at the spine compartment and regulate synaptic plasticity. Reprinted from [64] with permission from Elsevier, copyright 2007 (license no. 4640561450651).

1.3.1. Long-Term Potentiation and Long-Term Depression

One mechanism with which synaptic plasticity induces the strengthening or weakening of synapses at dendritic spines is through LTP and LTD, which are two electrophysiological and neurochemical processes that induce long-term structural changes at the synapse and therefore regulate the cellular basis of learning and memory [65, 69, 70]. LTP will result in spine enlargement, while LTD will result in spine shrinkage [71]. These two processes induce enlargement and shrinkage by initiating structural changes at the two subcellular compartments of dendritic spines, the postsynaptic density (PSD) and the actin cytoskeleton [72].

Upon pharmacological or electrical activation and subsequent depolarisation, LTP is initiated by Ca^{2+}-mediated NMDA activation [65, 71]. This activation results in the polymerisation of filamentous actin (F-actin), thereby elongating the actin cytoskeleton. In turn, glutamatergic receptor trafficking is initiated, such that more AMPA receptors are positioned along the spine membrane [66]. The increase in active AMPA receptors is accompanied by an increase in the size of the PSD and therefore the expansion of these dendritic spines [71]. These processes are consistent with reports that spine enlargement directly correlates with the size of the PSD and that changes in structural plasticity will result in parallel changes in scaffolding proteins localised to the PSD [70].

Long-term increases in spine size cannot occur without the activation of Ca^{2+}/calmodulin-dependent protein kinase II (CaMKII) during LTP induction [65, 73, 74]. CaMKII activation is crucial for the activation of the small GTPase proteins RhoA, Cdc42, Rac1 and Ras, which are required for structural remodelling of dendritic spines [71]. These downstream signalling molecules result in the activation of multiple signalling pathways that all have effects on spine remodelling. For example, RhoA activation results in the phosphorylation of the ADF/cofilin actin-binding protein family [75], while Cdc42 and Rac1

activation results in F-actin depolymerisation induced by ADF/cofilin, thereby resulting in sustained structural changes [65].

On the other hand, LTD results in spine shrinkage and is induced by NDMA receptor-mediated prolonged stimulation at low electrophysiological frequencies [76, 77], which is associated with calcineurin activation [71, 78]. For example, low-frequency stimulation in hippocampal slices of neonatal rats resulted in spine shrinkage and spine retraction via the activation of calcineurin [78]. This shrinkage was mediated by dephosphorylated cofilin activity, consistent with reports that activated (dephosphorylated) cofilin severs F-actin bundles and results in depolymerisation [78, 79]. Such depolymerisation of F-actin, and therefore spine shrinkage, during LTD via cofilin contrasts the polymerisation of F-actin, and therefore spine enlargement, during LTP via ADF/cofilin. Therefore, LTP and LTD are both associated with molecular reorganization at multiple locations within spines via the activation of multiple pathways that directly or indirectly influence the PSD and actin cytoskeletal substructures. This reorganisation ultimately results in larger or smaller spine size and in turn, the strengthening or weakening of synaptic connections [76].

1.3.2. Synaptic Plasticity in Neuropsychiatric Disorders

Because of the crucial role that dendritic spines, LTP and LTD have on the regulation of synaptic plasticity and synaptic communication, it is unsurprising that abnormal dendritic spine dynamics have been implicated in the neuropathology of MDD, SUDs and ASD [63]. For example, chronic stress-induced MDD has been associated with enhanced GR activation, which inhibits neurogenesis and results in the reduction of spine and synapse density [80]. The enhanced activation of stress hormones like GR, as well as epinephrine, leads onto aberrant synaptic transmission and spine dysfunction, particularly in the frontal cortex, hippocampus and amygdala via the activation of several kinases and phosphatases [63]. These reports are

consistent with studies showing that chronic mild stress in Wistar rats results in the reduction of dendritic arborisation, and by extension spine density, in hippocampal granular neurons [81]. This reduction is saved by fluoxetine, consistent with findings that SSRIs inhibit the effects of stress-induced LTD, and therefore protect against dendritic spine shrinkage, in both WT and SERT KO mice [82].

Moreover, Nietzer and colleagues examined changes in dendritic spine dynamics in SERT KO mice exposed to social defeat stress in the PFC, hippocampus and amygdala using Golgi-Cox staining [15]. The authors demonstrated higher dendric spine density in WT animals compared to SERT HOM in the infralimbic cortex of the PFC at basal (not exposed to social stress) levels. In contrast, spine density was increased in the basolateral amygdala in SERT HOM mice compared to WTs, indicating that spine density in the SERT KO model is differentially altered according to brain region. SERT HOM mice exposed to social defeat stress also had higher spine density in the lateral amygdala than WT and SERT HOM control mice. These findings support evidence showing that SERT KO animals, even at the baseline level, exhibit higher reactivity to stress via impaired HPA axis feedback, and that altered GR expression in stress-induced MDD is associated with abnormal synaptic transmission and density [51, 80]. The differential regulation of spine dynamics, and therefore glutamatergic transmission, in the PFC and amygdala is also suggestive of altered connectivity between these two regions, which is in line with the theory that MDD is associated with altered corticolimbic neuronal communication [83].

In contrast to MDD, ASD is generally associated with an aberrant upregulation of dendritic spines in the brain. A study on human brain tissue showed that ASD patients had higher spine densities in Golgi-impregnated cortical pyramidal neurons compared to age-matched controls [84], which is also the case for animal models of ASD [63]. ASD has also been linked to mutations in the neurexin and neuroligin synaptic cell adhesion molecules.

These molecules are necessary for establishing trans-synaptic signalling between presynaptic terminals and dendritic spines and form connections with the PSD found in spines, therefore regulating the structural integrity of synaptic communication [63]. Mutations in the genes that code for these trans-synaptic molecules will result in the increase of immature spines and filopodia, the upregulation of which is associated with the neuronal overexcitation observed in ASD individuals [63].

Not only is ASD associated with dysregulated spine structure at the level of the PSD, but abnormalities in the dendritic spine cytoskeleton have also been observed. Given the heterogeneity of ASD, it is unsurprising that many genes associated with the actin cytoskeleton have been identified as ASD risk genes (see [85] for review). These include actin binding proteins such as cortactin-binding protein 2, cross-linking proteins such as CaMKII and α-actinin, as well as the major scaffolding proteins found in dendritic spines such as the SHANK family [85]. Another major family of molecules heavily implicated in ASD is the Rho GTPase family. The synaptic abnormalities in ASD have been linked to Rho GTPase dysfunction [86, 87]. These GTPases, including RhoA, Ras, and Cdc42, are involved in the downstream signalling pathways that result in the reorganisation of the dendritic spine cytoskeleton, and therefore changes in spine morphology. Moreover, Rho GTPases interact heavily with other synaptic proteins implicated in ASD risk such as SHANK. These interactions suggest that synaptic abnormalities in ASD are associated with alterations at many points of the synapse, including the PSD, cytoskeleton, and its downstream effectors [86].

Because ASD is a heterogenous neurodevelopmental disorder, it is difficult to pinpoint how synapses are altered. It is evident that alterations at many locations along the dendritic spine complex can result in aberrant synaptic organisation, but the exact mechanisms with which these abnormalities occur remain to be elucidated. Moreover, only a small number of the genetic ASD animal models mimic the upregulated dendritic spine density identified in the

human condition [85]. This disparity between the human condition and the respective animal models for ASD must come down to the heterogeneity of the disorder and suggests that the increased spine density in ASD may or may not be linked to ASD symptomology [85].

In terms of SUDs and chronic exposure to drugs of abuse, reports generally observe an upregulation of dendritic spines. For example, methamphetamine, cocaine, MDMA and nicotine administration increases spine density and dendritic branching in the PFC and nucleus accumbens (NAcc). However, chronic alcohol and morphine administration reduces spine density and dendritic branching in these areas [88, 89, 90]. Regardless, drug use and abuse will induce rapid changes in dendritic spine density and morphology in brain regions associated with drug abuse, thereby indicating dysregulated glutamatergic neurotransmission.

More specifically, findings show trends towards increased F-actin and PSD95 in the NAcc and medial PFC (mPFC) after chronic cocaine exposure among Wistar rats using western blot [91]. Electron microscopic analysis from the same study also showed trends towards an increase in PSD thickness and length in both NAcc and mPFC dendritic spines. Upon short-term withdrawal from cocaine, dendritic spine density in the mPFC will decrease, complemented by a decrease in F-actin and PSD95 protein levels and an increase in immature filopodia [92]. These changes in dendritic spine dynamics after cocaine exposure are similar to findings that chronic exposure to methamphetamine also increases the expression of PSD95, SYP, neuroligin 1, and NMDA receptor subunit expression in mice [93], and in rats [94]. Moreover, all genes coding for these synaptic proteins were also significantly upregulated in the frontal cortex of rats (SERT WT, HET, HOM) after MDMA exposure as shown by the RNA-seq data from our lab (unpublished data). The upregulation in PSD95 and NMDA receptor subunits after cocaine and methamphetamine exposure is suggestive of synaptic remodelling and an enlargement of dendritic spines via LTP. Overall, it is evident that dendritic spine dynamics are heavily influenced by the molecular microenvironment, such that exposure

or withdrawal from drugs of abuse can rapidly alter the transient behaviour and expression of these dendritic spines, primarily via LTP- and LTD- based mechanisms [89].

1.4. Drebrin

As discussed, both the role of the SERT and changes in dendritic spine dynamics have been suggested as important hallmarks contributing to the aetiology and pathology of neuropsychiatric disorders. Dendritic spine changes require actin cytoskeletal remodelling, whether these changes are in spine shape (morphology), number (density), or both. The relationship between spine dynamics and actin cytoskeletal remodelling, by extension, highlights a crucial role for actin-associated proteins in regulating dendritic spine dynamics. The goal of this thesis is to expound upon the relationships between dendritic spine dynamics and the SERT in neuropsychiatric disorders by focusing on the actin-binding protein drebrin as a marker for changes to dendritic spines. Because drebrin was strongly upregulated after MDMA self-administration in our RNA-seq study (Figure 1.2.1), its potential role in regulating synaptic plasticity changes after drug use and abuse in SUDs was highlighted. Moreover, considering there is a dearth of research investigating the role of drebrin in neuropsychiatric disorders, despite its fundamental role in regulating dendritic spine density and morphology, it is the aim of this thesis to discern its potential role in synaptic plasticity changes induced by genetic reductions in the SERT.

Coded by the *DBN1* gene in humans and rodents, drebrin (developmentally-regulated brain protein) is an actin-binding protein that forms stable F-actin [95]. Drebrin undergoes a developmentally-regulated isoform conversion, where neuronal maturation results in the conversion of the embryonic isoform (drebrin E) into the adult isoform (drebrin A) [95, 96]. This isoform conversion is crucial to drebrin's function and is the result of alternative mRNA

splicing from the same *DBN1* gene (Figure 1.4.1), with a 46-amino-acid insertion in the middle of the drebrin A mRNA transcript [97, 98].

While drebrin E is located in neuronal and non-neuronal tissue, drebrin A is located exclusively at dendritic spines of glutamatergic synapses [96, 99]. A study by Hayashi and colleagues demonstrated in the rat brain that at postnatal day (PND) 14, drebrin A begins to accumulate in the cerebrum while drebrin E expression begins to decrease [96]. Moreover, drebrin A was shown to accumulate at a similar rate as synaptophysin expression, suggesting that isoform conversion of drebrin A occurs alongside synaptogenesis [100]. Drebrin A expression was also adjacent to synaptophysin expression, indicating its molecular localisation

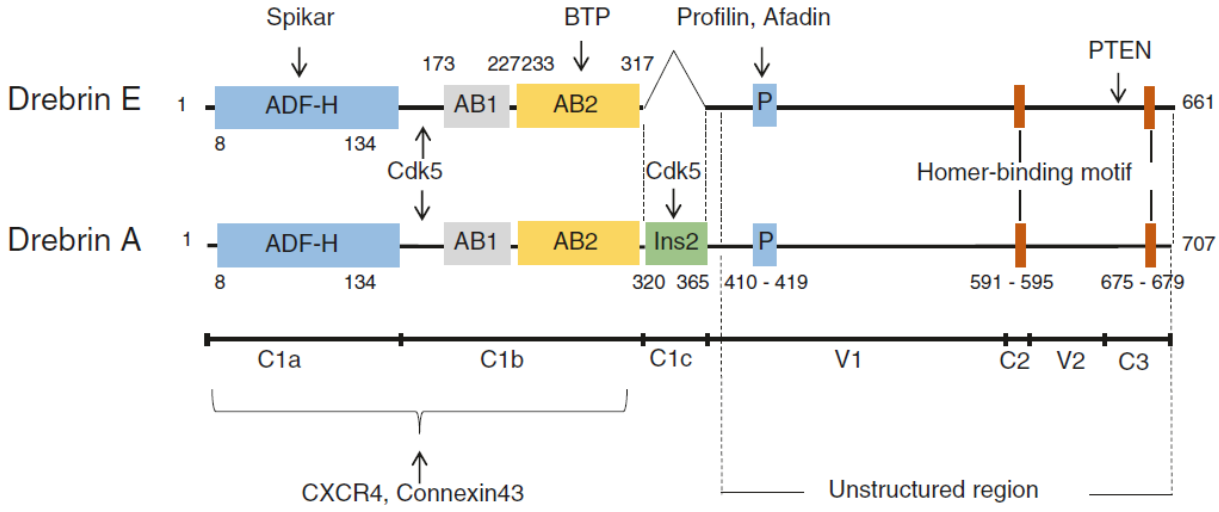

Figure 1.4.1 Domain structures for drebrin E and drebrin A isoforms in *Rattus norvegicus*. Drebrin E and A isoforms have the same domain structures except for a 46-amino-acid insertion ('Ins2') in drebrin A. Reprinted from [97] with permission by Springer Nature, copyright 2017 (licence no. 4665570871979).

at postsynaptic sites of synaptic junctions. The expression of drebrin A was high in the cerebral cortex but expressed at low levels in the cerebellum, further highlighting its high localisation at forebrain excitatory (glutamatergic) dendritic spines [96, 100].

The finding that drebrin A expression parallels synapse formation in cortical neurons is suggestive of the protein's role in synaptogenesis and synaptic function. *In vitro* characterisation of drebrin in cortical neurons also indicated that drebrin colocalised with F-actin and was present in all dendritic spines but absent in dendritic shafts, and that drebrin overexpression resulted in an elongation of spine shape, both highlighting drebrin's role in regulating dendritic spine morphology and density [101]. In hippocampal cultures, Takahashi and colleagues showed that drebrin A knockdown disrupted the clustering of PSD95 in dendritic spines [102]. However, reintroducing drebrin A into drebrin A-knockdown neurons counteracted these effects and reintroduced PSD95 clustering in spines, thereby indicating that PSD95 accumulation in spines is dependent on the presence of drebrin A. Drebrin A knockdown also reduced the width and density of both filopodia and dendritic spines and inhibited activity-dependent NMDA receptor trafficking along the spine membrane [103]. These findings are consistent with reports that drebrin A expression positively correlates with spine head size [104]. Further, the role of drebrin in regulating spine morphogenesis is mediated by AMPA receptor activity, such that blockade or activation of AMPA receptors will induce a decrease or increase in drebrin clustering in spines, respectively, and therefore inhibit or accommodate spine morphogenesis during development [105]. Taken together, these *in vitro* studies highlight that drebrin A is a major contributor to synaptogenesis by regulating the synaptic mechanisms involved in both dendritic spine density and morphology.

Not only is drebrin involved during the development of the synapse, but this actin-binding protein is also involved in regulating synaptic plasticity. After 10 min of exposure to glutamate (100 μM) in cortical neurons *in vitro*, there is an efflux of the subcellular localisation

of drebrin A from dendritic spines into the parent dendrite [106]. In the presence of an NMDA antagonist or jasplakinolide, an F-actin stabiliser, this drebrin efflux was blocked. Because this efflux was blocked in the presence of F-actin stabilisation, the authors proposed that NMDA-dependent drebrin efflux precedes the reorganisation of the actin cytoskeleton during synaptic plasticity. By extension, because of drebrin's high affinity binding to F-actin, drebrin A-bound F-actin (DA-actin) is also translocated from the spine to the parent dendritic shaft [107]. Mizui and colleagues extended these findings by showing that 5 min after chemically-induced LTP (cLTP), there is an exodus of DA-actin from dendritic spines [107]. This reduction in DA-actin recovered to baseline conditions at 30 min after cLTP, indicating that the exodus is only transient. Alongside this transient exodus of DA-actin, there was an increase in glutamate receptor subunit 1 (GluR1), an AMPA receptor subunit, density 30 min after cLTP induction. This GluR1 density increase is indicative of spine head enlargement, because AMPA receptor expression positively correlates with spine head size [67, 68]. These results are in line with LTP-induced distribution and expression of drebrin and F-actin identified *in vivo* [108]. Moreover, the findings from both Sekino and colleagues [106], and Mizui and colleagues [107], taken together, indicate that DA-actin exodus after LTP could be an initial process required for actin reorganisation to occur, ultimately resulting in F-actin polymerisation and spine enlargement by the time DA-actin is reinstated into the spine head (Figure 1.4.2). In contrast, while induction of LTD also results in DA-actin exodus, this exodus is not transient but induces AMPA receptor internalisation, F-actin depolymerisation, and therefore spine shrinkage (Figure 1.4.2) [69]. Moreover, drebrin expression is required for NMDA-induced LTD induction [109]. Thus, drebrin A activity is a regulator of not only dendritic spinogenesis and synaptogenesis, but also regulates the mechanisms involved in LTP- and LTD- mediated synaptic plasticity. Thus, drebrin activity contributes to the cellular basis of learning and memory [69].

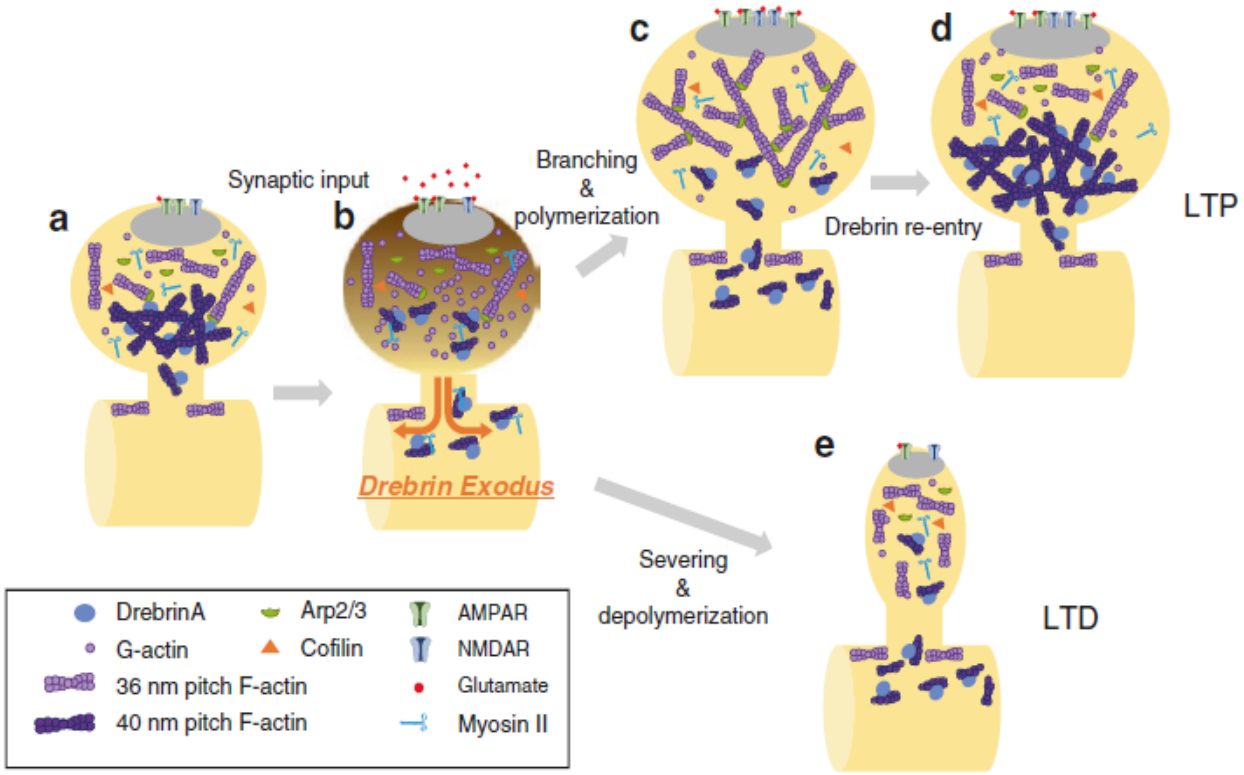

Figure 1.4.2 Role of drebrin in initiating LTP- and LTD- induced cytoskeletal remodelling. (a) Dendritic spines at a steady or resting state. (b) After glutamatergic activation of NMDA receptors, spine depolarisation results in DA-actin exodus from spine head and into the parent dendrite. (c) During DA-actin exodus, F-actin polymerisation is induced, resulting in enlarged spine head. (d) DA-actin re-enters the spine and stabilises the newly-polymerised F-actin, thereby maintaining the spine enlargement established by LTP. (e) LTD induction results in drebrin exodus and the subsequent severing of the polymerised DA-actin complex, inducing spine shrinkage. Reprinted from [69] with permission from Springer Nature, copyright 2017 (licence no. 4671531013771).

Because drebrin plays a crucial role during both the development of the synapse and during synaptic plasticity, the functional and behavioural consequences of changes in drebrin expression have also been studied, albeit not extensively. The establishment of a drebrin A knockout (DAKO) murine model, where the drebrin isoform conversion is disrupted, showed that drebrin A is required for homeostatic synaptic plasticity. In this respect, NMDA antagonism resulted in the trafficking of NMDA receptors onto the spine head membrane in WT mice but not DAKO mice, highlighting that homeostatic plasticity cannot be maintained without drebrin A expression [110]. Moreover, hippocampal LTP was disrupted, and

hippocampus-dependent fear memory was impaired, in adult DAKO mice [111]. These two processes, however, were unaffected in adolescent DAKO mice. Because the isoform conversion occurs during adolescence, this indicates that the conversion from drebrin E to A is crucial for maintaining LTP and establishing fear memory during adulthood. As well, in a drebrin A antisense knockdown rat model, locomotor activity and grooming in an open-field test was increased compared to controls, indicative of an increase in anxiety-like behaviour [112]. Drebrin A knockdown rats also showed impaired pre-pulse inhibition as well as hypersensitivity to amphetamine exposure as indicated by enhanced amphetamine-induced locomotor activity, both indicative of aberrant excitatory synaptic transmission.

Therefore, altering the expression of drebrin A in murine knockout and knockdown models results in abnormalities not only at the cellular level, but also the behavioural and cognitive levels. Despite the role of this protein in regulating synaptogenesis, plasticity, memory and behaviour, drebrin's role in regulating these mechanisms at the human level has been scarcely studied. Some research has shown that drebrin expression is reduced in both Alzheimer's Disease (AD) and Down's syndrome [112]. Drebrin expression was reduced in the frontal and temporal cortices in brain samples of Down's syndrome patients but not the cerebellum [113]. Drebrin protein expression was also reduced in AD patients compared to non-AD controls in both the hippocampus [114] and cerebral cortex [115], indicating that this neurodegenerative disease results in the dysfunction or loss of dendritic spine activity. This drebrin downregulation in AD patients was also identified at the mRNA level using *in situ* hybridisation in the parietal and temporal cortices and hippocampus [116]. Moderate drebrin downregulation has also been observed as a function of normal brain aging [115] and in patients with mild cognitive impairment (MCI) in the temporal cortex and hippocampus [117, 118]. Although this decline in aging and MCI is not as severe as in AD, it suggests that drebrin downregulation occurs naturally as a function of age but is exacerbated by neurodegenerative

diseases, and therefore may be involved in the underlying mechanisms governing cognitive impairments evident in these aged populations.

Other than in Down's syndrome, AD, and MCI, the link between drebrin and neuropsychiatric disorders has not yet been elucidated. Despite the major role drebrin possesses in regulating dendritic spine morphogenesis, morphology and plasticity, this protein has been scarcely studied in relation to neuropsychiatric disorders, even though disorders such as MDD, SUDs, and ASD all involve dynamic changes to dendritic spine activity. Evidence diverges towards a relationship between drebrin expression at dendritic spines and the aberrant synaptic and spine dynamics evident in neuropsychiatric disorders, not only at the human level but also in animal models. Given that the SERT KO model is a valid model for studying the cellular mechanisms underlying neuropsychiatric disorders and their respective synaptic dysfunction, it is surprising that drebrin expression has not been assessed in this model despite its major role in regulating dendritic spine morphogenesis and plasticity.

1.5. Aims and Hypotheses

To date, only one recent study has begun to elucidate how excitatory synapses in general are altered in the SERT KO model. This study examined synaptic markers such as PSD95 and the NMDA subunit glutamate receptor subunit zeta-1 (GluN1) in the PFC of SERT HOM and WT rats at PND 7, 21 and 100 [119]. The authors showed that GluN1 and PSD95 protein levels were reduced in the PFC of SERT KO rats at both PND 21 and 100, but not at PND 7, compared to WT. At the mRNA level, both GluN1 and PSD95 were reduced in SERT KO animals at PND21, a trend which persisted only for GluN1 mRNA at PND100 but not PSD95 mRNA. This finding is indicative of abnormal synaptic functioning at glutamatergic synapses, particularly spine formation, which may in turn contribute to this model's efficacy in mimicking neuropsychiatric disorders that are associated with abnormal spine dynamics.

However, this study was preliminary and an in-depth examination of the changes in both dendritic spine density, by examining drebrin expression, in the SERT KO model is warranted. Because changes in both density and morphology converge on drebrin activity and its resultant cytoskeletal remodelling, analysing drebrin expression offers a novel pathway to further understand the synaptic dysfunction involved in neuropsychiatric disorders. This examination will not only elucidate how drebrin is regulated in the SERT KO model, and by extension in disorders such as MDD, ASD and SUDs, but it may pinpoint novel therapeutic avenues for the treatment of these disorders.

Therefore, the aim of this thesis was to examine the regulation of drebrin expression in dendritic spines in the SERT KO rat model and the potential implications this regulation may have on understanding neuropsychiatric disorders, given that in murine animals genetic SERT deletion is intended to model MDD, ASD, and SUDs. This thesis offers the first assessment into how drebrin is differentially expressed in SERT WT, HET, and HOM animals. Drebrin expression will be used as a marker for assessing dendritic spine density and will be compared to pre- and post- synaptic markers (synaptophysin and PSD95, respectively) to determine whether any potential changes observed are occurring synapse-wide or are limited to the postsynaptic compartment. Drebrin expression in the frontal cortex of SERT WT, HET, and HOM animals will be assessed at both the mRNA and protein levels. The frontal cortex was chosen as the area of interest given that MDD, ASD, and SUDs are all associated with abnormalities in this brain region [63, 91]. This examination will be tracked at two weeks of age and at adulthood, given that drebrin A begins to accumulate at the two-week timepoint and is fully expressed by adulthood [96]. Dendritic spine density will also be assessed in SERT WT, HET, and HOM neurons *in vitro* using drebrin immunofluorescent labelling. Therefore, if the SERT KO model is associated with abnormal dendritic spine dynamics, it is hypothesised that drebrin expression will be differentially regulated in SERT HET and HOM compared to

WT. Because PSD95 activity at dendritic spines is dependent on the presence of drebrin A [102], and PSD95 mRNA and protein is reduced among SERT KO animals across the lifespan [119], it was expected that drebrin expression would also be lower among SERT KO animals at both timepoints compared to WT. This downregulation will result in changes to the density and morphology of dendritic spines, which will in turn have implications for the mechanisms involved in the neurobiology of neuropsychiatric disorders that are associated with the SERT polymorphism at the human level.

CHAPTER 2. GENERAL METHODS

2.1. Animals

A total of 104 animals, of mixed sex, were used for the four methods employed in this thesis. Table 2.1.1 details the number of animals for each method and their genotypes and ages. Subjects were one of three genotypes: SERT WT, SERT HET or SERT HOM. All animals came from SERT HET x HET breeding pairs with a Wistar background. There were 13 litters in total, which came from 6 breeding pairs. Animals lived in standard housing conditions in polycarbonate cages in a temperature (21ºC ± 2) and humidity-controlled environment (55-60%) and were housed under a reverse light cycle (lights on between 7pm-7am), with access to standard chow and water *ad libitum*.

Animals were sacrificed at two timepoints: PND12-14 (referred to as PND14) and PND60-67 (referred to as PND60). Having a window of time to conduct the brain extractions at these timepoints was decided due to practical limitations, but time windows were minimised to ensure little synaptic changes occurring within said timepoints and to avoid increased variability. Animals at PND14 stayed housed with their respective SERT HET dam until brain tissue was taken for experimentation. Otherwise, animals sacrificed at PND60 were weened at PND21 and were placed in single-sex group housing conditions. Handling was minimised for both the pup and adult subjects to avoid any substantial plasticity-related changes in the synaptic markers used in this study, an effect which has been previously suggested as a consequence of human handling [120, 121]. Animals were bred and housed at Victoria University of Wellington (VUW) and all procedures were approved by the VUW Animal Ethics Committee prior to experimentation (Animal Ethics Number: 25766).

Table 2.1.1 Number of animals used in this thesis. Genotype and age information is provided alongside a description of the intended method the tissue was collected for. Animals for primary neuronal culture were taken at PND0-1.

	PND 14			PND 60			Primary Neuronal Culture		
	Western Blot	qPCR	RNAscope®	Western Blot	qPCR	RNAscope®	No. of cultures	No. of cultures also used for dendritic spine analysis	
WT	8	7	1	8	8	3	14	7	
HET	9	7	7	9	9	3	14	7	
HOM	6	4	4	10	10	1	7	5	
Sub Total	23	18	12	27	27	7	35	19	
Total Animals		**35**			**34**			**35**	**104**

2.2. Tissue Dissection and Preparation

The frontal cortex was the region of interest for qPCR, western blot and RNAscope® methods used in this thesis. Frontal cortex dissection protocols were tailored to each method as described below. For all methodologies, a section of the animals' tails was snipped upon sacrifice and stored at -80ºC for subsequent genotyping (Transnetyx; TN, USA).

2.2.1. Quantitative Polymerase Chain Reaction (qPCR) and Western Blot

Animals intended for qPCR and western blot at both PND14 and PND60 were sacrificed using CO_2 asphyxiation followed by decapitation. The brains were then removed and placed on a brain block (Figure 2.2.1), with two 1 mm sections dissected out (Figure 2.2.2). These sections were placed onto a petri dish and the tissue approximately 45º from the midline of the section, from both hemispheres, was removed from the rest of the section to isolate the frontal cortex (Figure 2.2.2). A total of four sections of the frontal cortex were therefore dissected out (two per 1 mm section). It was ensured that two sections were randomly designated for qPCR and two were randomly designated for western blot.

If intended for qPCR, frontal cortex tissue was homogenised using a razor blade and placed into 1.8 ml Eppendorf tubes containing 500 µl of TRIzol® Reagent (ThermoFisher Scientific, #15596018; MA, USA). Tissue was then homogenised further with sterile pestles. If intended for western blot, frontal cortex tissue was homogenised using a razor blade and placed into 1.8 ml Eppendorf tubes with 300 µl of radioimmunoprecipitation assay (RIPA) buffer to lyse the cells. To prevent protein degradation, the RIPA buffer contained Halt™ Protease Inhibitor (PI) Cocktail, Ethylenediaminetetraacetic acid (EDTA)-free 100x (ThermoFisher Scientific, #87785; MA, USA) at a concentration of 10 µl/ml. Tubes for both qPCR and western blot were then moved into dry ice to snap freeze the samples, then were subsequently stored at -80ºC until ready for further processing.

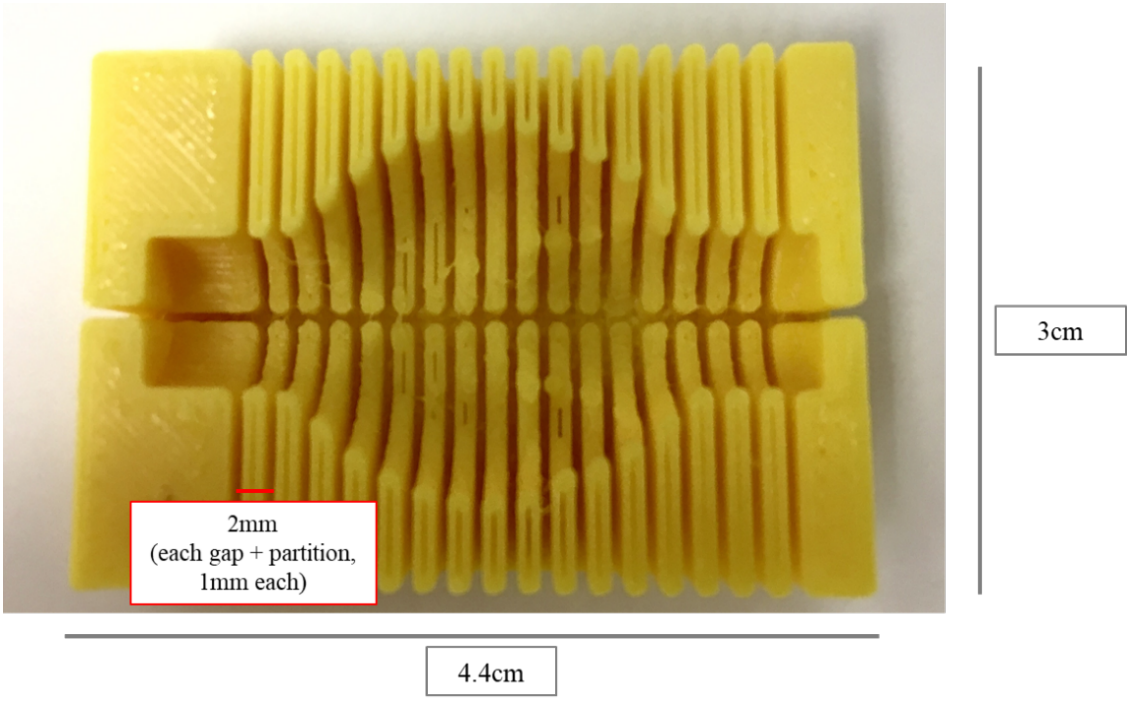

Figure 2.2.1 Brain block used for qPCR, western blot and RNAscope® frontal cortex dissections. These brain blocks were used for both PND14 and PND60 animals.

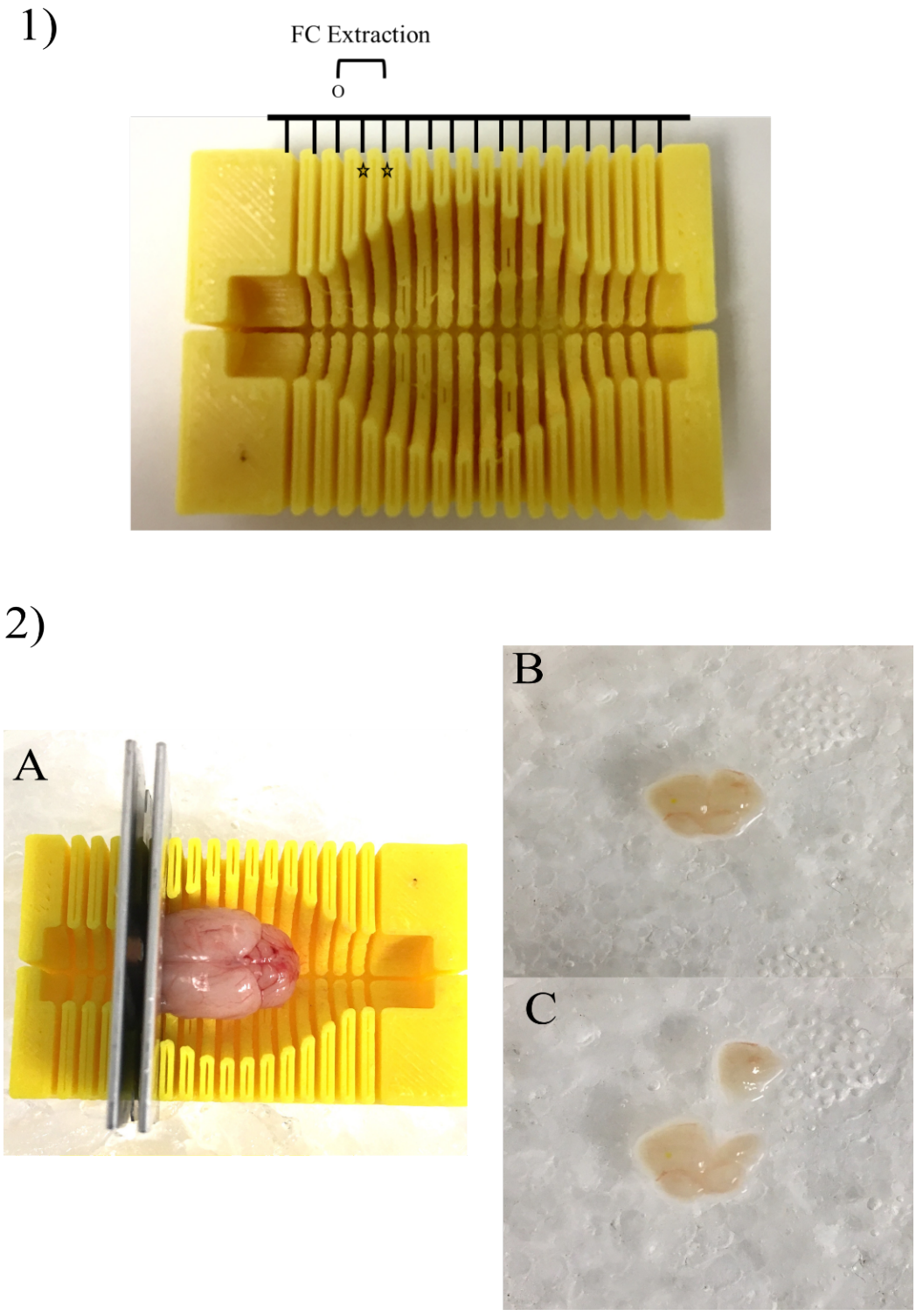

Figure 2.2.2 Dissection of the frontal cortex for qPCR and western blotting. 1) The brain was placed on a brain block, with a razor blade placed perpendicular to the olfactory bulb (designated as 'O'). Two 1 mm frontal cortex (FC) cuts were then made (designated by the stars across two partitions). 2A) A PND12 brain placed on the brain block prior to FC extraction. 2B) Both 1 mm cortical slices were removed and placed on a petri dish on ice. 2C) The frontal cortex from both 1 mm slices were removed by collecting the tissue at 45º angles from the midline of the slices. This tissue was then placed in the appropriate buffer and rapidly frozen in dry ice.

2.2.2. RNAscope®

Animals at PND14 and PND60 were given a lethal intraperitoneal injection of pentobarbital at a concentration of 50-100 mg/kg. They were then transcardially perfused using 4% paraformaldehyde (PFA) in 0.1 M phosphate buffered saline (PBS). Brains were extracted and whole brains were post-fixed in 10 ml of 4% PFA in 0.1 M PBS for 16-24 hrs and stored at 4ºC. After post-fixation, brains were transferred into 70% ethanol (EtOH) at 4ºC until ready for further processing.

The whole brain was then placed on a brain block as shown in Figure 2.2.3, and one razor blade was placed at the rostral end of the brain perpendicular to the olfactory tubercles. An additional blade was inserted 5 mm back from the olfactory tubercles, resulting in a 5 mm coronal section of the cerebrum. These sections were placed in individual Citotest® Embedding Cassettes (Interlab Ltd, #0106-1106; Wellington, NZ) which were placed in a container with 70% EtOH at 4ºC until ready for tissue processing and embedding.

Tissue was then processed in a Leica Semi-enclosed Benchtop Tissue Processor (Lecia Biosystems TP1020; Wetzlar, Germany) in increasing concentrations of EtOH (75%, 80%, 95%, 100%), a 50/50 mix of EtOH/xylene, xylene, and finally paraffin wax. Tissue processing lasted a total of 16.5 hrs. Once processed, cassettes were moved onto a melted paraffin wax compartment in a Leica paraffin embedding station (Lecia Biosystems, EG1160; Wetzlar, Germany). All sections were then embedded in paraffin wax. These moulds were allowed to set, after which they were stored at room temperature (RT).

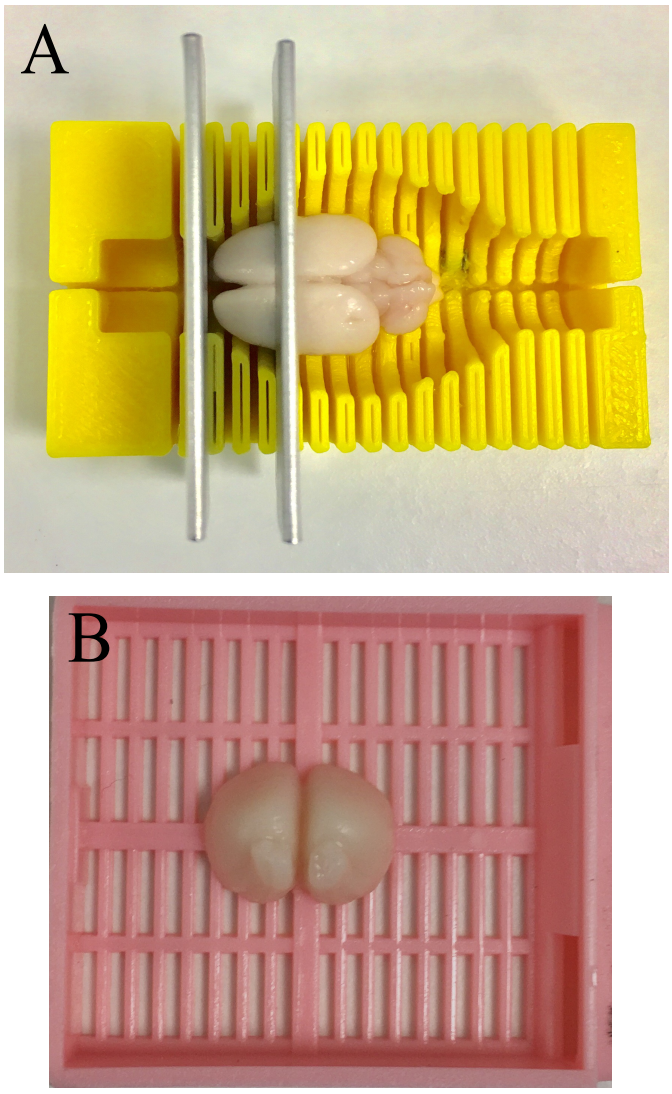

Figure 2.2.3 Dissection of the frontal cortex for RNAscope®. A) The post-fixed brain was placed onto a brain block and a razor blade was placed at the rostral end of the brain. A 5 mm slice of the cerebrum was then obtained by placing an additional razor blade three partitions back from the initial blade. B) The 5 mm section was then placed into a cassette and immersed in 70% EtOH before tissue processing and paraffin embedding. Figure displays a brain extracted at PND12.

2.3. Experimental Design and Statistical Analyses

In general, this thesis employed a 3 x 2 factorial design, with two between-subjects variables: genotype (SERT WT, HET, HOM) and age (PND14, PND60). During the data acquisition and analysis stages, the experimenter was blind to the genotypes of the tissue samples (for qPCR, western blot, RNAscope®) and of the cultured neurons (primary neuronal culture). When performing inferential statistical analyses, Levene's test of homogeneity was first conducted to satisfy the assumption of equal variance between the groups. Where appropriate, this was followed by a 3 (genotype: WT, HET, HOM) x 2 (age: PND14, PND60) factorial analysis of variance (ANOVA) to determine the effects of both genotype and age on dependent variables. If the assumption of homogeneity of variances was not satisfied, alternative analyses were conducted.

Significant results were followed up by either Bonferroni or Tukey post hoc tests. Bonferroni post hoc tests were conducted when there were planned comparisons between the six groups (primarily used for qPCR and western blot chapters). However, if all groups were to be compared with each other, Tukey post hoc tests were opted for (primarily used for primary neuronal culture chapter). Details of these analyses, and of all other statistical tests and analyses, are as stated within each individual chapter.

CHAPTER 3. QUANTIFICATION OF mRNA EXPRESSION OF SYNAPTIC GENES IN SERT KO USING qPCR

3.1. Aim and Rationale

The aim of this chapter was to determine the relative mRNA expression of drebrin specifically, but also SYP and PSD95 (as pre- and post- synaptic markers), in the frontal cortex across the SERT genotypes at two developmental timepoints using quantitative polymerase chain reaction (qPCR). This experiment was expected to extend the results obtained from the RNA-seq study (Section 1.2.3) by obtaining data from more animals per genotype to provide a robust analysis of mRNA expression in the frontal cortex for these genes.

As stated, previous reports indicate that PSD95 mRNA levels are reduced in the PFC of SERT HOM animals at PND21, but not PND100 [119]. Moreover, given that drebrin A expression directly influences the morphology of dendritic spines and PSD95 clustering in these spines during synaptogenesis [101, 102], a proportional relationship between drebrin and PSD95 activity was expected. This relationship would in theory also be expected between drebrin and SYP, given that studies in the rat demonstrate a proportional accumulation between drebrin and SYP during both synaptogenesis and into adulthood [96]. Therefore, if the SERT KO animal model is a valid model of synaptic alterations in neuropsychiatric disorders, it was hypothesised that drebrin, PSD95 and SYP mRNA expression among SERT HOMs would be downregulated compared to SERT WT animals. Because SERT HETs only express half the SERT compared to WT, this downregulation was also expected among HETs, but at a less severe level than HOMs. This pattern of expression was expected primarily during early stages of development, that being at PND14, but not at PND60.

3.2. Methods

3.2.1. Animals

A total of 45 animals were used in the qPCR experiments. Animals were kept under standard housing conditions and came from SERT HET dams as described previously (Section 2.1). Table 3.2.1 denotes the number of animals per genotype (WT, HET, HOM), age (PND14, PND60), and sex at adulthood (male, female).

Table 3.2.1 Number of animals used for qPCR across genotype, age, and sex (at adulthood).

	PND 14	PND 60			
		Male	Female	Combined sex	Combined age
WT	7	3	5	8	15
HET	7	4	5	9	16
HOM	4	6	4	10	14
Total	18	13	14	27	45

3.2.2. RNA Extraction and Purification

The frontal cortex was dissected, immersed in TRIzol® Reagent and stored at -80ºC, as described previously (Section 2.2.1). After thawing the samples on ice, the tissue was homogenised using pestles to break up remaining tissue chunks. The homogenised samples were then left at RT for 5 min. Chloroform was added to each sample at a ratio of 0.2 ml per every 1 ml of TRIzol®, after which tubes were vortexed. The tubes were then incubated for 5 min at RT, then centrifuged at 14,000 x g for 15 min at 4ºC. The aqueous phase (upper layer) from each sample containing the RNA was then collected and placed into a fresh tube. The RNA was purified further using a GeneJET RNA Cleanup and Concentration Micro Kit (ThermoFisher Scientific, K0841; MA, USA). Briefly, 100% EtOH was added to the aqueous

phase at 0.5x volume and triturated to mix. The entire contents were then transferred to individual GeneJET columns and centrifuged at 14,000 x g for 1 min. After discarding the flow-through, a series of three washes using two wash buffers was added to the column. At each wash, the tubes were centrifuged at 14,000 x g for 1 min and the flow-through discarded. To discard any remnants of the wash buffers, the contents were centrifuged once more. The columns were moved into fresh microcentrifuge tubes and the RNA was eluted in 20 µl of nuclease-free water.

The purified RNA was quantified using a NanoDrop® ND-1000 Spectrophotometer (ThermoFisher Scientific; MA, USA) in ng/µl. Measurements of RNA purity were also calculated. These were derived from absorbance (A) ratios A280/A260 and A260/A230. Ratios of 2.0 for A280/A260 and 1.8-2.20 for A260/A230 are suggestive of pure RNA.

3.2.3. DNase Treatment and Reverse Transcription

DNase I treatment (ThermoFisher Scientific, #18068015; MA, USA) was performed to remove any contaminating gDNA, following the manufacturers' instructions. Briefly, isolated RNA was added to a 0.6 ml microcentrifuge tube along with 10x DNase I reaction buffer (1x final concentration) and DNase I Amplification Grade. The reaction was incubated at RT for 15 min, after which 25 mM EDTA was added to the tube (2 mM final concentration) to inactivate the DNase I and prevent RNA degradation. To further ensure the reaction was inactivated, reactions were also heated at 65ºC for 10 min. DNase-treated non-reverse transcribed (NRT) controls for each primer were used during qPCR to assess the efficacy of this DNase treatment.

DNase-treated RNA was then reverse transcribed with Superscript III reverse transcriptase (ThermoFisher Scientific #18080-044; MA, USA) following the manufacturer's protocol. Briefly, 1-3 µg of RNA was added to a nuclease-free microcentrifuge tube with

random hexamers at a concentration of 50 ng/µl, and 10 mM deoxyribonucleotide triphosphate (dNTP) mix. The mixture was heated at 65ºC for 5 min then incubated on ice for 1 min. Superscript III, RNaseOUT™, 0.1 M dithiothreitol and 5x First-strand buffer were then added to each tube. The reaction was incubated at RT for 5 min, then at 50ºC for at least 60 min, after which the reverse transcription reaction was inactivated by heating the tubes at 70ºC for 15 min. The cDNA was then used for qPCR immediately or was stored at -20ºC until subsequent use.

3.2.4. qPCR

cDNA was quantified in 25 µl reactions in duplicate using a SensiMix™ SYBR® & Fluorescein Kit (Bioline Meridian Bioscience QT615-05; OH, USA), following the manufacturer's instructions. Each reaction contained 12.5 µl of 2x SensiMix SYBR® & Fluorescein, forward and reverse primers for each target gene (Table 3.2.2) at a concentration of 0.2 µM, and 200 ng cDNA. No template control (NTC) and DNase-treated RNA NRT control reactions were used for each primer pair. NTCs and NRT controls were used to eliminate the possibility of contaminating PCR product or contaminating gDNA, respectively, and to ensure the PCR products were specific to each cDNA sequence.

qPCR was conducted using a Bio-Rad CFX96™ Real-Time PCR Detection System (Bio-Rad, #185-5096; CA, USA). Cycling conditions constituted an initial denaturation step at 95ºC for 10 min, after which there were 35 cycles of 95ºC for 15 s (denaturation phase), 52ºC for 15 s (annealing phase), and finally 72ºC for 15 s (elongation phase).

3.2.5. Melt Curve Analysis

Melt curve analysis was conducted after the completion of the 35 PCR cycles by heating the products from 65ºC to 95ºC at 0.5ºC intervals. Melt curve analysis determines the specificity of the PCR products by manipulating the fluorescent nature of these products.

Because double-stranded PCR products contain SYBR-infused primer sequences, the separation of these products into their single stranded components at specific temperatures will result in the decrease in SYBR green fluorescence. Therefore, relative fluorescent units (RFU) is plotted over temperature (65-95ºC). When plotting the derivative of this function, a single PCR product will be characterised by a single peak at one temperature. A diffuse peak, or two peaks, is indicative of primer dimer or multiple PCR products in each reaction, respectively.

3.2.6. Agarose Gel Electrophoresis

Agarose gel electrophoresis was used to visualise the PCR products and to determine whether the products were of the expected band size. Two percent agarose gels were made up by microwaving 1.5 g of agarose (Bioline Meridian Bioscience BIO-41025; OH, USA) in 75 ml of 1x tris-acetate-EDTA (TAE) buffer until the agarose was dissolved, for approximately 2-3 min. SYBR® Safe DNA Gel Stain, 10,000x (ThermoFisher Scientific, S33102; MA, USA) was then added to the heated agarose mixture (1x final concentration). The mixture was then poured into a casting tray and allowed to set at RT. PCR products were mixed with 6x xylene cyanol loading dye (1x final concentration) by trituration, of which 10 µl was loaded into each gel lane while gels were immersed in 1x TAE buffer. Electrophoresis was conducted at 100 V for approximately 50 min. SYBR green fluorescence was visualised using an Omega Lum™ G Imaging System (Gel Company, Inc., #81-12100-00; CA, USA). Product size was determined using a GeneRuler 50 bp DNA ladder (ThermoFisher Scientific, SM0371; MA, USA), which was loaded onto the first lane of the gel.

3.2.6.1. Gel Extraction and Product Purification

Gel extraction was performed to excise and purify the PCR products for the five genes used in the qPCR experiments. These isolated products were then used for primer efficiency tests to determine the amplification efficiency of the primers used. Gel extraction was

performed using a GeneJET Gel Extraction Kit (ThermoFisher Scientific, K0691; MA, USA) following the manufacturer's instructions. Briefly, PCR products were extracted from the agarose gel and placed into individual 1.8 ml Eppendorf tubes. Bands were then weighed. A proportional amount of binding buffer was added into each tube (1:1 ratio of product mass to buffer volume). Bands were heated at 60ºC for 10 min to dissolve the gel, following which 100% isopropanol was added to the dissolved product (1:1 ratio of isopropanol to original product mass). Next, 800 µl of the solubilised gel solution was transferred into a GeneJET column. Columns were centrifuged at 12,000 x g for 1 min. The flow-through was discarded. Next, 700 µl of wash buffer was added to the columns, which were then centrifuged once more at 12,000 x g for 1 min, with the flow-through discarded. The columns were then centrifuged alone, before eluting the DNA in 50 µl of elution buffer, both at 12,000 x g for 1 min. Purified DNA was stored at 4ºC and was used for primer efficiency tests.

Table 3.2.2 Primer sequences used for qPCR analysis.

Primer Target *(Gene Name)*	Forward Primer (+)		Reverse Primer (-)		Product Size (bp)
	Sequence (5'-3')	Tm (ºC)	Sequence (3'-5')	Tm (ºC)	
Drebrin (*Dbn1*)	CTGACCAATGGAGAGACCAC	55.0	GGTGATGTCGATTTCTGGAG	53.0	156
PSD95 (*Dlg4*)	AGTACCCGCTGTAGGGATGCAGG	62.7	GTGTGAAAGACAGGGGACCCTCAG	61.1	193
Synaptophysin (*Syp*)	CTATGGGCAGCAAGGCTATG	55.8	CAGGCCTTCTCTTGAGCTCTT	56.8	120
Hypoxanthine-guanine phosphoribosyltransferase *(Hprt1)*	TCCTCATGGACTGATTATGGACA	55.3	TAATCCAGCAGGTCAGCAAAGA	56.3	132
Ribosomal Protein L31A *(Rpl13a)*	TCTCCGAAAGCGGATGAACAC	57.4	CAACACCTTGAGGCGTTCCA	58.0	145

3.3. Results

3.3.1. Agarose Gel Electrophoresis and Melt Curve Analyses

Agarose gel electrophoresis and melt curve analyses were conducted to determine the product specificity of the five primers used for qPCR. PCR products from these five genes, amplified under the same cycling conditions as the qPCR experiments, were loaded and run on an agarose gel. Bands for each product were compared against a DNA base pair ladder to ensure the products were of the expected size.

Figure 3.3.1 displays the PCR products electrophoresed on an agarose gel. Products of all five genes resolved at the expected base pair size (see Table 3.2.2), with no evidence of multiple products or primer dimer. These results therefore indicate that the primers and cycling conditions used resulted in the amplification of one specific product.

To complement the results of the gel electrophoresis experiment, melt curve analyses were also conducted alongside each qPCR experiment. Melt curve analysis is another method to ensure that the primers used are producing one single PCR product. A representative image of the derivative function of RFU over temperature is displayed in Figure 3.3.2. One single peak is evident for all primers, except for PSD95 which is comparatively more diffuse. While a diffuse peak is indicative of primer dimer, no evidence of primer dimer for PSD95 was detected on the agarose gel. In contrast, no melt peaks were observed for NRTc and NTC reactions (Figure 3.3.3). Overall, the melt curve analyses and agarose gel results, taken together, suggest the amplification of one single PCR product, thereby validating the primer design and cycling conditions used for the qPCR experiments.

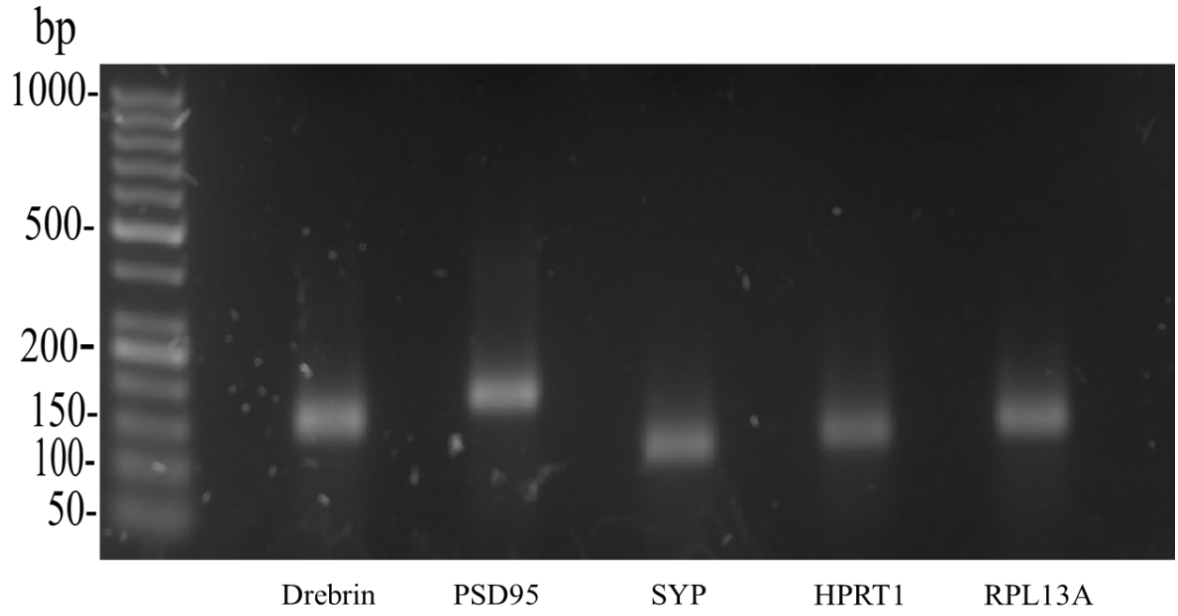

Figure 3.3.1 Agarose gel electrophoresis was used to ensure PCR products were of the expected size. Gel presents drebrin (*Dbn1*; 156bp), PSD95 (*Dlg4*; 193bp), Synaptophysin (*Syp*; 120bp), *Hprt1* (132bp) and *Rpl13a* (145bp) against GeneRuler 50 bp DNA ladder (lane 1), all of which were of the expected product size.

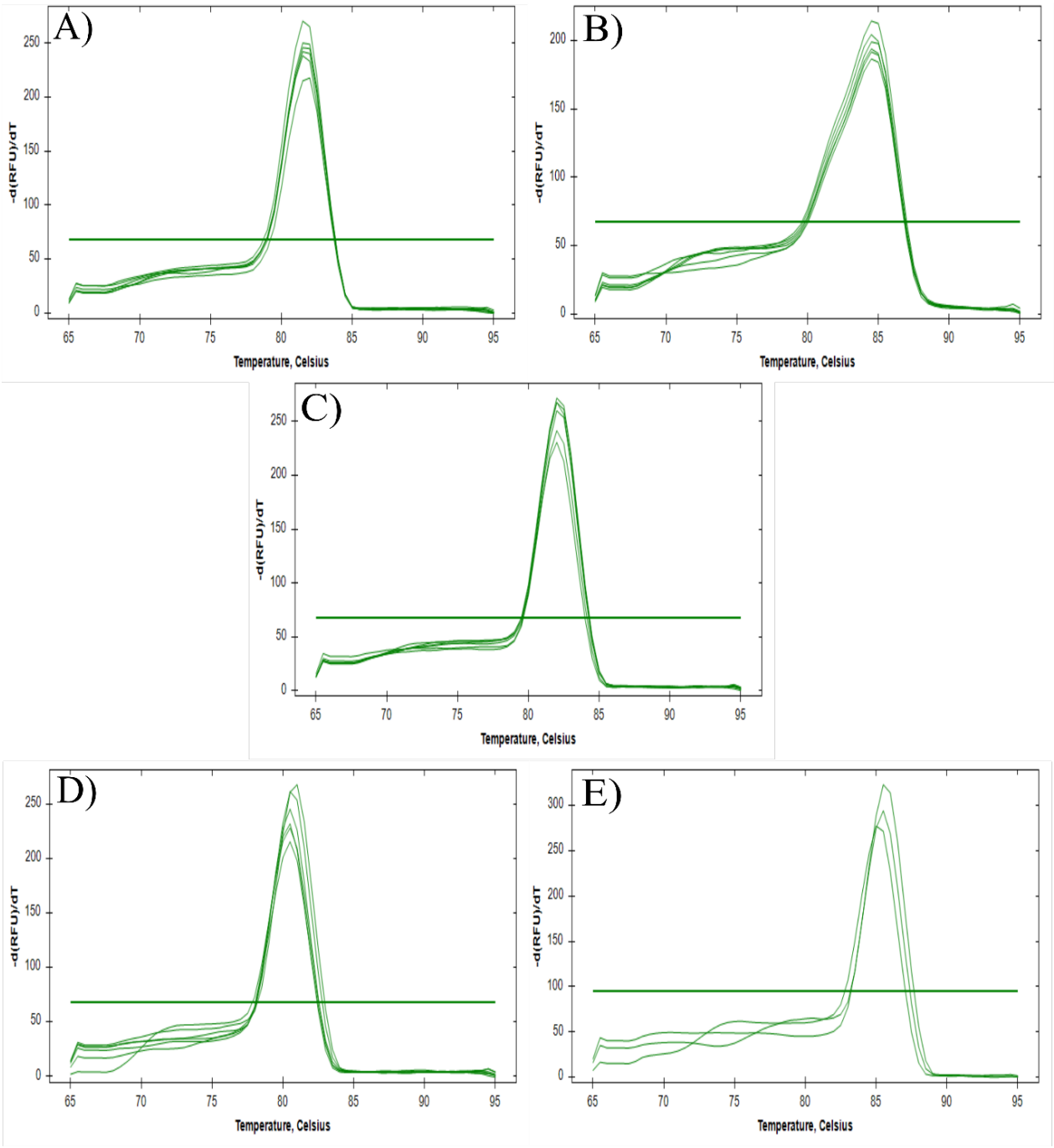

Figure 3.3.2 Representative melt peaks for all five primers, taken from melt curve analyses. The derivative of RFU is plotted over temperature (ºC) for A) *Dbn1*, drebrin (82ºC), B) *Dlg4*, PSD95 (84.5ºC), C) Synaptophysin (81ºC), D) *Hprt1* (81ºC), and E) *Rpl13a* (85ºC). Green line = threshold line.

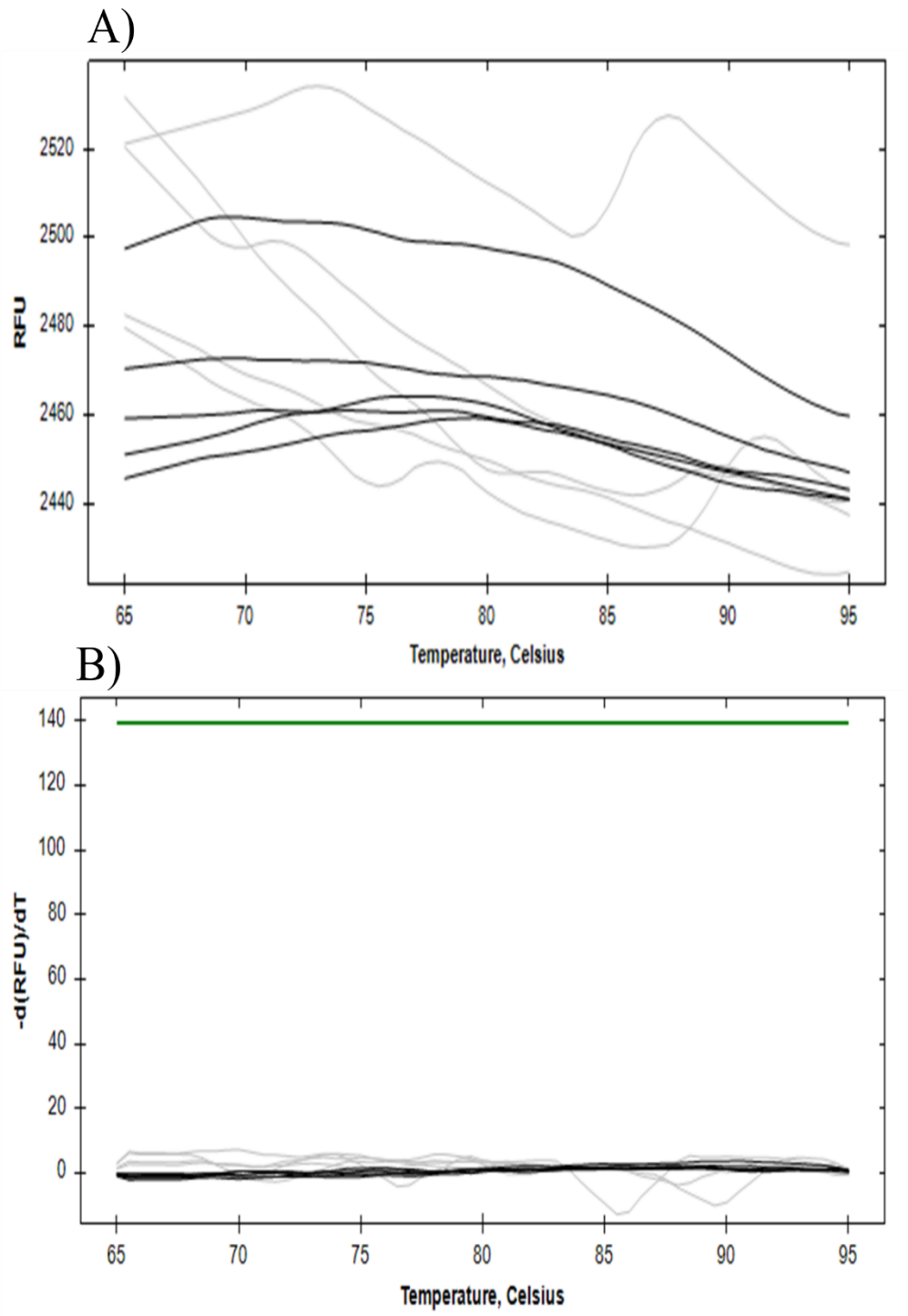

Figure 3.3.3 Representative melt curve plots for NTC (black) and NRTc (grey) reactions. Undifferentiated (A) and differentiated (B) plots are shown, indicating no observable melt peaks. Green line = threshold line.

3.3.2. Primer Efficiencies

To determine the amplification efficiency of the five primers used, primer efficiency tests were conducted. Primers should have an efficiency of close, or equal to, 100%, which indicates that the product amount doubles after each PCR cycle [122]. Moreover, target genes must have similar efficiencies to housekeeping or reference genes for any accurate comparisons to be made using ΔCq or ΔΔCq methods [122].

After gel extraction and product purification (Section 3.2.6.1), ten-fold serial dilutions were made for the purified products of all five genes over a 6-log scale (dilution series down to $1:10^6$). A dilution series of $1:10^2$ to $1:10^6$ was amplified in duplicate by PCR using the same cycling conditions as the qPCR experiments. The Cq values obtained in these primer efficiency tests were then plotted against the log of the dilution (-2 to -6). A difference of 3.32 Cq between ten-fold dilutions corresponds to an efficiency of 100%. Data points that did not align with the trend were omitted from the analyses. Moreover, points that fell below a Cq of 20 were also omitted, to ensure the efficiency calculations were conducted with values that fell within the range of the Cq values obtained in the qPCR experiments. However, at least three points for each gene were included in the analyses. The slope of the trend and R^2 values were then calculated. Primer efficiency (taken from Bustin and colleagues [122])was calculated as:

$$Primer\ Efficiency = 10^{-\frac{1}{m}} - 1$$

Where m = slope of the trend line

Percent efficiency was then calculated:

$$\%\ Efficiency = Primer\ Efficiency * 100$$

Figure 3.3.4 displays the results of the primer efficiency tests. For accurate and optimal qPCR analysis and quantification, efficiencies of between 80-120% and R^2 values of ≥ 0.95

are required [123]. Only the efficiencies for synaptophysin (107%) and *Rpl13a* (89%) fell within this range. However, the R^2 value for *Rpl13a* (0.88) fell below the required value, indicating suboptimal PCR amplification, in contrast to the R^2 for the remaining genes (all > 0.99).

The efficiencies for both drebrin (77%) and *Hprt1* (73%) were close to the desired minimum efficiency of 80%. However, PSD95 produced low primer efficiency (65%). Because of time constraints, the cycling conditions were not able to be reoptimized nor the primers redesigned. Therefore, the qPCR analysis was still conducted. However, caution must be taken when interpreting any potential differences in the mRNA expression of the target genes (drebrin, PSD95, SYP) between the groups, due to the suboptimal primer efficiencies identified, particularly for PSD95.

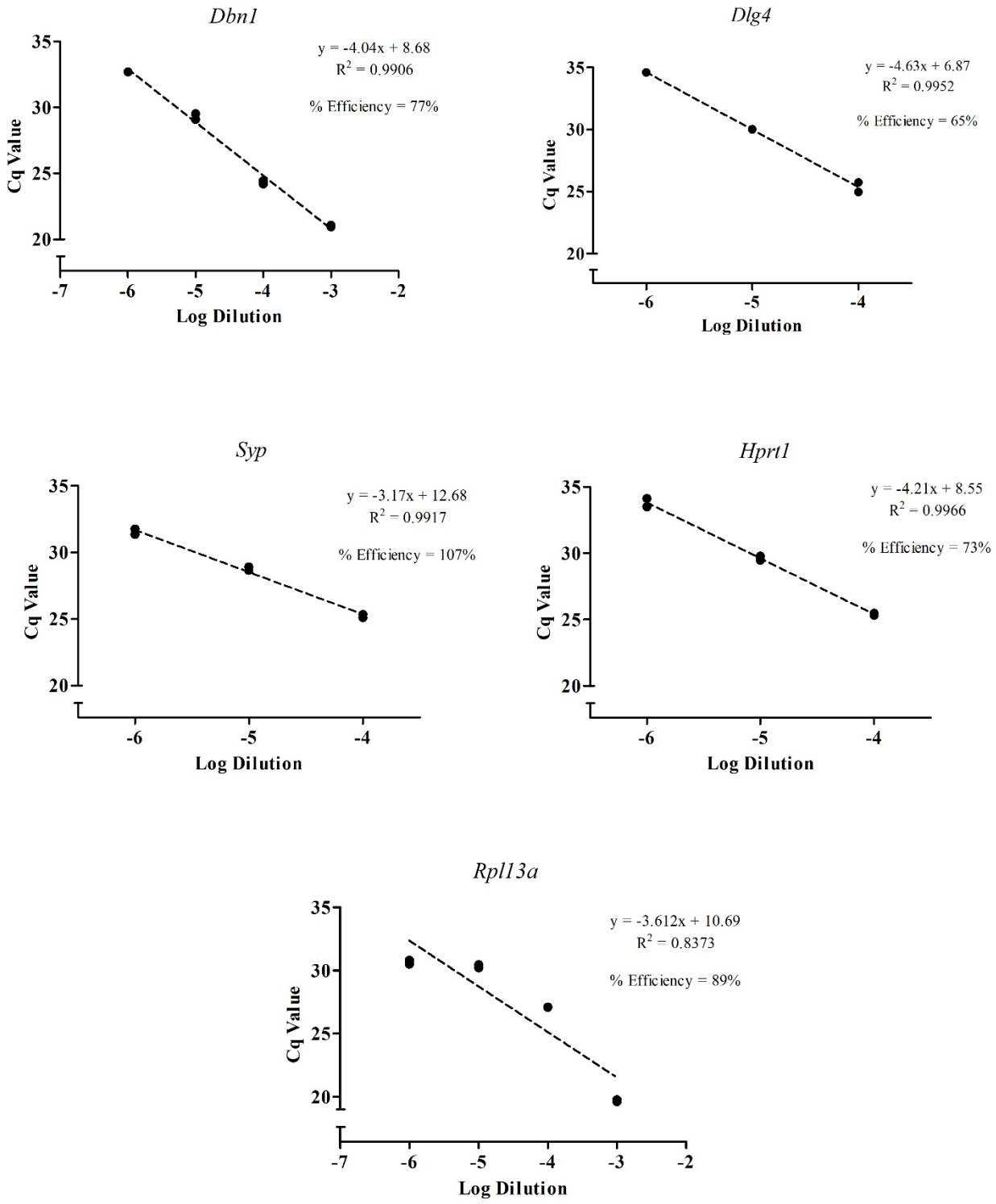

Figure 3.3.4 Primer efficiencies for all genes used in the qPCR experiments. Cq value plotted over log dilution, with trend line, R^2 value and efficiency (%), are presented for each primer.

3.3.3. Housekeeping Gene Analysis

Next, *Hprt1* and *Rpl13a* were evaluated for their suitability as reference genes to normalise drebrin, SYP, and PSD95 expression against using the ΔCq and ΔΔCq methods. The variance in Cq values across the six groups for both potential housekeeping genes are displayed in Figure 3.3.5. Results indicated more variance in Cq values for *Rpl13a*, with a range of 6.505 Cq (Min Cq: 20.5; Max Cq: 27.005), compared to *Hprt1*, which had a range of 3.505 Cq (Min Cq: 22.42; Max Cq: 25.925). Reference genes with less variability are desirable, to ensure that the expression of these genes is constant across the groups. In this case, *Hprt1* is less variable and has a smaller range, thereby suggesting its suitability to be used as a reference gene for the qPCR analysis.

However, visual observation demonstrates a potential developmental trend, such that expression of both genes increases at PND60 compared to PND14. This trend is demonstrated by comparatively lower Cq values for *Hprt1* and *Rpl13a* at adulthood than at PND14. As a result, 3 (genotype: WT, HET, HOM) x 2 (Age: PND14, PND60) factorial ANOVAs were performed for both genes to determine whether there was a difference in *Hprt1* or *Rpl13a* mRNA expression between the groups. Levene's test of homogeneity indicated the assumption of equal variance across the six groups was met for *Hprt1* ($p = .072$), but not for *Rpl13a* ($p = .017$).

A 3x2 ANOVA was then conducted to determine whether *Hprt1* expression differed across the groups. This analysis indicated a main effect of age ($F(1, 39) = 9.04$, $p = .005$, $\eta_p^2 = .188$), but not a main effect of genotype ($F(2, 39) = .47$, $p = .626$, $\eta_p^2 = .024$, *ns*) , nor an age * genotype interaction ($F(2, 39) = 1.78$, $p = .182$, $\eta_p^2 = .084$, *ns*). Post-hoc Tukey tests indicated that the main effect of age was driven by a difference in *Hprt1* expression between the HOMs at PND60 ($M = 23.35$, $SD = 0.47$) and PND14 ($M = 24.9$, $SD = 0.91$), such that expression was higher in the adult HOMs ($p = 0.44$). No other differences between age groups were observed.

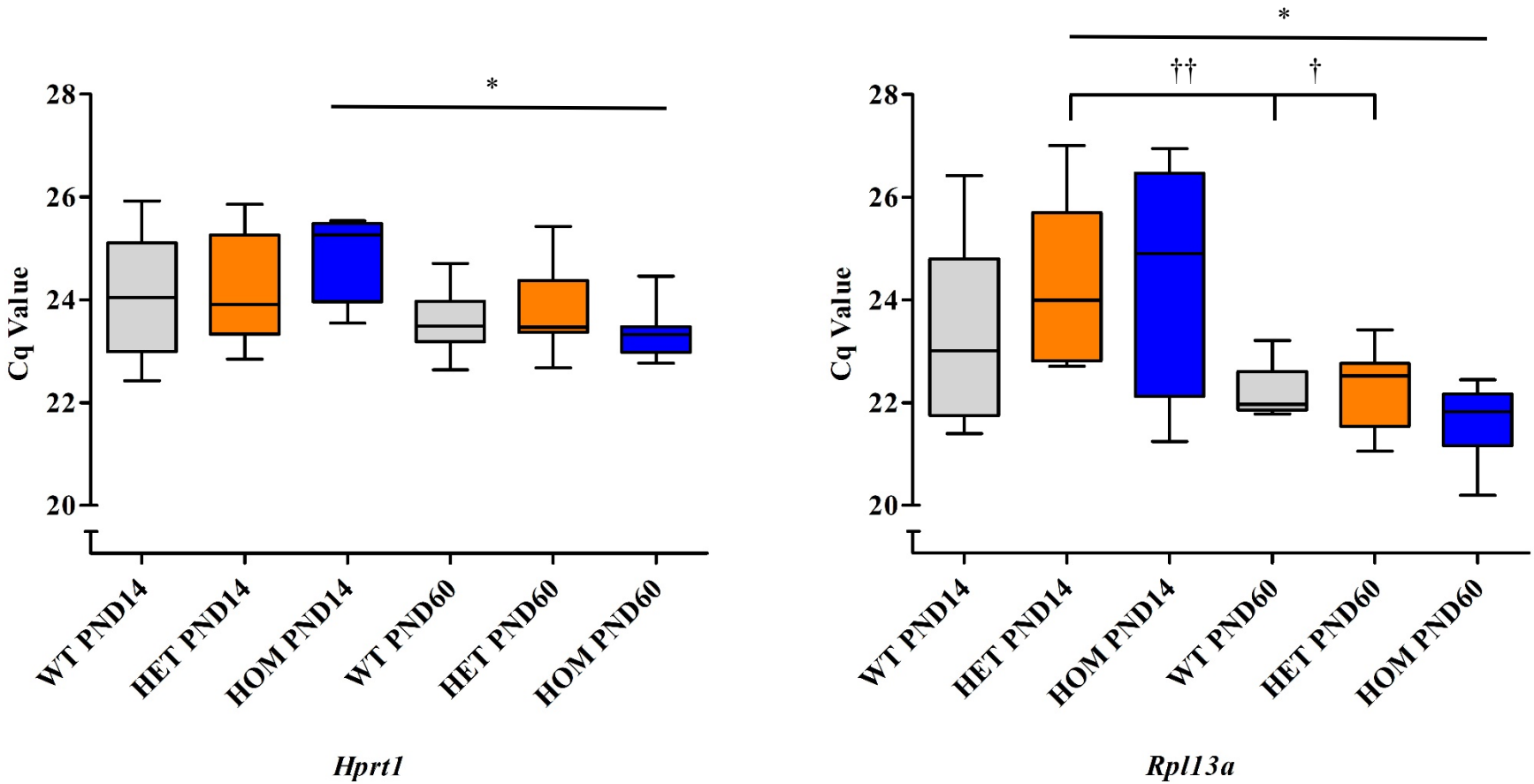

Figure 3.3.5 Cq values for both potential housekeeping genes, *Hprt1* and *Rpl13a*. Cq values for WT (grey), HET (orange), and HOM (blue) animals across the two time points are plotted. Variance is greater between the groups in *Rpl13a* than in *Hprt1*. * $p < .05$, † $p = .067$, †† $p = .066$.

Because equality of variances for *Rpl13a* was not assumed, a 3x2 factorial ANOVA was substituted for a Welch's ANOVA followed by Games-Howell post-hoc analyses. Welch's ANOVA indicated a significant difference between the six groups, $F(5, 39) = 6.57$, $p < .001$. Follow-up Games-Howell post-hoc analyses indicated that the Cq values for *Rpl13a* differed between PND14 HET ($M = 24.39$, $SD = 1.54$) and PND60 HOM ($M = 21.64$, $SD = 0.75$), $p = .020$. Differences between PND14 HET animals and both adult WT ($M = 22.22$, $SD = 0.50$) and adult HET ($M = 22.22$, $SD = 0.77$) animals, were marginally significant, $p = .066$ and $p = .067$, respectively. Therefore, across all cases, HET pups displayed less *Rpl13a* expression than adult animals of all genotypes.

Both the findings for *Hprt1* and *Rpl13a* were consistent with the observed visual trend, such that higher mRNA expression of these genes was observed in adult animals compared to pups. However, less variation was observed for *Hprt1* mRNA expression between the six groups compared to *Rpl13a* expression, as well as fewer differences. In contrast, the Cq variation was greater for *Rpl13a* expression and three significant or marginally significant differences were obtained between HET pups and all animals at adulthood. Moreover, all samples were normalised against total RNA input at RT phase, such that 3 µg of RNA was reverse transcribed for each sample, which is an alternative normalisation method if potential housekeeping genes differ between experimental conditions [124]. Taken together, *Hprt1* was chosen as the housekeeping gene for the qPCR analysis. However, the difference in *Hprt1* expression between pup and adult HOMs was not disregarded; any potential differences in drebrin, PSD95, or SYP expression between these two groups was interpreted with caution.

3.3.4. qPCR

Amplification functions displaying RFU over Cq indicated adequate amplification of the target genes and no amplification of NTC or NRT control reactions (Figure 3.3.6). qPCR analysis was then conducted using the ΔCq and ΔΔCq methods to determine whether there were differences in drebrin, PSD95, and SYP mRNA expression between the six groups, using *Hprt1* as the housekeeping gene. ΔCq and ΔΔCq values were calculated as (based on Rao and colleagues [125]):

$$\Delta Cq = Cq_{target\ gene} - Cq_{Hprt1}$$

$$\Delta\Delta Cq = \Delta Cq_{Experimental\ Group} - \Delta Cq_{\bar{X}_{WT\ Control}}$$

Where:

- Target gene = Cq value for each sample, across genotype and age, for each gene.
- Experimental group = ΔCq value for HET or HOM samples.
- $\overline{X}_{\text{WT Control}}$ = Sample average of WT ΔCq for the target gene.
- ΔCq/ΔΔCq values < 0 indicate more mRNA expression relative to *Hprt1* (ΔCq) or WT (ΔΔCq).
- ΔCq/ΔΔCq values > 0 indicate less mRNA expression relative to *Hprt1* (ΔCq) or WT (ΔΔCq).

Before comparing the mRNA expression of drebrin, PSD95 and SYP between the two timepoints, a sex analysis was performed to ensure that there were no sex effects on ΔΔCq values for drebrin, PSD95 and SYP among male and female adult SERT animals. This analysis was omitted for PND14 animals because at this timepoint both male and female rats are prepubescent and sexual maturity is reached among both sexes only after PND30 [126, 127, 128]. The analysis showed no significant differences in mRNA expression between male and

female SERT adults (Appendix A). Next, the sexes at adulthood were combined and compared to effects at PND14. Three 3 (genotype: WT, HET, HOM) x 2 (Age: PND14, PND60) factorial ANOVAs were conducted to determine whether drebrin, PSD95, or SYP mRNA expression differed between genotypes and across developmental timepoints, where HET and HOM mRNA expression were normalised against WT (such that WT = 0). For drebrin ΔΔCq values (Figure 3.3.7), Levene's test of homogeneity was satisfied (p = .645). Moreover, the ANOVA indicated a main effect of age ($F(1, 39) = 6.68$, p = .014, η_p^2 = .146) and a marginally significant age * genotype interaction ($F(2, 39) = 2.87$, p = .069, η_p^2 = .128). No main effect of genotype was observed ($F(2, 39) = 0.13$, p = .881, η_p^2 = .006, *ns*). Post-hoc Bonferroni analyses indicated that the main effect and interaction for drebrin ΔΔCq was due to a difference between PND14 HET animals (M = 0.53, SD = 0.70) and HET animals at adulthood (M = -0.58, SD = 0.50), p = .016, such that drebrin mRNA expression for HET animals increases over time. While the differences in drebrin mRNA expression between PND14 and adult HOM animals did not reach significance, a visual trend towards an increase in expression was also observed, albeit at a lower rate than HET animals.

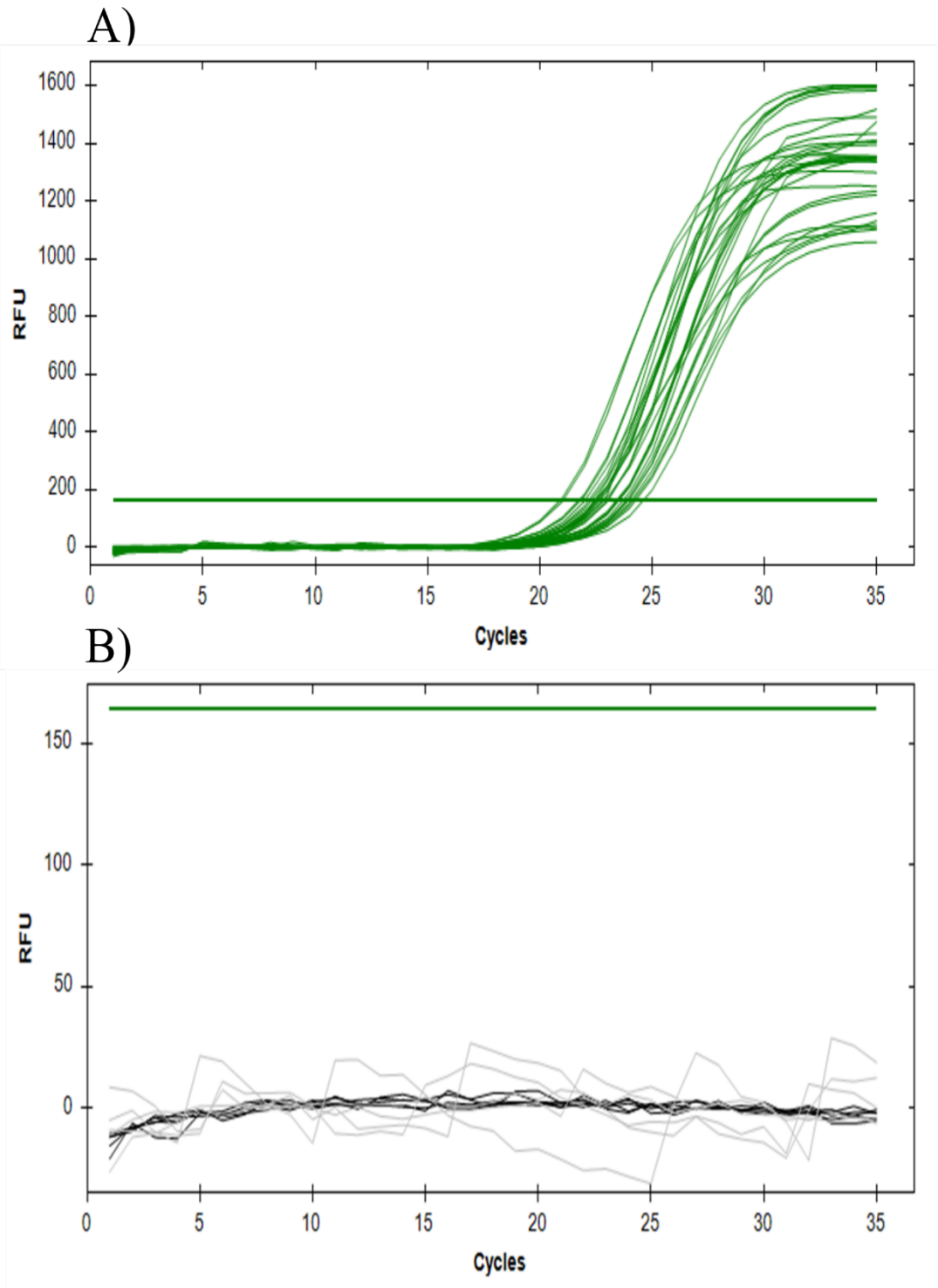

Figure 3.3.6 Representative plots of amplified target genes in the qPCR experiments. A) All five genes (*Dbn1*, *Dlg4*, *Syp*, *Hprt1*, *Rpl13a*) amplified adequately. B) NTC (black) and NRTc (grey) reactions did not amplify, as expected. Green line = threshold line.

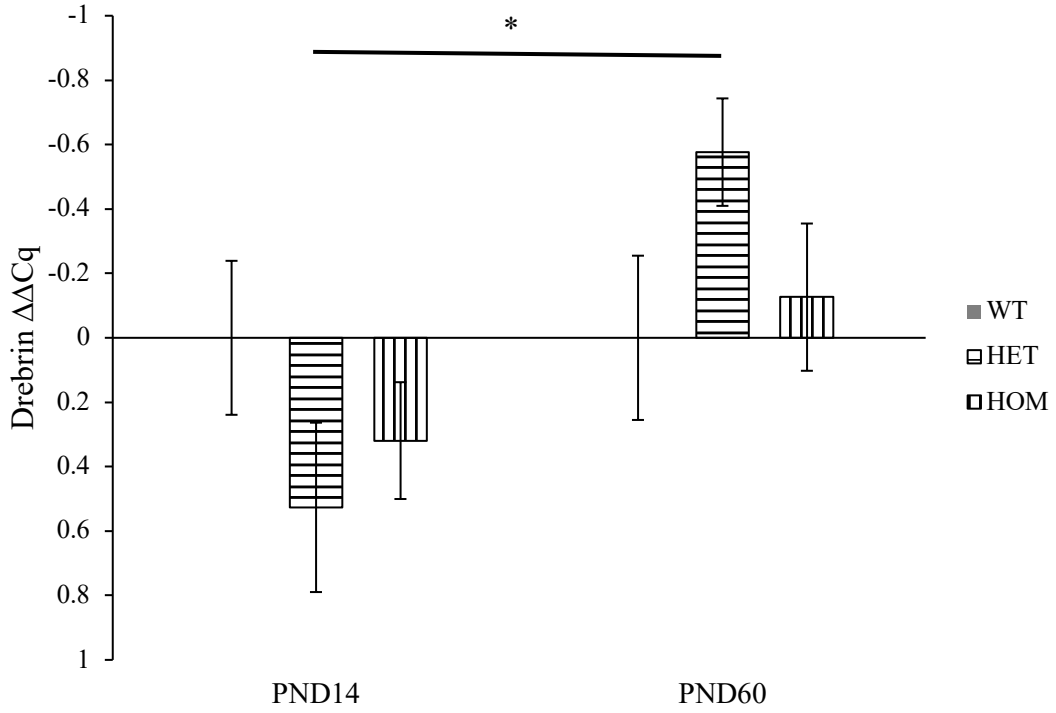

Figure 3.3.7 Mean drebrin ΔΔCq values for SERT HET and HOM animals normalised against WT at PND14 and adulthood. * $p < .05$. Error bars indicate ± SEM. Y-axis is inverted for graphical presentation purposes.

The analysis for differences in PSD95 ΔΔCq values (Figure 3.3.8) indicated that the assumption of equal variances was met ($p = .493$). Once again, a main effect of age was observed ($F(1, 39) = 6.26$, $p = .017$, $\eta_p^2 = .138$). However, no main effect of genotype ($F(2, 39) = 2.24$, $p = .120$, $\eta_p^2 = .103$, *ns*), nor an age * genotype interaction ($F(2, 39) = 2.26$, $p = .118$, $\eta_p^2 = .104$, *ns*) was found. Bonferroni post-hoc analyses indicated greater PSD95 mRNA expression among adult HET animals ($M = -0.33$, $SD = 0.55$) compared to HETs at PND14 ($M = 0.77$, $SD = 0.95$), $p = .032$.

For SYP ΔΔCq values (Figure 3.3.9), Levene's test of equality of variances was significant ($p = .002$). Quantile-Quantile (Q-Q) plots were used to determine whether the data were normally distributed (Appendix B). Visual observation indicated this assumption was supported. Therefore, Welch's ANOVA was conducted, followed by Games-Howell post-hoc tests, to determine whether there were any differences in SYP ΔΔCq values between the six

groups. As shown in Figure 3.3.9, no significant differences between genotype across developmental timepoints were observed using Welch's ANOVA ($F(5, 39) = 1.44$, $p = .231$, *ns*).

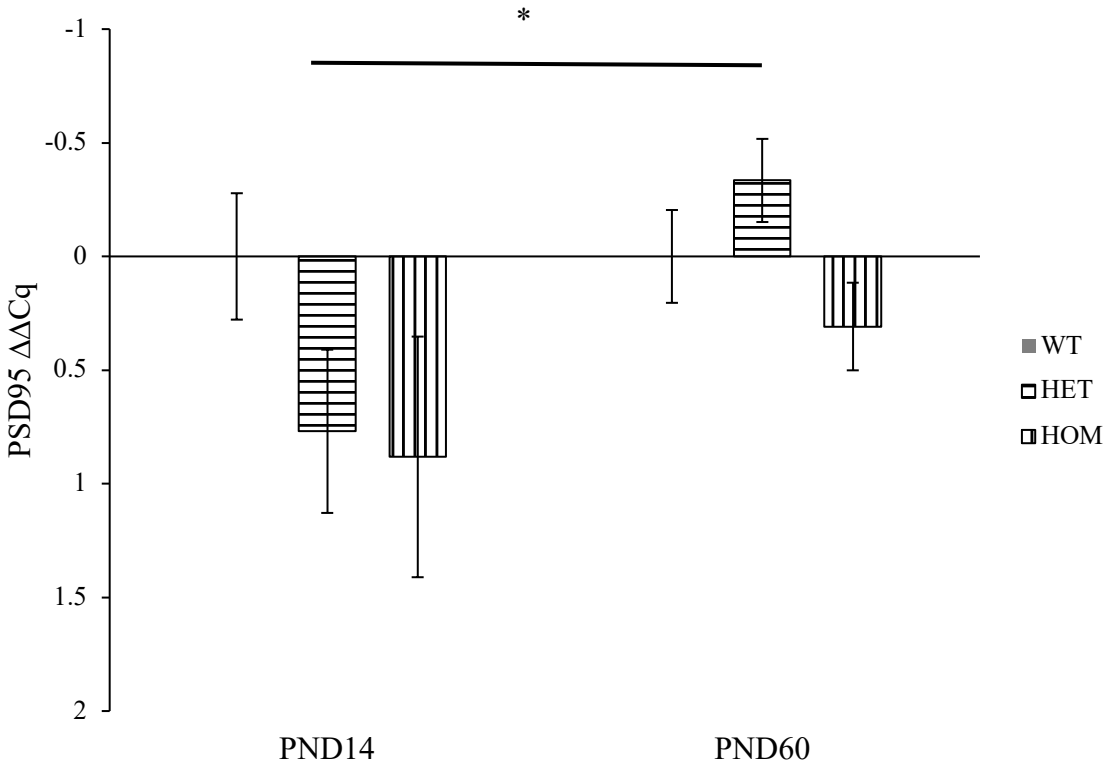

Figure 3.3.8 Mean PSD95 ΔΔCq values for SERT HET and HOM animals normalised against WT at PND14 and adulthood. * $p < .05$. Error bars indicate ± SEM. Y-axis is inverted for graphical presentation purposes.

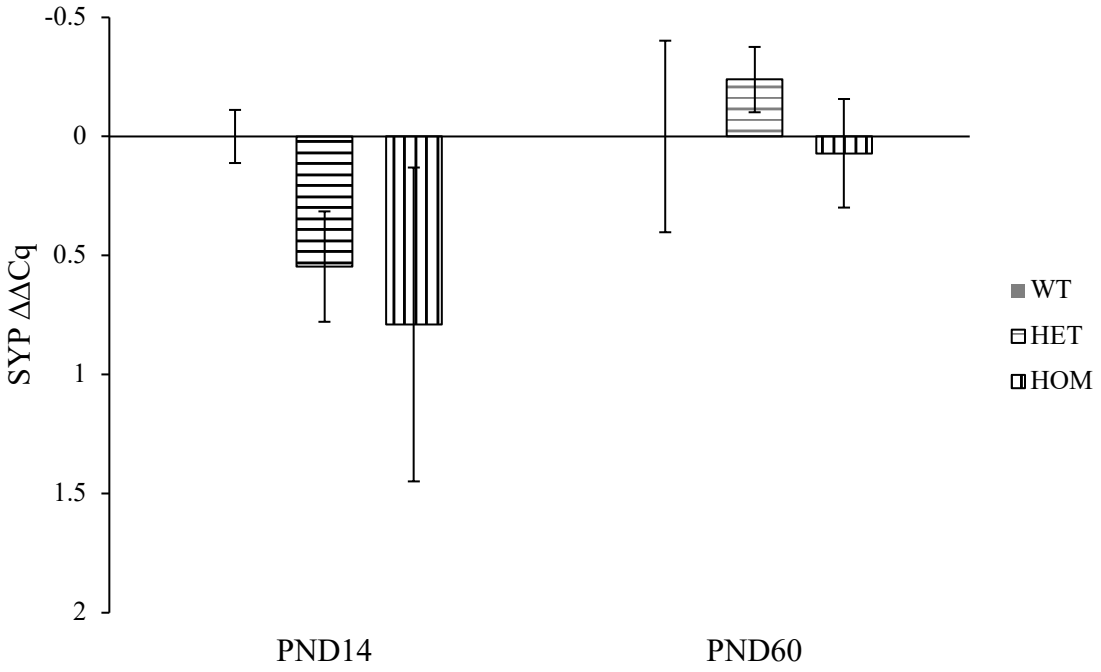

Figure 3.3.9 Mean SYP ΔΔCq values for SERT HET and HOM animals normalised against WT at PND14 and adulthood. Error bars indicate ± SEM. Y-axis is inverted for graphical presentation purposes.

Lastly, correlational analyses between the ΔCq values for the three target genes were performed to determine whether the normalised mRNA expression for these synaptic markers were correlated. This analysis was performed first on the entire dataset, pooling both genotype and age together, which showed that mRNA expression for all synaptic genes were correlated (Figure 3.3.10). Significant moderate-strong, positive correlations were found between drebrin and PSD95 ΔCq ($r = .664$, $p < .001$), drebrin and SYP ΔCq ($r = .590$, $p < .001$), and SYP and PSD95 ΔCq ($r = .514$, $p < .001$). When observing the ΔCq correlations at PND14 alone (Figure 3.3.11), these strong, positive correlations were upheld between drebrin and PSD95 ($r = .806$, $p < .001$), and PSD95 and SYP ($r = .659$, $p = .003$), but not drebrin and SYP ($r = .394$, $p = .105$, *ns*). Finally, mRNA expression for all synaptic genes were positively correlated at PND60 (Figure 3.3.12), with drebrin and PSD95 ($r = .685$, $p < .001$), and drebrin and SYP ($r = .670$, $p < .001$), showing strong correlations, whereas PSD95 and SYP showed a comparatively weaker association ($r = .448$, $p = .019$).

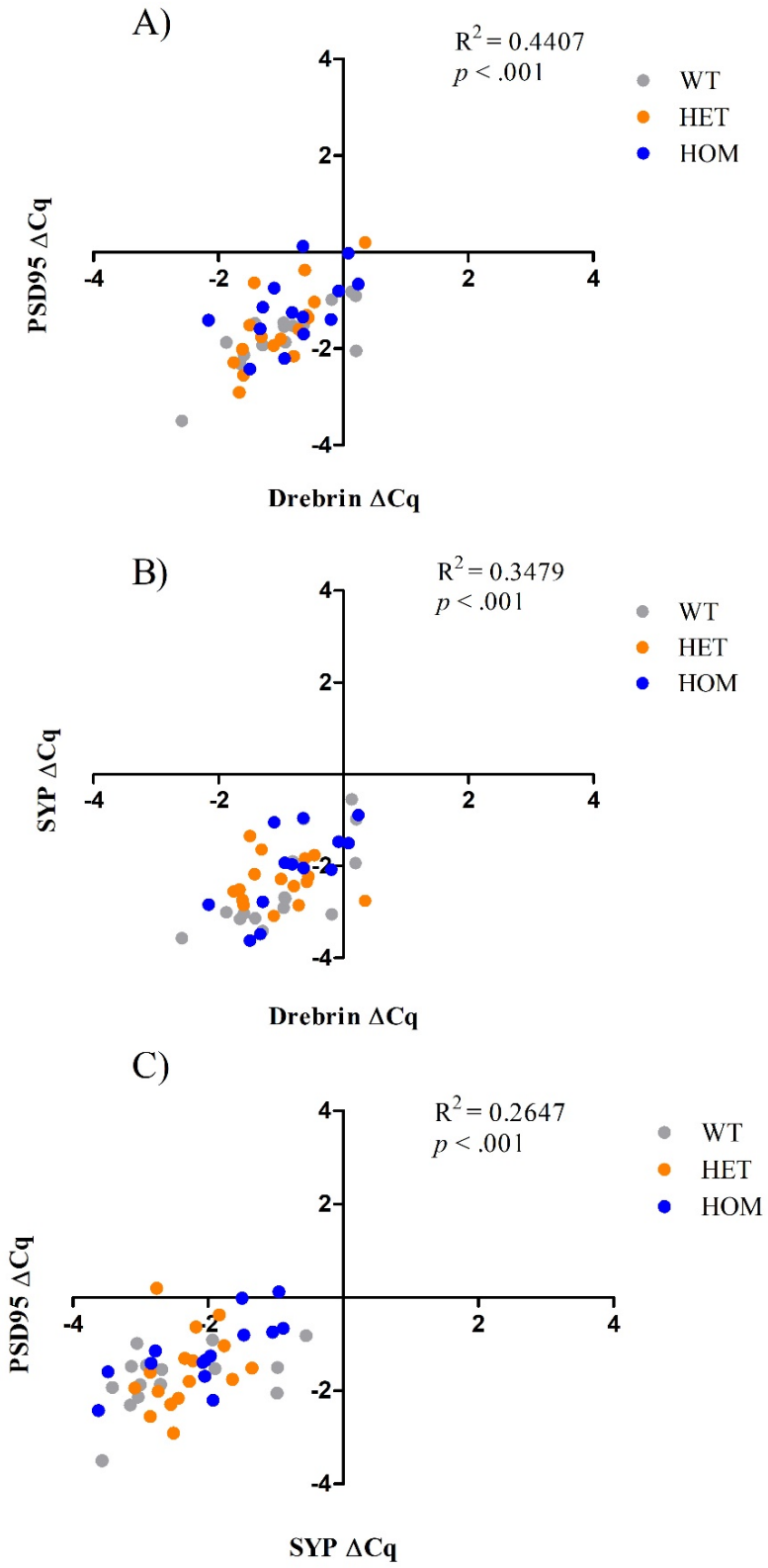

Figure 3.3.10 Correlations between A) drebrin and PSD95, B) drebrin and SYP, and C) SYP and PSD95 ΔCq values, pooled across developmental timepoints. R^2 and p values depicted on each graph.

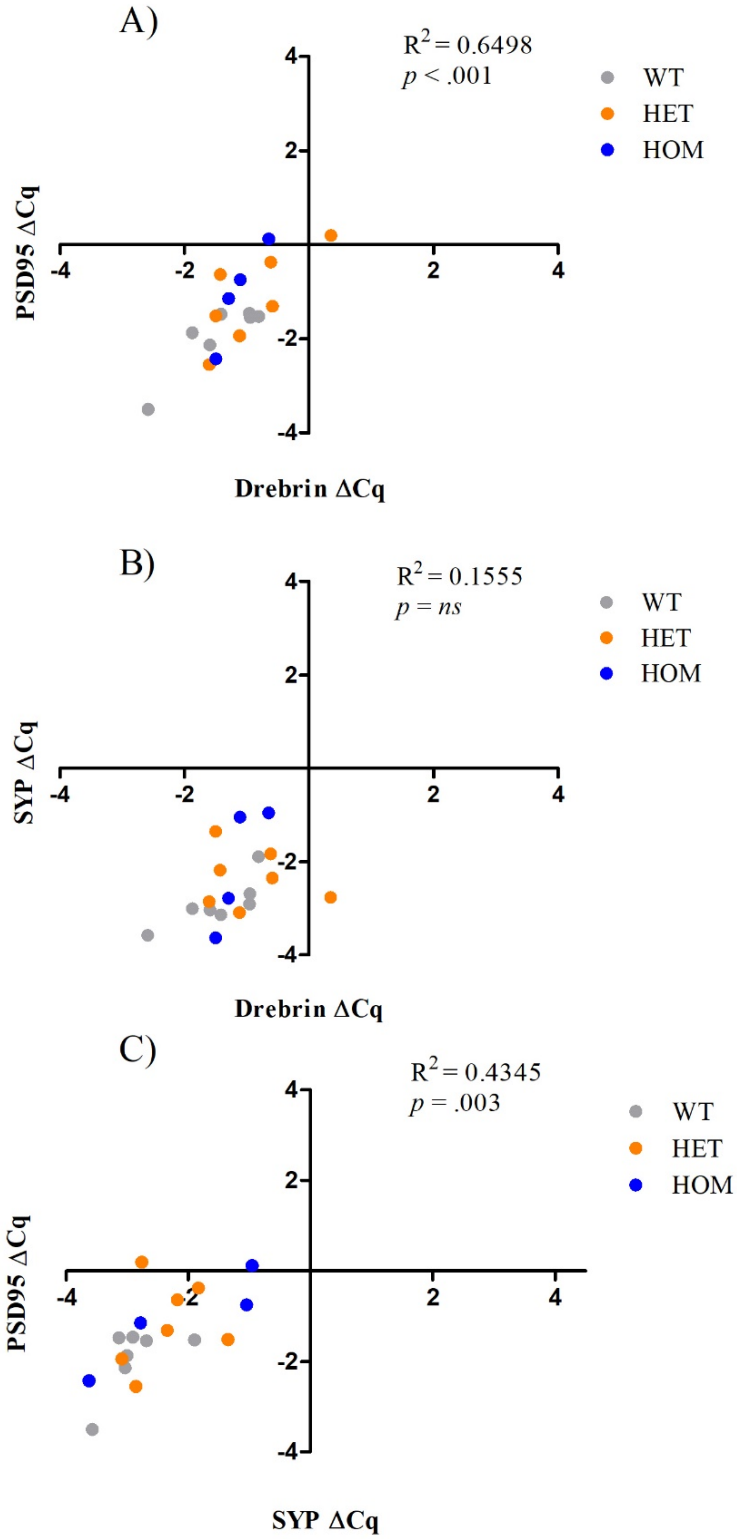

Figure 3.3.11 Correlations between A) drebrin and PSD95, B) drebrin and SYP, and C) SYP and PSD95 ΔCq values at PND14. R^2 and *p* values depicted on each graph.

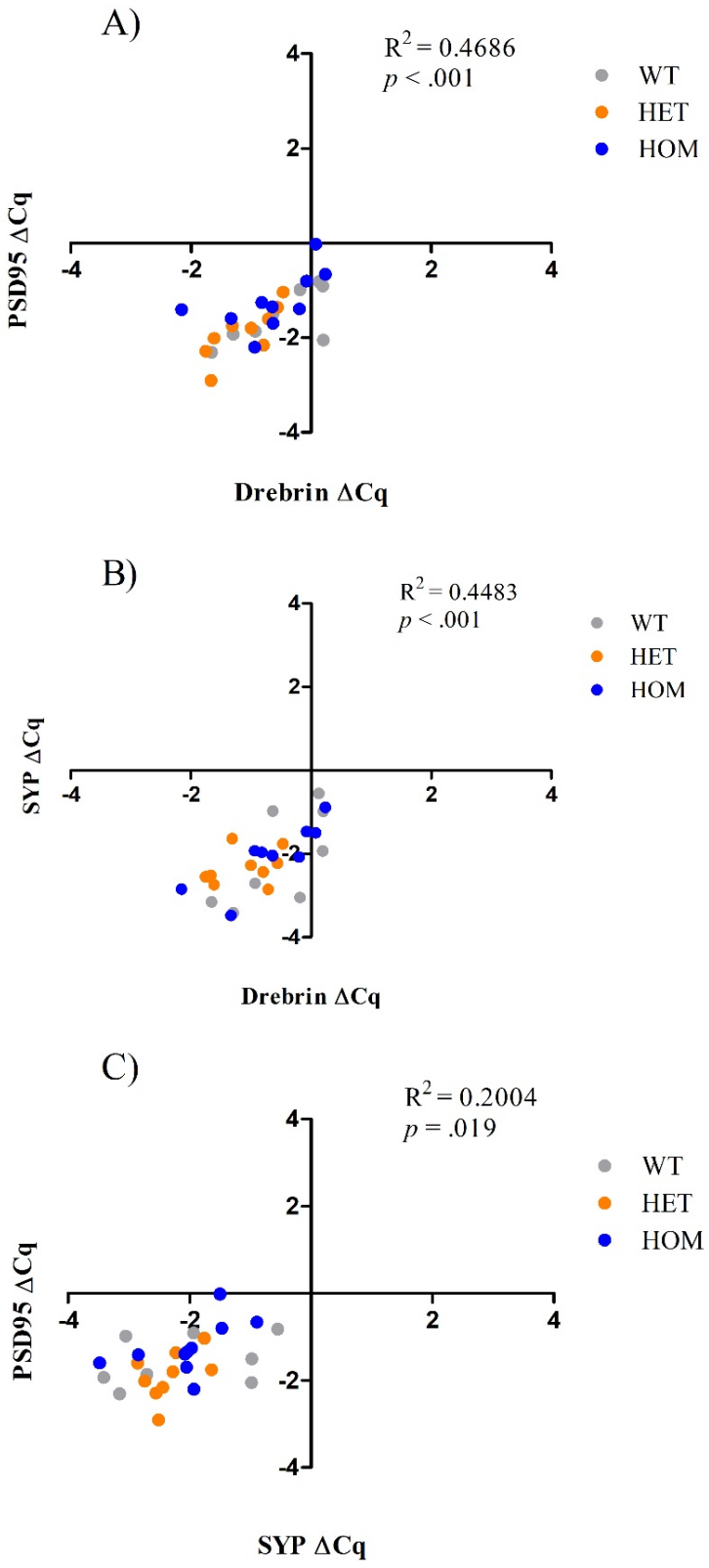

Figure 3.3.12 Correlations between A) drebrin and PSD95, B) drebrin and SYP, and C) SYP and PSD95 ΔCq values at PND60. R^2 and *p* values depicted on each graph.

3.4. Discussion

The aim of this chapter was to determine whether the mRNA expression of drebrin, PSD95, and SYP was downregulated in the frontal cortex of SERT HET and HOM animals relative to WT. By measuring across two timepoints, at PND14 and PND60, the developmental trajectory of this mRNA expression was also assessed. It was hypothesised that mRNA expression of these synaptic genes would be differentially downregulated among SERT KO animals relative to WT, particularly at PND14. Overall, the data are supportive of this hypothesis that during early development, synaptic genes in the frontal cortex of SERT KO animals are downregulated compared to WT.

A major pattern suggestive of these alterations observed in the data was the lower ΔΔCq values for *Dbn1*, *Dlg4*, and *Syp*, at PND14, with mRNA expression being reduced for all these genes in both HET and HOM pups compared to WT. Except for drebrin mRNA expression in SERT HOMs, both genotypes expressed these synaptic genes at least 0.5 ΔΔCq values lower than WT. However, no signs of downregulated mRNA expression at adulthood were observed. While this downregulation at PND14 may not have reached significance, due to low n and high SEM values, the consistently reduced mRNA expression at PND14 across all synaptic genes is a pattern that cannot be disregarded. Because this consistent downregulation at PND14 is resolved by adulthood, this pattern may be suggestive of some developmental delay in the molecular mechanisms governing synaptogenesis in the frontal cortex among SERT HET and HOM animals, at least at the genetic level. To speculate further, there may be compensatory mechanisms developing over time in these animals that may allow for this aberrant mRNA downregulation evident at PND14 to be resolved once these animals reach adulthood.

In support of the idea of a developmental delay among HETs and HOMs during the pre-pubescent period which may be resolved by adulthood was the finding that mRNA expression for drebrin and PSD95 significantly increased over time in HETs. More drebrin and

PSD95 mRNA was evident among HET adults than HET pups. Because drebrin and PSD95 mRNA expression in adult HETs did not differ to adult WTs, this increase in mRNA expression further suggests that the developmental delay resolves over time for HETs. It is interesting that this increase in mRNA expression for these postsynaptic genes was not also observed in HOM adults. The difference between pup and adult ΔΔCq values was much smaller in SERT HOMs, suggesting if there are compensatory mechanisms protecting SERT KO animals in adulthood, that these may occur more slowly in HOM animals compared to HET animals.

It is also interesting that no significant developmental increase in SYP mRNA expression was observed for HET and HOM animals. While a trend for SYP mRNA expression to increase over time is evident, these effects were smaller compared to the same effects seen in the postsynaptic genes. Whether this can be attributed to pre- and post- synaptic compartments being affected by genetic SERT deletion in different ways at adulthood is yet to be determined and cannot be supported by the current data.

Moreover, the data at adulthood were pooled across male and female animals. When determining whether there were any sex differences at adulthood in the mRNA expression of these synaptic genes, no differences between male and female animals were observed. A substantial increase in drebrin mRNA expression among HET and HOM males, compared to WT males and females across all genotypes, was observed. However, these differences did not reach significance, likely due to low sample sizes in each group. It is worth noting that the samples sizes for adult males and females were low because these differences were not a priority in this thesis, so more power would be required to provide an accurate account of any potential sex differences. There is a tendency to include only male animals in preclinical research as effects from female animals may be influenced by different stages in their oestrous cycle, in turn increasing statistical variability [129]. However, results from recent meta-analyses indicate that in neuroscience research, females are not affected by oestrous cycle

fluctuations as previously thought and are by extension not significantly more variable than males [130, 131], thereby suggesting that including females in the present experiment would not have created greater statistical variability. Moreover, such findings justify the pooling of both males and females at adulthood in this experiment to provide one single group at PND60 to be compared to data at PND14.

Finally, the correlational analysis provides some insight into how mRNA expression is involved in the regulation of synaptic proteins. Regardless of genotype, strong, positive correlations between ΔCq values were found. Of interest was that at both timepoints, and when pooling across timepoints, PSD95 and drebrin ΔCq values were correlated. Therefore, greater mRNA expression for PSD95 is correlated with greater mRNA expression for drebrin, and vice versa. Correlations between these synaptic genes were also maintained at adulthood, whereby all correlations were positive and moderate-strong. Importantly, these correlations involved both presynaptic (*Syp*) and postsynaptic (*Dbn1*, *Dlg4*) genes, suggesting some level of cross-talk between pre- and post- synaptic sites in regulating the expression of synaptic mRNA. While the correlation between drebrin and SYP ΔCq values at PND14 was not significant, the reason for which is presently unclear, a correlation between pre- and post- synaptic sites at PND14 was indeed evident between PSD95 and SYP. Taken together, the robust correlations between synaptic genes within postsynaptic sites and across the synaptic cleft are important indications that mRNA expression is tightly regulated both at the stage of synaptogenesis (PND14) and at the stage of dendritic spine maturity and maintenance (PND60).

3.4.1. Concluding Remarks

This chapter used qPCR to determine whether genetic SERT KO resulted in changes to mRNA expression of drebrin, PSD95 and synaptophysin, relative to WT. Overall, the results were suggestive of a developmental delay in the frontal cortex, such that mRNA expression for

all synaptic genes were reduced in HET and HOM pups compared to WT pups, albeit not reaching statistical significance. Moreover, the data showed that this reduction was not observed at adulthood, particularly for HET animals, indicating that the aberrations observed at PND14 wane by PND60. Complementary analyses also showed strong correlations between mRNA expression for all synaptic genes at both timepoints, highlighting that mRNA expression is closely regulated at the synapse across both synaptic sites. Altogether, this chapter begins to expound the effects of genetic SERT deletion on the synapse at the genetic level and extends on the mRNA changes to these genes found in the RNA-seq experiment performed by our lab as well as the mRNA changes in SERT KOs reported previously [119].

CHAPTER 4. QUANTIFICATION OF SYNAPTIC MARKER PROTEIN EXPRESSION IN SERT KO USING WESTERN BLOT ANALYSIS

4.1. Aim and Rationale

The aim of this chapter was to examine the protein expression of drebrin, PSD95 and synaptophysin across the SERT genotypes at PND14 and PND60 using western immunoblotting. This experiment aimed to extend and complement the results from the qPCR analysis, which demonstrated that these synaptic markers at the mRNA level were reduced at PND14 among SERT HET and HOM animals, to determine whether changes are also occurring at the protein level. While the efficacy of mRNA levels predicting protein expression has been challenged, markers of synaptic activity show one of the highest levels of predictability between mRNA transcript and subsequent protein levels, at least in the human brain [132]. Therefore, this analysis was expected to delineate whether there are functional effects of genetic SERT deletion on drebrin, PSD95 and SYP, and to parallel the findings of the previous qPCR chapter.

If the changes found at the mRNA level in Chapter 3 also translate into functional consequences at the protein level, as expected, it was hypothesised that drebrin, PSD95 and SYP protein expression among SERT HET and HOM animals would be downregulated relative to WT. This downregulation was expected foremost at PND14, given that the mRNA expression for all these genes was reduced among the SERT KO animals at this pre-weaning timepoint. This hypothesis would align with the finding that PSD95, as well as GluN1, expression is downregulated at PND21 in the PFC of SERT HOM animals [119]. Moreover, in line with the postulation established in the previous chapter that SERT reduction (HETs) and deletion (HOMs) results in developmentally-limited aberrations to synaptic markers, it was

further hypothesised that the reduction in these proteins at PND14 would be resolved by adulthood.

4.2. Methods

4.2.1. Animals

A total of 50 animals were used for the western blot experiments. Animals were kept under standard housing conditions and came from SERT HET dams as described previously (Section 2.1). Table 4.2.1 denotes the number of animals per genotype (WT, HET, HOM), age (PND14, PND60), and sex (male, female) at adulthood.

Table 4.2.1 Number of animals used for western immunoblotting across genotype, age, and sex (at adulthood).

	PND 14	PND 60			
		Male	Female	Combined sex	Combined age
WT	8	3	5	8	16
HET	9	4	5	9	18
HOM	6	6	4	10	16
Total	23	13	14	27	50

4.2.2. Tissue Preparation

The frontal cortex from each animal was dissected, immersed in RIPA buffer with PI and stored at -80ºC as described in detail in Section 2.2.1. To further prepare the frontal cortex tissue lysates for western blot, the samples were thawed on ice when ready for processing. Tissue was then homogenised with pestles to break up large tissue chunks. After adequate homogenisation, samples were sonicated using a SONOPLUS Mini20 Ultrasonic Homogeniser (Bandelin Electronic - GmbH & Co. KG; Berlin, Germany) to further dissociate the tissue remaining after the previous homogenisation steps. Samples were sonicated on ice for 15 s at

3 Watts, with 10 s intervals to prevent heat-mediated protein degradation. Each sample was sonicated for a total of 1 min.

After sonication, homogenised samples were centrifuged at 16000 x g for 20 min at 4ºC to sediment out any cellular debris. The supernatant was then transferred into a fresh microcentrifuge tube to isolate the homogenised protein lysate from each sample, while the precipitate and cellular debris were discarded. The isolated lysates were stored at -20ºC and were used for all subsequent protein quantification and western blot assays.

4.2.3. Protein Quantification

Protein concentrations for each isolated lysate were quantified using a Pierce bicinchoninic acid (BCA) assay kit (ThermoFisher Scientific, #23227; MA, USA). The BCA assay reaction results in the reduction of Cu^{2+} (cuprous) ions to Cu^{1+} (cupric) ions by the protein in each sample, which is then chelated by the BCA. This molecular complex induces absorbance at 562 nm, which directly correlates with the concentration of protein found in each sample lysate. The BCA assay was conducted on JET BIOFIL 96-well tissue culture plates (Interlab Ltd, KJ511-3VL; Wellington, NZ) and absorbance was measured on a CLARIOstar® microplate reader (BMG Labtech; Ortenberg, Germany).

Samples were diluted in RIPA buffer with PI at a ratio of 1:9 for accurate interpolation of the protein concentrations in each sample. At least two replicates for each sample lysate were used and the absorbance values averaged between replicates. Protein concentrations were calculated in µg/µl after correcting for both the dilution factor and the absorbance emitted by the diluent (RIPA+PI) alone.

4.2.4. SDS-PAGE and Membrane Transfer

Protein samples were diluted in either RIPA+PI or 1x Tris-EDTA (TE) buffer containing 0.5% sodium dodecyl sulphate (SDS), and 2x Laemmli Buffer (LB), with a 1:1 ratio

of sample and RIPA+PI/1x TE to 2x LB. Proteins were denatured via the β-mercaptoethanol in the 2x LB, and also heat denatured for 5 min at 95ºC. Ten percent acrylamide separating gels were made using 30% bis-acrylamide (Bio-Rad, #1610156; CA, USA). The separating gels were made fresh or in advance and kept at 4ºC immersed in 1x SDS-PAGE running buffer. Stacking gels, at a concentration of 4%, were made fresh. For each sample, 20 µg of protein was loaded at a volume of 20 µl per lane (1 µg/µl). The Precision Plus Protein™ dual colour standard (Bio-Rad, #1610374; CA, USA) was also loaded into the first lane for a standard reference of the separated molecular weights.

The 20 µg of protein in each lane was resolved by sodium dodecyl sulphate polyacrylamide gel electrophoresis (SDS-PAGE) in 1x SDS-PAGE running buffer at 120 V for 1.5 hrs or until the dye front moved adequately to the bottom of the separating gel. Protein was then transferred onto an Immobilon-FL Polyvinylidene difluoride (PVDF) membrane (Millipore #IPFL00010; MA, USA) activated in 100% methanol for at least 5 min. Transfer was carried out at 80 V for 4.5 hrs in transfer buffer at 4ºC, with the transfer tank placed into a box containing ice to prevent overheating.

4.2.5. Protein Detection

After proteins were transferred onto the PVDF membrane, the membrane was washed in 1x tris-buffered saline (TBS) for 5 min twice. It was then blocked in 5% skim milk powder for 1 hr at RT. After membranes were washed twice in 1x TBS with 0.1% Tween-20 (TBST) for 5 min each, they were incubated with the required primary antibody (Table 4.2.2) overnight at 4ºC, diluted in 1% milk powder in 1x TBST. The next day, membranes were washed twice for 5 min each in 1x TBST, then incubated with the appropriate secondary antibody for 2 hrs at RT (Table 4.2.2), diluted in 1% milk powder in 1x TBST. For the loading control bands, membranes were incubated with an α-Tubulin antibody for 1 hr at 4ºC, then with the

appropriate secondary antibody for up to 2 hrs at RT. For both the loading control and proteins of interest, the membranes were protected from light during the incubation with the secondary antibody. After washing in 1x TBST twice for 5 min each, membranes were scanned using a Fujifilm FLA5000 fluorescence scanner (Fujifilm Medical System; CT, USA) at 400 V to detect antibody-bound transferred proteins. Proteins fluorescently tagged with Alexa Fluor™ 488 were scanned using the 473 nm laser, while proteins tagged with Alexa Fluor™ 647 were scanned using the 635 nm laser.

Densitometry analysis using ImageJ software was used to quantify the expression of each protein of interest across genotypes and age, which was normalised to the loading control (α-Tubulin), to ensure that the same amount of protein (20 µg) was loaded for each sample. Negative control membranes where the primary antibody was omitted were also used alongside the test membranes to ensure specificity of the primary antibody binding.

Table 4.2.2 Primary and secondary antibodies used for western blot analysis.

Primary Antibodies			
Marker (clone)	Antibody Raised in	Antibody Dilution	Manufacturer (Code)
Drebrin (M2F6)	Mouse	1:1000	Invitrogen (MA1-20377)
PSD-95 (6G6-1C9)	Mouse	1:1000	Abcam (ab2723)
SYP (EP1098Y)	Rabbit	1:2500	Abcam (ab52636)
α-Tubulin (DM1A)	Mouse	1:10000	Abcam (ab7291)
Secondary Antibodies			
Secondary Antibody	Host x Raised Against	Antibody Dilution	Manufacturer (Code)
Alexa Fluor™ 488	Goat x Mouse	1:4000	Invitrogen (A11001)
Alexa Fluor™ 488	Goat x Rabbit	1:4000	Invitrogen (A11008)
Alexa Fluor™ 647	Donkey x Mouse	1:4000	Invitrogen (A31571)

4.3. Results

An initial set of western blot experiments were conducted to ensure that all markers appear as distinct, specific bands corresponding to the expected molecular weights of each antigen. These tests confirmed that all antibodies produced specific bands with expected molecular weights (Figure 4.3.1).

Densitometry analysis was then conducted to determine the effect of genetic SERT deletion on drebrin, SYP and PSD95 across the two developmental time periods. The relative density for each band was calculated against the loading control (α-Tubulin). Density change for SERT HETs and HOMs at both timepoints was then calculated relative to WT to determine the relative expression of these synaptic markers compared to WT control (where WT = 1).

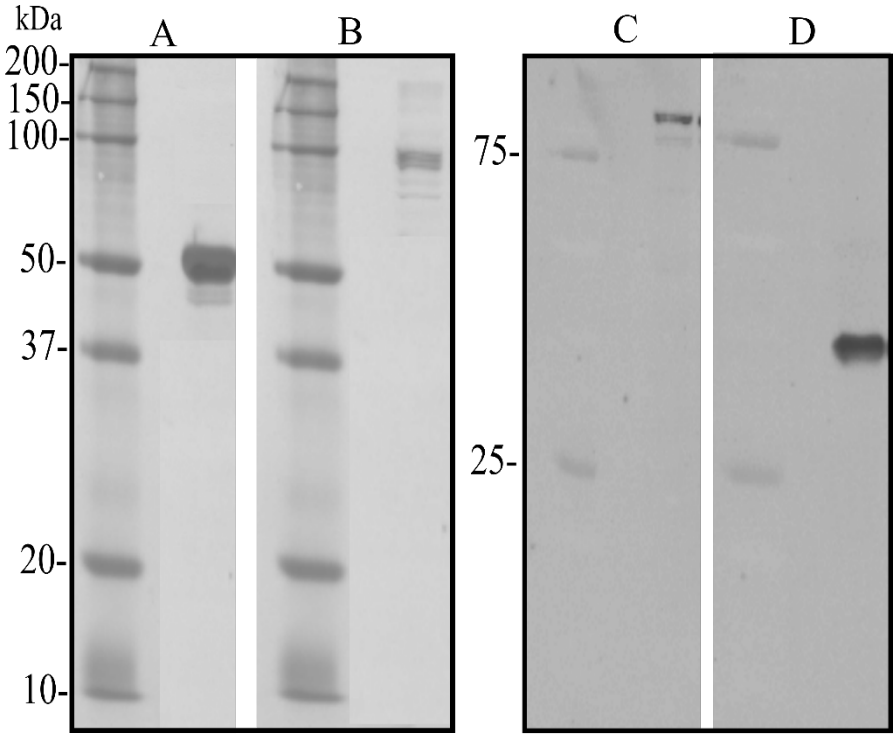

Figure 4.3.1 Validation of protein size against Precision Plus Protein™ dual colour standard molecular weight marker for the antibodies used in this study: A) α-Tubulin (51 kDa), B) PSD95 (95 kDa), C) Drebrin (110 kDa), and D) SYP (42 kDa).

As with the qPCR experiments, a sex analysis was performed to ensure drebrin, PSD95 and SYP protein expression did not differ between adult male and female SERT animals. The sex analysis showed no significant differences between males and female adults in protein expression for these synaptic proteins (Appendix C). Thus, protein expression at PND60 was pooled across sex and compared with the PND14 timepoint. An initial 3 (genotype: WT, HET, HOM) x 2 (age: PND14, PND60) factorial ANOVA was conducted to assess main effects and interactions of the relative densities of drebrin, PSD95, and SYP across age and genotype. However, for all proteins, Levene's homogeneity test of variance indicated that equal variance between the groups was not assumed. As a result, the distribution for all relative density measures was assessed using Q-Q plots. Visual observation indicated the relative density measures of SYP, PSD95 and drebrin were approximately normally distributed (Appendix D). Because the relative density data for all target proteins had non-constant variance but were approximately normally distributed, Welch's ANOVA was conducted for all target proteins to assess whether there was a difference in synaptic protein expression between the groups, which was followed-up with Games-Howell post-hoc tests to determine where these differences occurred.

Welch's ANOVA indicated for both drebrin (Figure 4.3.2) and PSD95 (Figure 4.3.3), protein expression did not significantly differ between the groups: drebrin, $F(5, 44) = .1.324$, $p = .272$, *ns*; PSD95: $F(5, 44) = .454$, $p = .808$, *ns.* However, Welch's ANOVA indicated a significant difference in SYP expression between the six groups, $F(5, 44) = 8.036$, $p < .001$ (Figure 4.3.4). Games-Howell post-hoc analyses demonstrated that at PND14, there was a 58% reduction in SYP expression in SERT HOM animals ($M = 0.48$, $SD = 0.15$) compared to WT animals ($p = .045$). Moreover, there was a 52% reduction of SYP expression in SERT HET animals ($M = 0.42$, $SD = 0.18$) compared to WT, which showed a trend towards significance ($p = .076$). Comparing across developmental timepoints at PND14 and PND60 indicated a 92%

increase in SYP expression in HET adults (M = 1.40, SD = 0.65) compared to HET pups (p = .022), and a more than 100% increase in SYP expression in HOM adults (M = 1.43, SD = 0.57) compared to HOM pups (p = .002), such that SYP expression at adulthood was increased compared to PND14. No differences were identified between HET and HOM animals at adulthood compared to WT controls.

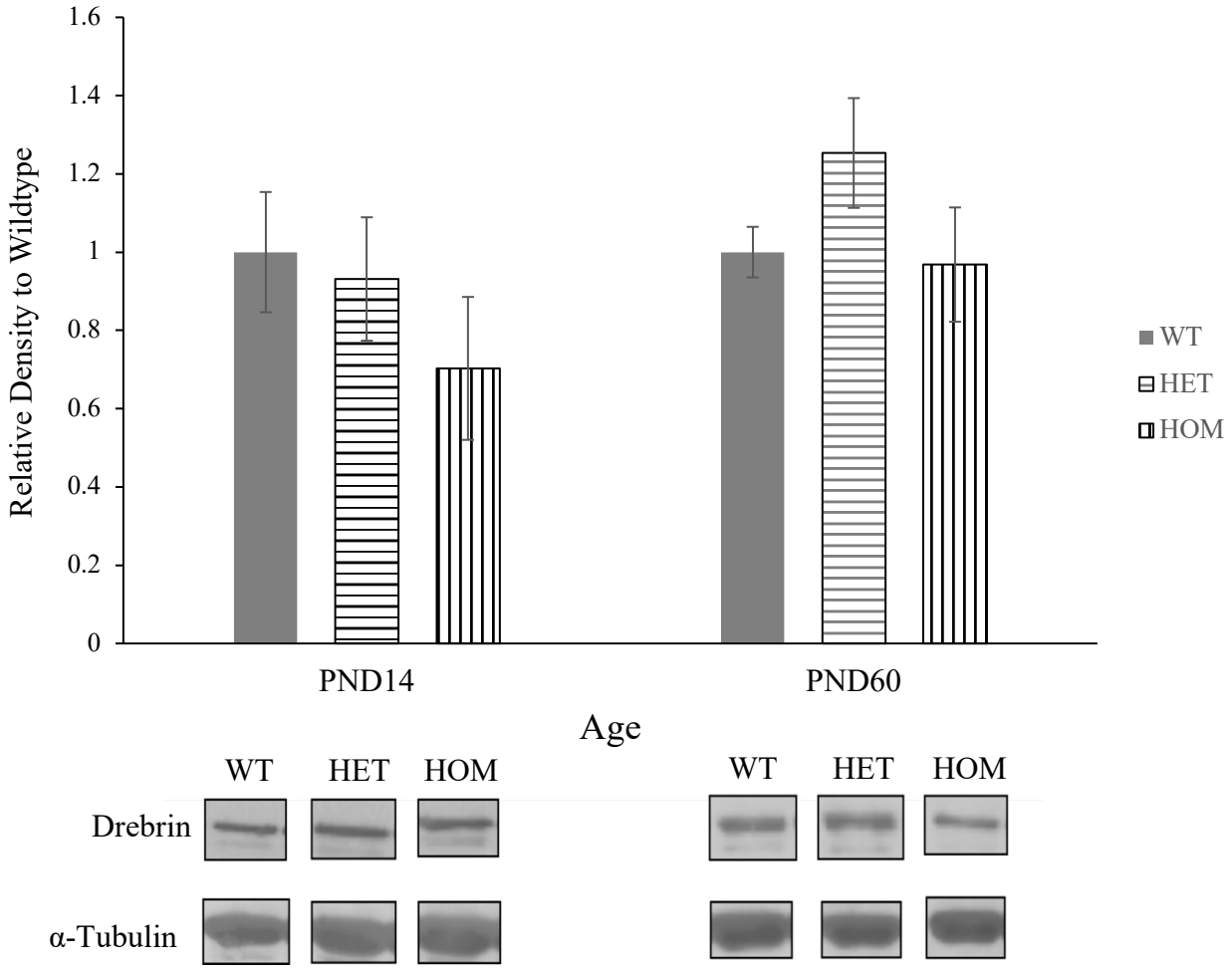

Figure 4.3.2 Mean relative density of drebrin expression in the frontal cortex of SERT HET and HOM animals at PND14 and PND60 relative to WT control. Representative bands for each group for both drebrin and loading control (α-Tubulin) are also displayed. Error bars indicate ± SEM.

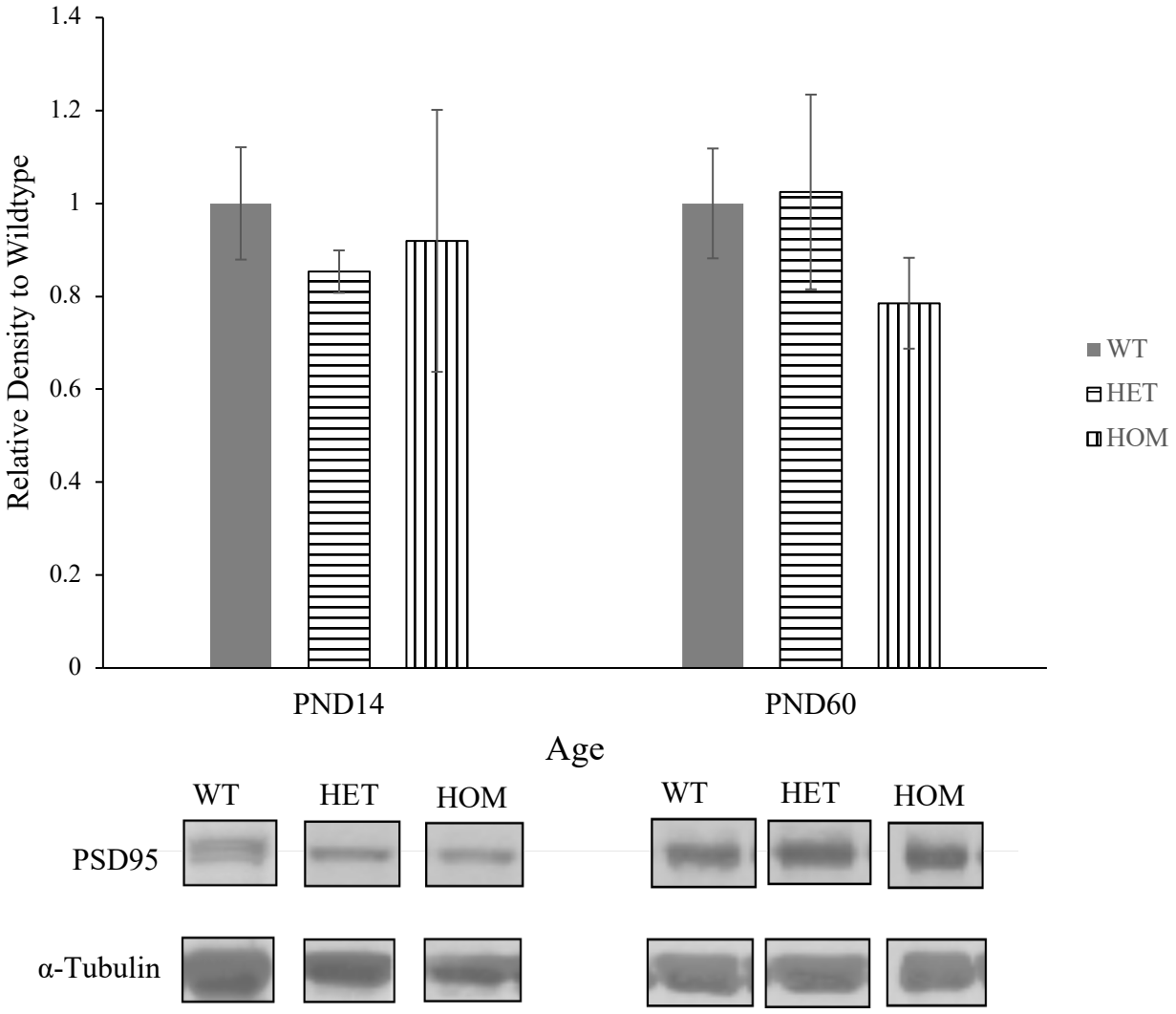

Figure 4.3.3 Mean relative density of PSD95 expression in the frontal cortex of SERT HET and HOM animals at PND14 and PND60 relative to WT control. Representative bands for each group for both PSD95 and loading control (α-Tubulin) are also displayed. Error bars indicate ± SEM.

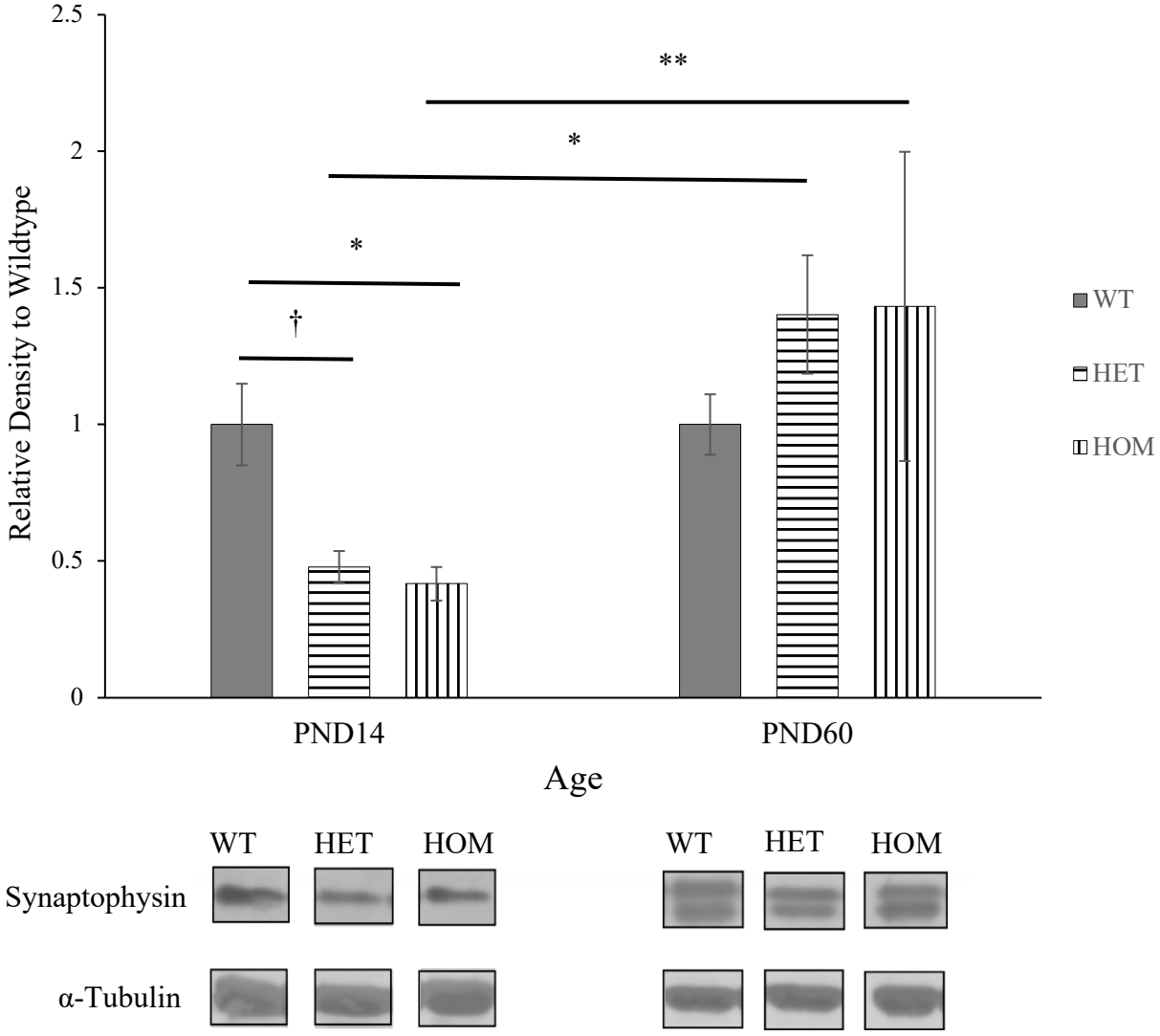

Figure 4.3.4 Mean relative density of synaptophysin expression in the frontal cortex of SERT HET and HOM animals at PND14 and PND60 relative to WT control. Representative bands for each group for both synaptophysin and loading control (α-Tubulin) are also displayed. * $p < .05$, ** $p < .01$, † $p = .076$. Error bars indicate ± SEM.

Finally, a correlational analysis was performed on the relative density to loading control measurements to determine whether there were any correlations between the three target proteins. This analysis was performed first on the entire dataset, pooling both genotype and age together. Results indicated a significant, positive correlation between SYP and drebrin relative density expression, $r = 0.35$, $p = .013$ (Figure 4.3.5). This result was further investigated, with the dataset separated by age to determine whether this correlation was evident at both timepoints. The follow-up analysis indicated that the initial correlation identified was driven by a significant, positive correlation between SYP and drebrin expression at PND14 ($r = .50$, $p = .02$), but not at PND60 ($r = 0.29$, $p = .141$, *ns*; Figure 4.3.5).

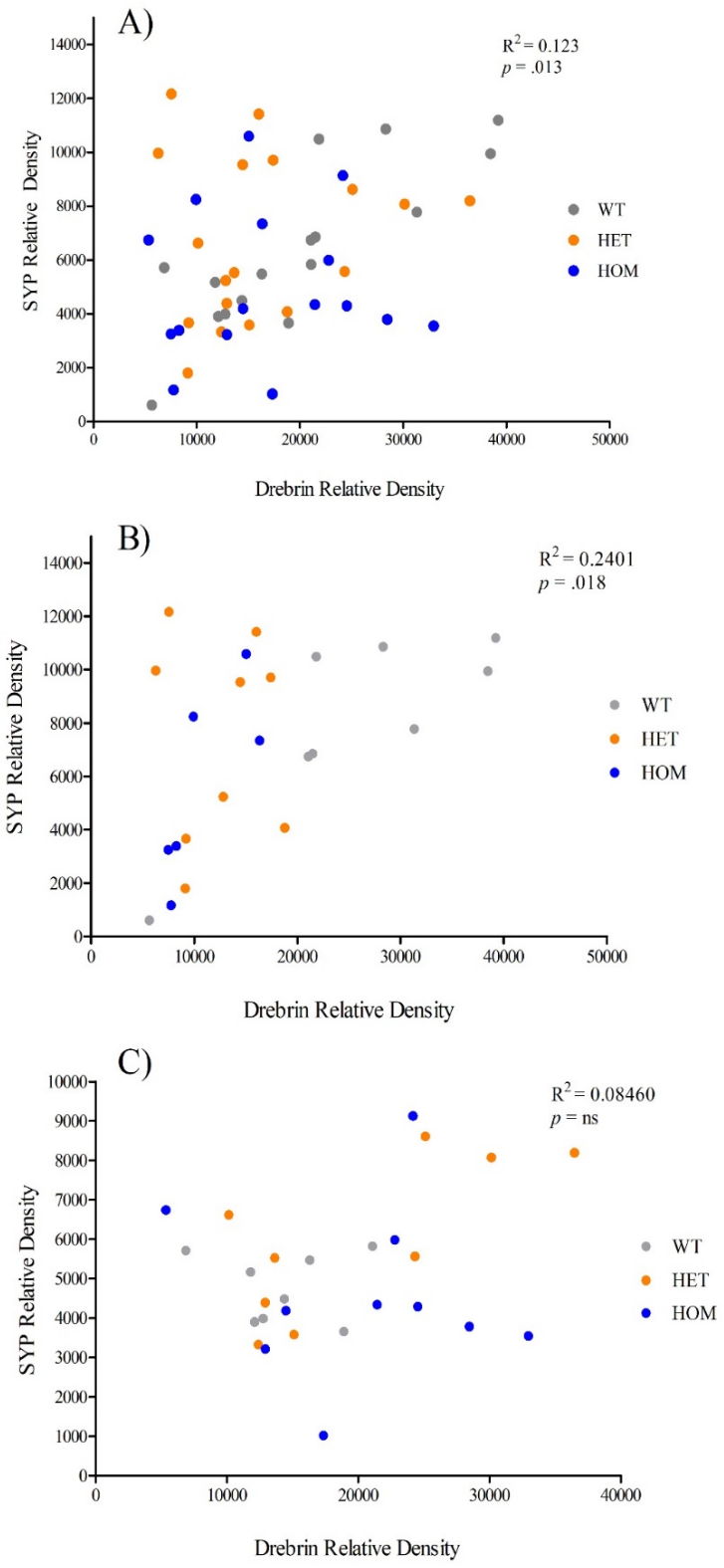

Figure 4.3.5 Pearson's correlations for SYP and drebrin expression relative to loading control, with R^2 and p values depicted on each graph. A) A significant correlation between SYP and drebrin was found when combining both PND14 and PND60 data. When separating the timepoints, the SYP and drebrin correlation was significant at PND 14 (B), but not at PND60 (C).

4.4. Discussion

The aim of this chapter was to extend upon the results from the qPCR analysis in Chapter 3 by determining the protein expression of drebrin, PSD95, and SYP in the frontal cortex of SERT HET and HOM animals relative to WT, using western blot. Two timepoints were assessed to determine how this protein expression may change over time, alongside a sex analysis at adulthood to assess whether any sex differences were evident. It was hypothesised that drebrin, PSD95 and SYP protein expression among SERT HETs and HOMs would be reduced relative to WT, especially at PND14, with results providing partial support for this hypothesis.

One of the most salient findings from this chapter in support of the hypothesis was that SYP expression was reduced after genetic SERT deletion at PND14. Results indicated that at PND14, SYP in the frontal cortex was substantially reduced in HETs and HOMs, with these animals expressing less than half the amount of SYP than those expressed in WTs. However, at adulthood, SERT KO animals no longer demonstrated reduced SYP expression compared to WT, indicating that the reduction in presynaptic SYP expression is specific to this period of postnatal development and that there is a resolution of this aberrant reduction occurring between this early timepoint and PND60. Because SYP expression is directly correlated with synaptogenesis [96], this aberrant SYP reduction exclusive to PND14 is suggestive of a reduction, or delay, in synaptogenesis and synapse formation in SERT HETs and HOMs. Synaptophysin is involved in neurotransmitter vesicular trafficking at presynaptic terminals and is correlated with the number of synaptic sites [133]. Thus, the reduced expression of this protein after genetic SERT deletion only during early development and not adulthood suggests that processes related to synaptogenesis are stunted in these animals.

If this hypothesis that genetic deletion of the SERT results in stunted synaptogenesis is supported, it would imply that proteins at both pre- and post- synaptic sites would be reduced.

Therefore, it is interesting that neither drebrin nor PSD95 was significantly reduced among SERT KO animals alongside SYP. Visual observation did indeed show that drebrin expression among HOM pups was reduced by nearly one third of the expression of WT pups, indicative of some level of aberration even at postsynaptic sites of the synaptic cleft. However, this effect failed to reach significance. Perhaps the combination of non-equal variance and low power yielded insignificant results with the current data set. A replication of the current experiment with improved, constant variance is therefore warranted to confirm whether this postulated stunted synaptogenesis among SERT KO animals occurs at both pre- and post- synaptic sites or is exclusive to presynaptic processes, as the current data only show support for the latter.

Moreover, the additional sex analysis at PND60 did not indicate any major expression differences between adult males and females for these synaptic proteins. The lack of sex differences between drebrin, PSD95 and SYP at the protein level complements the same null findings from the qPCR analysis, once again justifying the pooling of both sexes at PND60 to be compared to pups at PND14. Interestingly, however, the correlational analysis showed that drebrin and SYP protein expression were correlated. When pooling the timepoints together, a positive, moderate correlation was found between postsynaptic drebrin and presynaptic SYP. Separating the timepoints indicated that this effect was driven by a strong correlation at PND14, but not at PND60. It is clear that both drebrin and SYP expression begin to accumulate from PND14, and continue to accumulate at a similar rate over time [96]. This parallel accumulation coincides with synaptogenesis, a process that requires the expression of drebrin A in dendritic spines and SYP in presynaptic terminals [96]. Therefore, it is unsurprising that drebrin and SYP are correlated at this early developmental timepoint, but the reasons for why this association is not held at adulthood are unclear.

4.4.1. Concluding Remarks

This chapter aimed to complement the results from Chapter 3 by determining whether genetic SERT ablation also affects the expression of synaptic proteins, as well as having an impact at the genetic level. Results indicated that SYP protein expression was substantially reduced in SERT HETs and HOMs at PND14 relative to WT. Additionally, SYP expression was correlated with drebrin expression at PND14, providing further support for reports from previous literature that the accumulation of these two proteins coincides with synapse formation. Altogether, this chapter highlights the potential consequences of genetic SERT deletion, as the results suggest that SERT deletion results in an aberration of presynaptic processes during development that would lead on to stunted synaptogenesis and developmental delays, which is resolved by young adulthood.

CHAPTER 5. OPTIMISATION OF A NOVEL *IN SITU* HYBRIDIZATION METHOD, RNASCOPE®, FOR *IN SITU* DETECTION OF DREBRIN mRNA

5.1. Aim and Rationale

The aim of this chapter was to optimise a protocol for a novel *in situ* hybridization (ISH) method, RNAscope®, to assess the expression of drebrin mRNA within tissue. RNAscope® is a novel ISH method designed to increase the sensitivity of hybridization while reducing background noise, in contrast to the poor signal-to-noise ratios engendered using ordinary RNA ISH methods [134, 135]. This method employs a unique probe design, whereby the target probe is comprised of two contiguous, but separate sequences complementary to the target transcript, referred to as a "double-Z" design (Figure 5.1.1) [135]. Because of this unique double-Z design, only when these two contiguous sequences are hybridized to the target, will the signal amplify, thereby enhancing the signal-to-noise ratio (Figure 5.1.1). Using this RNA ISH method, each single punctate dot corresponds to a single mRNA transcript. RNAscope® allows for visualisation of mRNA puncta either using a diaminobenzidine-based (brightfield microscopy) method or using fluorescent signals. Simultaneous labelling of multiple target probes, and dual ISH and immunohistochemistry/immunocytochemistry are also possible using RNAscope® [134]. By optimising an RNAscope® protocol for the expression of drebrin mRNA, the results of the qPCR experiments in Chapter 3 would be extended upon. Specifically, utilising this alternative method could identify any region-specific differences within a single section across genotype and age, such as between cortical and subcortical regions, and could provide an understanding of drebrin mRNA localisation, both of which cannot be explored using standard qPCR methodology.

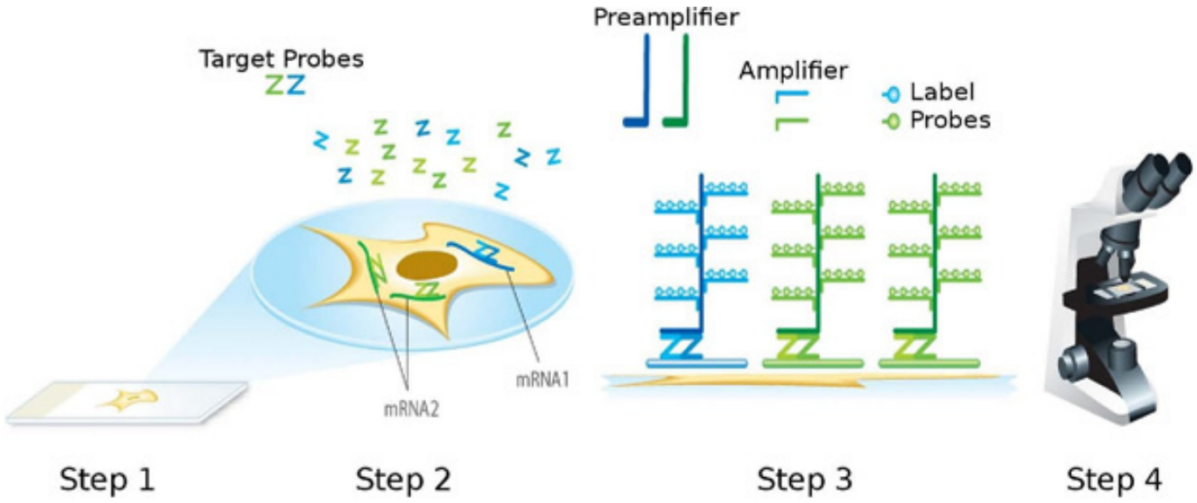

Figure 5.1.1 Schematic diagram for RNAscope® assay procedure. Step 1: tissue is fixed and permeabilized. Step 2: the double-Z probe is hybridized to the mRNA targets. Step 3: The signal is amplified via the presence of the preamplifier hybridizing to the contiguous target probes, alongisde unique labels and probes to amplify the signal. Step 4: signal is detected using brightfield or fluorescent microscopy. Figure redistributed from [135] under Attribution-nonCommercial-NoDeriavtives 4.0 International (CC BY_-NC-ND) License (https://creativecommons.org/licenses/by-nc-nd/4.0/).

5.2. Methods

5.2.1. Animals

A total of 19 animals were processed for RNAscope®. Before tissue collection, all animals were kept under standard housing conditions and came from SERT HET dams as described in Section 2.1. Table 5.2.1 denotes the number of animals per genotype (WT, HET, HOM) and age (PND14, PND60).

Table 5.2.1 Number of animals processed for RNAscope® across genotype and age

	PND 14	PND 60	Combined Age
WT	1	3	4
HET	7	3	10
HOM	4	1	5
Total	12	7	19

5.2.2. Tissue Sectioning

After processing and embedding in paraffin wax (Section 2.2.2), tissue was stored at RT until ready for the sectioning. Frontal cortex tissue was sectioned at 5 µm using a Lecia Manual Rotary Microtome (Lecia Biosystems, RM2235; Wetzlar, Germany) alongside a Lecia Water Bath (Lecia Biosystems, HI1210; Wetzlar, Germany). Because the 5 mm tissue section was placed onto FFPE cassettes rostral-side-down, brains were sectioned along the caudal-to-rostral plane. These FFPE sections were then mounted on LabServ Superfrost® Plus microscope slides (ThermoFisher Scientific, LBS4951+; MA, USA) and allowed to dry at RT before proceeding onto the RNAscope® protocol.

5.2.3. RNAscope®

The RNAscope® protocol was provided by Advanced Cell Diagnostics (ACD bio; CA, USA), comprising of a sample preparation and pre-treatment manual (document #322452) and an RNAscope® 2.5 HD detection reagent manual (document #322360-USM). The RED RNAscope® detection reagent kit was used in this experiment, which allows for the individual mRNA transcripts to be visualised using both brightfield and fluorescent microscopy as red puncta.

Briefly, FFPE sections were baked at 60ºC for 1 hr. As an optional stopping point, the sections were stored for up to 1 week at RT with desiccant. Otherwise, sections were then deparaffinized. Sections were immersed in xylene for 5 min at RT with mild agitation, with one change into fresh xylene for another 5 min. They were then immersed in 100% EtOH twice, for 1 min each at RT with agitation then air dried for up to 10 min at RT. Sections were quenched with RNAscope® hydrogen peroxide for 10 min, then washed in fresh distilled water twice. Target retrieval was then performed in a standard pressure cooker. Slides were placed in a Coplin jar containing 1x RNAscope® Target Retrieval Reagent, heated to 95-100ºC, for 15 min. After target retrieval, slides were immediately washed in distilled water at RT and then dipped briefly in 100% EtOH. Slides were then airdried at RT, and a hydrophobic barrier was created around each individual section using an ImmEdge™ Hydrophobic Barrier PAP pen (Vector Laboratories, H-4000; CA, USA). To complete the sample preparation and pre-treatment protocols, sections were permeabilised with RNAscope® Protease Plus at 40ºC in a HybEZ™ Oven provided by ACD for 30 min. Finally, slides were washed in distilled water before proceeding onto the hybridization and amplification procedure.

The target probe (drebrin, *Dbn1*) was applied to each section and hybridized for 2 hrs at 40ºC in the HybEZ™ Oven. At least one section was designated as a negative control, in which a negative control probe for the *Escherichia coli* gene 4-hydroxy-tetrahydrodipicolinate reductase (*DapB*) was used. After hybridization, slides were washed twice in 1x RNAscope® Wash Buffer for 2 min each at RT with gentle agitation. The hybridization was then amplified 6 times (AMP 1-6), by adding the appropriate amplification solution onto each section. For AMP 1, 3, and 5, slides were incubated for 30 min, AMP 1 and 3 at 40ºC in the HybEZ™ Oven, while AMP 5 at RT. For AMP 2, 4, and 6, slides were incubated for 15 min, with AMP 2 and 4 at 40ºC in the HybEZ™ Oven, while AMP 6 at RT. Between each amplification step,

the slides were washed twice in 1x RNAscope® Wash Buffer for 2 min each at RT, with gentle agitation.

The signal was then detected by pipetting on each section the RED working solution, made by combining Fast RED-A and Fast RED-B at a ratio of 60:1. Sections were incubated for 10 min at RT, then washed twice with tap water to remove all remnants of the RED working solution. The sections were subsequently counterstained with 50% Haematoxylin staining solution for 2 min at RT, then washed with tap water repeatedly until the slides were clear from the Haematoxylin staining but the sections remained purple. Slides were then immersed in 0.02% Ammonia water briefly, then washed in tap water once more.

Finally, slides were dried at 60ºC for at least 15 min. They were then dipped in xylene, covered with a small amount of VectaMount® Permanent Mounting Medium (Vector Laboratories, H-5000; CA, USA) and immediately affixed with coverslips. Slides were air dried before examination under the microscope.

5.2.4. Dual RNAscope® ISH-IHC

A protocol was also optimised for dual labelling of mRNA puncta using RNAscope® and protein labelling using immunohistochemistry (IHC). Dual ISH-IHC has been previously shown to be successful in free-floating brain tissue [134]. The dual ISH-IHC protocol optimised in this thesis was adapted from these previous methods, using the *Dbn1* probe, to make it possible for a greater variety of experimental questions relating to drebrin mRNA activity to be posed and addressed.

The standard RNAscope® protocol as described in this thesis was followed up until staining with the fast RED solution and washing the hybridized sections with tap water - the counterstaining sections were omitted from this dual ISH-IHC protocol. After washing in tap water, sections were blocked in 5% bovine serum albumin (BSA) in 1x TBST at RT for 1 hr.

Slides were then washed three times for 5 min each in 1x TBST, followed by incubation with the primary antibody, SYP (1:100), overnight at 4ºC. A high concentration of SYP was used to account for any potential blocked epitope sites caused by the RNAscope® protocol. The next day, slides were washed three times in 1x TBST for 5 min each, then incubated with Alexa Fluor™ goat anti-rabbit 488 for 2 hrs. After washing three times in 1x TBST for 5 min each, sections were mounted with ProLong™ Gold Antifade Reagent with DAPI (ThermoFisher Scientific, P36934; MA, USA). They were then affixed with a coverslip and allowed to cure overnight before imaging. Additional information on the primary and secondary antibodies used for this dual ISH-IHC test are provided in Table 4.2.2.

5.2.5. Imaging

Two microscopes were used for acquiring images of RNAscope®-treated tissue. Brightfield (Figure 5.3.1) and fluorescent (Figure 5.3.3, Figure 5.3.4) images of RNAscope®-treated sections were examined using an Olympus 1X58 inverted microscope with an Olympus TH4-200 Halogen lamp (Olympus Corporation; Tokyo, Japan) used for brightfield detection of mRNA puncta or an X-Cite® 120Q light source for fluorescent detection of mRNA puncta (Excelitas Technologies; MA, USA). Examination of the dual RNAscope® ISH-IHC treated tissue (Figure 5.3.2) was conducted on an Olympus FLUOVIEW FV1000 Confocal laser Scanning Microscope (Olympus Corporation; Tokyo, Japan), with image acquisition conducted on the Olympus FV10-ASW software (version 4.0).

5.3. Results

The RNAscope® protocol for a drebrin (*Dbn1*) probe was first tested on 5 µm FFPE coronal sections from a randomly selected PND14 rat brain obtained from a SERT litter, following the protocol as outlined by the two RNAscope® manuals provided. Hybridization with the *Dbn1* probe showed intense red staining corresponding to the individual mRNA

drebrin transcripts, while hybridization with the negative control *DapB* resulted in no mRNA expression (Figure 5.3.1). *Dbn1* transcripts were particularly clustered in cell nuclei, which made identifying individual puncta, and therefore any subsequent quantification, difficult (Figure 5.3.1-A). Therefore, as suggested by the RNAscope® manual (document #322360-USM) the incubation time for AMP5 was reduced from 30 min to 15-20 min to reduce the intensity of the red staining. As shown in Figure 5.3.1-B, this alteration reduced the intensity of the staining in highly-clustered areas which allowed for the identification and distinction between individual mRNA puncta.

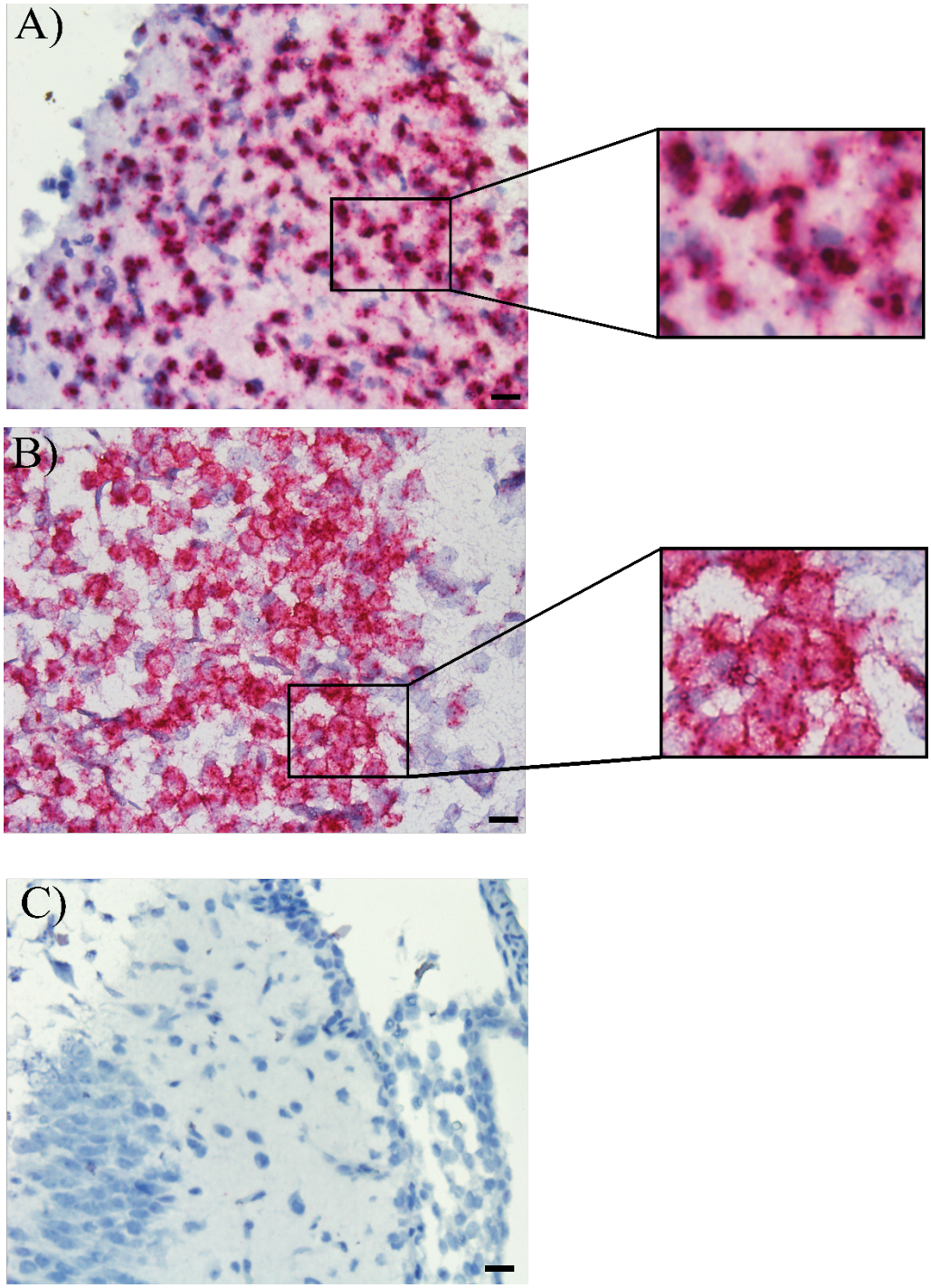

Figure 5.3.1 Images of the frontal cortex hybridized with the *Dbn1* probe, showing that reducing the AMP5 incubation time from 30 min (A) to 15-20 min (B) reduces the intense staining of drebrin mRNA puncta in cell nuclei. Magnified images of the rectangular areas in (A) and (B) are shown. Decreasing AMP5 time therefore allows for more visible distinct puncta that can be distinguished from each other. C) Negative control hybridized with *DapB* showed no mRNA puncta. Scale bar = 20 µm.

Next, a method for dual ISH-IHC was optimised by hybridizing tissue with the drebrin probe, followed by fluorescent IHC labelling of SYP, using coronal sections from a randomly selected PND21 brain. Dendritic spines contain polyribosomes at the spine base as well as endoplasmic reticulum, which would allow for local transcription within the spine itself [63]. For this reason, dendritic spines are considered semi-autonomous compartments [63]. Such capability for local transcription would be particularly important during instances where high turnover would be required, such as during LTP and LTD. SYP was chosen as the labelled protein to determine whether co-localisation of SYP at presynaptic terminals with drebrin mRNA puncta at postsynaptic dendritic spines was evident. If dual ISH-IHC showed parallel localisation of SYP with drebrin mRNA, this would suggest that neither drebrin mRNA localisation, nor drebrin transcription, are exclusive to cell nuclei, but are also present in dendritic spines.

A projected Z-stack image of this dual ISH-IHC test is shown in Figure 5.3.2, demonstrating the high localisation of drebrin mRNA puncta in cell nuclei. However, it was also evident that some drebrin puncta are localised outside cell nuclei. The white arrows indicate co-localisation of drebrin mRNA puncta and SYP. This co-localisation provides support for the notion that drebrin mRNA may not be exclusive to cell nuclei but may also be found in dendritic spines themselves. In light of this preliminary data, a more thorough analysis of drebrin mRNA puncta and SYP parallel localisation is required to confirm this hypothesis. Moreover, dual ISH-IHC staining using the *Dbn1* probe alongside postsynaptic markers such as PSD95 or markers for the glutamatergic AMPA and NMDA receptors, can provide further support that drebrin mRNA is also localised at dendritic spines. Nonetheless, a protocol for dual ISH-IHC was successfully optimised, providing an interesting avenue for future experiments to examine how drebrin mRNA expression is involved in dendritic spine activity, especially during important processes relating to learning and memory, such as LTP and LTD.

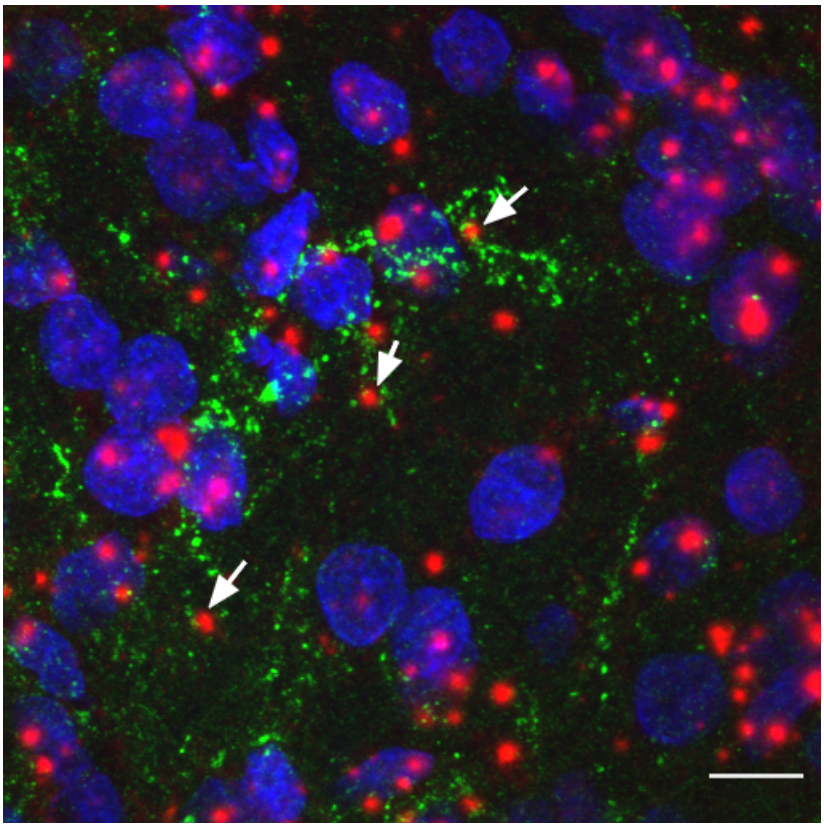

Figure 5.3.2 Representative image of a dual RNAscope® ISH-IHC test using the *Dbn1* mRNA probe (red) followed by SYP fluorescent IHC (green), with DAPI (counterstain). White arrows indicate examples where parallel localisation of drebrin mRNA puncta and SYP are evident, suggestive of drebrin localisation and transcription at dendritic spines. Scale bar = 10 µm

Finally, an analysis of drebrin mRNA expression across SERT genotype at PND14 and 60 was attempted, using the optimised RNAscope® method with the reduced AMP5 incubation time. However, due to time constraints and difficulties with mRNA puncta quantification, conducting a semi-quantitative analysis to determine the relative expression of drebrin mRNA across genotype and age was not possible. Instead, an experiment was performed to provide representative images of drebrin mRNA expression across these six groups (1 n per group), which would provide preliminary results for future RNAscope® experiments. Representative images depicting drebrin mRNA puncta in the outer layer of the cortex for each group, using fluorescent microscopy, are shown in Figure 5.3.3, compared to a negative control (Figure 5.3.4).

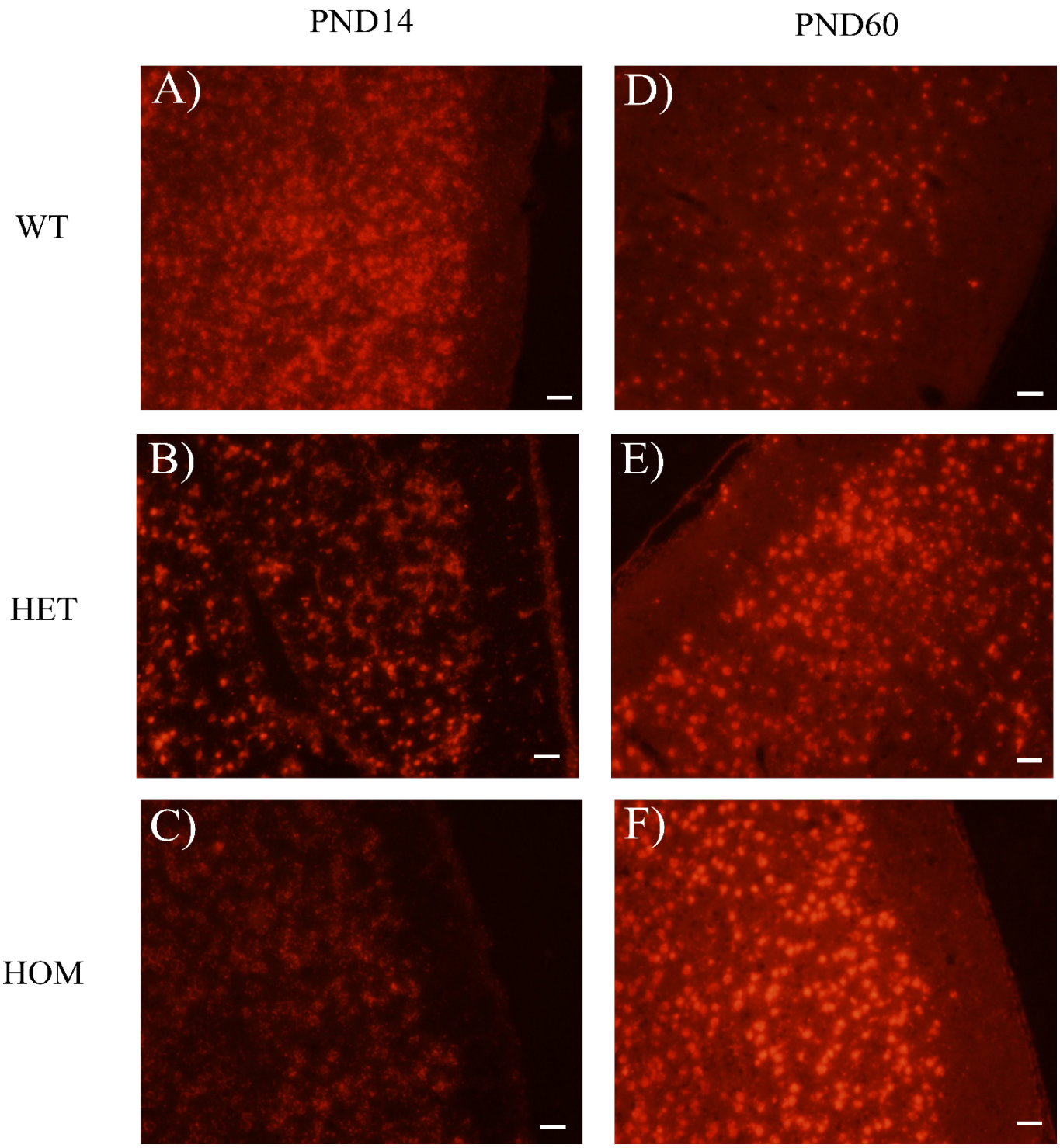

Figure 5.3.3 Representative images of drebrin mRNA expression across SERT genotype and age in the outer layer of the frontal cortex using RNAscope®. Coronal sections from PND14 animals (A-C) and PND60 (E-F) animals show differential mRNA expression across WT (A, D), HET (B, E), and HOM (C, F) genotypes for the SERT. Scale bar = 20 µm.

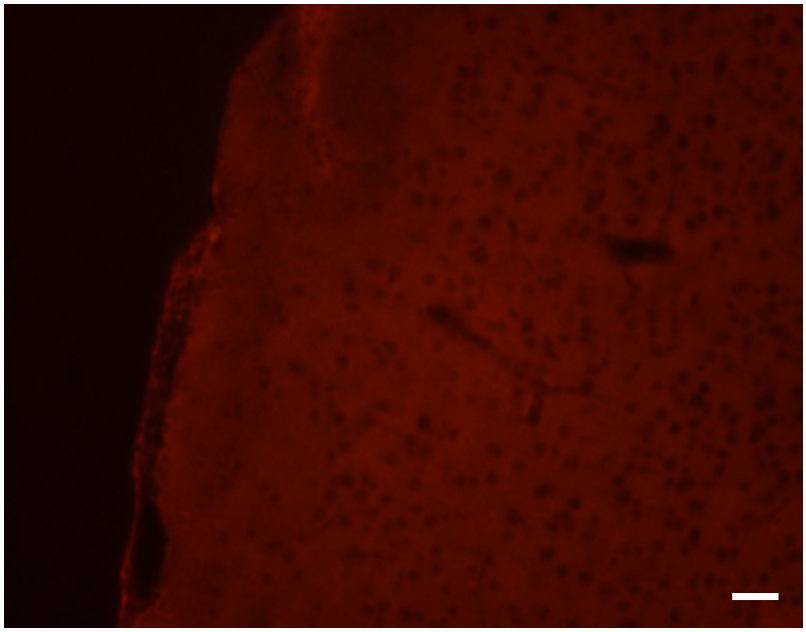

Figure 5.3.4 Negative control tissue for the final RNAscope® experiment, using *DapB* as the hybridized probe. The outer layer of the cortex is depicted, showing some level of autofluorescence but no distinct red fluorescent puncta when compared to drebrin mRNA puncta (shown in Figure 5.3.3). Scale bar = 20 µm.

Results indicated varying levels drebrin mRNA puncta across genotype and age, as evidenced by differences in fluorescent intensity across the groups. At PND14, red fluorescent intensity is greater in the WT section than the HET and HOM sections. In contrast, the adult WT section showed less fluorescent intensity compared to the adult HOM section. Because this experiment was a preliminary test, sections across the six brains may not have been taken at the same neuroanatomical location along the rostral-to-caudal plane. Therefore, the varying levels of fluorescent intensity may be due to different areas of the outer cortex layer being tested, which was not a factor controlled for in this experiment. Nonetheless, visual observation of drebrin mRNA puncta intensity across the six sections does show substantially different levels of mRNA puncta, a finding that warrants further investigation.

5.4. Discussion

The aim of this chapter was to establish and optimise a protocol for RNAscope®, a novel ISH method, to assess the expression of drebrin mRNA *in situ* using FFPE sections. A protocol for drebrin RNAscope® was successfully optimised, as well as a dual ISH-IHC protocol for examining the relationship between drebrin mRNA and synaptic proteins. Finally, preliminary results from an RNAscope® experiment examining drebrin mRNA puncta across genotype (SERT WT, HET, HOM) and age (PND14, PND60) was conducted and was suggestive of differing cortical levels of drebrin mRNA in tissue.

While a detailed, semi-quantitative, analysis of drebrin mRNA puncta across genotype and age was not possible at this time, it is interesting that visual observation suggested varying levels of fluorescent intensity for drebrin mRNA expression between the groups. All images were taken from the outer cortical layer, yet different levels of drebrin mRNA were observed between the SERT genotypes at the two timepoints. Interestingly, the observed reduction in fluorescence in SERT HET and HOM sections compared to WT at PND14 is in line with the reduced drebrin mRNA expression in HETs and HOMs found using qPCR at this same timepoint (see Chapter 3). Therefore, across two different methods, there are indications that at PND14, drebrin mRNA expression is reduced in the frontal cortex after genetic SERT reduction or deletion. A more rigorous analysis is required to substantiate this idea and extend upon the findings produced in this chapter, particularly by establishing measures to quantify drebrin mRNA puncta across the genotypes using fluorescent intensity levels.[1]

[1] It should be noted that RNAscope® quantification in brain tissue can be conducted under both brightfield [134] and fluorescent [174] microscopy RNAscope® methods. Brightfield microscopy is more suited for analysing both the expression of mRNA puncta alongside determining mRNA puncta/cell nuclei ratios, while fluorescent microscopy would allow for fluorescent intensity measures to be employed and would allow for labelling of both mRNA and fluorescently-tagged proteins using dual ISH-IHC. Therefore, these ideas for future drebrin RNAscope® experiments are based on the use of fluorescent microscopy.

Not only was an RNAscope® protocol optimised and applied to tissue from animals across SERT genotype and age, a dual ISH-IHC protocol was also established. Drebrin mRNA expression using RNAscope® was followed by immunohistochemical detection of SYP in the same section. This test proved successful and indicated that in addition to being localised in the cell body, drebrin mRNA also colocalises with the SYP protein. This parallel labelling of postsynaptic mRNA with presynaptic protein suggests that not only cell bodies but also dendritic spines are capable of drebrin mRNA synthesis. By extension, this finding would provide empirical evidence that drebrin transcription is an essential process necessary for dendritic spine activity. To speculate, it would be hypothesised that instances of LTP and spine enlargement would require more local drebrin mRNA at these semi-autonomous postsynaptic spines over and above those found in cell nuclei, compared to instances of spine maintenance or instances of LTD. Overall, the findings produced from optimising a dual ISH-IHC protocol provides interesting avenues for future research to further assess the nature of drebrin mRNA activity *in situ*.

5.4.1. Concluding Remarks

This chapter aimed to establish an RNAscope® protocol for the detection of drebrin mRNA. Such a protocol was successfully optimised, as well as one for dual ISH-IHC using drebrin mRNA and SYP at the protein level. The results from this chapter are particularly important for future research that could employ novel, yet robust, techniques such as RNAscope® to pose and answer questions about drebrin and drebrin mRNA activity that could not be addressed previously. Employing RNAscope® therefore can complement and extend upon standard laboratory techniques such as qPCR and ISH by allowing for a greater suite of hypotheses to be investigated.

CHAPTER 6. *IN VITRO* DENDRITIC SPINE ANALYSIS OF SERT KO CORTICAL NEURONS USING PRIMARY NEURONAL CULTURE

6.1. Aim and Rationale

Both qPCR and western immunoblotting in this thesis have been used to assess the mRNA and protein levels of drebrin, PSD95 and SYP across SERT genotypes. However, these methods only provide indirect indications of dendritic spine density and how this density may change after genetic SERT reduction or deletion. Therefore, it was the aim of this chapter to culture primary cortical neurons from SERT WT, HET, and HOM animals and then to assess the dendritic spine density across these genotypes using immunocytochemistry (ICC). Examining dendritic spine density *in vitro* is a common method to analyse density and morphology of dendritic spines in isolation [105, 136]. This method was employed to complement the results from the qPCR and western immunoblotting experiments by providing a comparatively more direct methodology to determine whether there are any differences in dendritic spine density across the SERT genotypes, at least in an *in vitro* system.

To the best of our knowledge, an *in vitro* analysis of dendritic spine density in ENU mutagenesis-based KO of the SERT in the rat has not been investigated previously. This *in vitro* investigation is therefore warranted to determine whether SERT KO neurons in culture mirror the effects of genetic SERT KO in tissue. While this experiment has not been conducted before, some indirect evidence is indicative that dendritic spines would be reduced in SERT KO neurons in culture. A recent study determined the dendritic spine density of WT and 5-HT_7 receptor KO neurons *in vitro* in both primary cortical neurons and primary striatal neurons from mice [137]. Dendritic spine density was carried out by 12 days *in vitro* (DIV). The authors showed that dendritic spine density was reduced in cortical and striatal 5-HT_7 receptor KO neurons relative to WT neurons. Spine density was also reduced in WT cortical and striatal

neurons after administration of a 5-HT_7 receptor antagonist. These findings indicate that the constitutive activity of the 5-HT_7 receptor is necessary for dendritic spine formation and for synaptogenesis.

Interestingly, other studies have shown that agonism of the 5-HT_{2A} receptor also reduced drebrin cluster density, and by extension dendritic spine density, in WT primary hippocampal neurons at 21 DIV [138]. At 21 DIV, dendritic spines are said to be matured [139], suggesting that overstimulation of the 5-HT_{2A} receptor results in the reduction of mature dendritic spines. Perhaps the KO of 5-HT_7 receptors as found by Speranza and colleagues [137] would result in an increased availability for 5-HT to stimulate other receptors, such as the 5-HT_{2A} receptor, thereby converging on the same effects, that being the reduction of dendritic spine density in cultured neurons. Moreover, the SERT KO model is associated with prolonged serotonergic activity in the synapse [40], suggesting that these same effects may be engendered in SERT KO neurons. Therefore, considering the reduction of PSD95 and GluN1 expression in SERT KO animals found in tissue [119], as well as these studies on 5-HT_7 and 5-HT_{2A} receptors performed *in vitro* [137, 138], it was hypothesised that there would be a reduction in dendritic spine density in cultured SERT HOM and HET cortical neurons compared to WT neurons.

6.2. Methods

6.2.1. Animals

A total of 7 WT, 7 HET and 5 HOM cultures were used for dendritic spine analysis, with the dendritic spines from a total of 29 WT, 27 HET, and 32 HOM neurons analysed for this experiment. All 19 pups came from litters across three different HET x HET breeding pairs and lived in standard housing conditions up until dissection as previously described (Section

2.1). Once the pups were removed from the dam at either PND0 or PND1, the dissection and culturing protocol was performed immediately.

6.2.2. Frontal Cortex Dissection

The primary neuronal culture protocol used in this experiment, which was a mixed culture system, was based on protocols established previously [140]. PND0-1 pups were decapitated, and their brains extracted, then placed on an ice-cold petri dish containing 0.3 ml of ice-cold dissection media. Dissections were performed using a Zeiss Stemi 305 Compact Greenough Stereo Microscope (Carl Zeiss AG; Oberkochen, Germany). First, the meninges were removed from brain. Two diagonal cuts were then made at the rostral end of the cerebellum to remove this region from the rest of the brain. Next, one cut was made along the longitudinal fissure to separate the two cerebral hemispheres. Each hemisphere was then placed lateral side down, and the cortical regions separated from the subcortical regions. The subcortical regions were then discarded while the cortical regions were collected into individual Eppendorf tubes containing 1 ml of ice-cold dissection media. All tubes were kept on ice until ready for the subsequent phase.

6.2.3. Cell dissociation and Seeding

After dissection, all subsequent steps were performed in a biohazard cabinet to ensure sterility. After the tissue settled to the bottom of the tube, 90-95% of the dissection media was removed gently with a pipette. The tissue was washed twice by adding 1 ml of fresh dissection media into the tube, waiting for the tissue to settle to the bottom of the tube, then aspirating the media.

After washing, cells were digested by adding 450 µl of fresh dissection media into the tubes with 50 µl of 2.5% trypsin, 10x (ThermoFisher Scientific, #15090046; MA, USA). Tubes were then incubated for 18-20 min at 37°C, with agitation every 5 min by tapping. The media

was removed and 500 µl of fresh dissection media was added. The tubes were then centrifuged for 5 min at 600 x g. After aspirating the supernatant, the pellet was resuspended in 500 µl of fresh dissection media. DNase I, 50 mg/ml (Roche Diagnostics, #10104159001; Mannheim, Germany), was then added to each tube and incubated for 4 min (1 mg/ml final concentration). The media was aspirated, and the tissue was washed twice in 1 ml of fresh dissection media each time. Tissue was washed twice more using 1 ml of warm plating media to inactivate the trypsin via the foetal bovine serum.

After washing, 500 µl of fresh warm plating media was added, followed by trituration approximately 15 times with a flame-constricted Pasteur pipette to break up any remaining tissue clumps. An additional 500 µl of plating media was added and the suspension was centrifuged at 600 x g for 5 min. The media was then aspirated, and the pellet resuspended in 500 µl of plating media.

A cell viability assessment was then carried out using a haemocytometer to determine cell yield, by combining the cell suspension with 0.4% trypan blue at a dilution factor of 5. Based on these counts, cells were seeded in 12-well Nunc™ Cell-Culture Treated plates (ThermoFisher Scientific, #150628; MA, USA) at a concentration of 150,000 cells/ml with plating media (2 ml total volume). Each well contained coverslips pre-treated with HistoGrip™, Concentrate (ThermoFisher Scientific, #008050; MA, USA), prepared according to the manufacturer's protocol. HistoGrip™ was used to facilitate cell adhesion to the coverslip for use in the subsequent ICC experiments. After seeding, cells were incubated for 4 hrs at 37ºC (5% CO_2). At 4 hrs, cells were examined under the microscope to ensure adequate adhesion on the substrate. Plating media was then replaced with warm Neurobasal-A maintenance media. After 24 hrs, the media was removed, and the cells were washed once with maintenance media. This was decanted, and fresh maintenance media was added into each well. The cells were then placed back into the incubator to mature for 21 days. Every 5 days the cells

were given 1/5th of the media volume with fresh maintenance media. ICC was then conducted to determine spine density in cortical neurons across all neurons across all genotypes, given that spine density accumulates until the end of three weeks *in vitro*, resulting in matured dendritic spines [139]. The components and their concentrations used to make up the dissection, plating, and maintenance media are presented in Table 6.2.1.

Table 6.2.1 Media components and concentrations used for primary neuronal culture.

Dissection Medium			
Component	Initial Concentration	Final Concentration	Volume (for 50 ml)
Hanks Buffered Saline Solution (HBSS)	10x	1x	5 ml
Sodium Pyruvate	100 mM	1 mM	0.5 ml
Penicillin Streptomycin	100x	0.5x	0.25 ml
HEPES	1 M	10 mM	0.5 ml
Glucose	20%	0.1%	0.25 ml
ddH_2O	-	-	Up to 50 ml
Plating Medium			
Component	Initial Concentration	Final Concentration	Volume (50 ml)
Glutamax	100x	1x	0.5 ml
Penicillin-Streptomycin	100x	1x	0.5 ml
Glucose	20%	0.45%	1.125 ml
Minimum Essential Medium (MEM) Vitamins	100x	1x	0. 5 ml
Foetal Bovine Serum (heat inactivated at 55ºC)	100%	10%	5 ml
Sodium Pyruvate	100 mM	1 mM	0.5 ml
MEM	-	-	Up to 50 ml
Neurobasal-A Maintenance Medium			
Component	Initial Concentration	Final Concentration	Volume (50ml)
Glutamax	100x	1x	0.5 ml
Penicillin-Streptomycin	100x	1x	0.5 ml
B-27 Supplement	50x	1x	1 ml
Neurobasal-A Medium	-	-	Up to 50 ml

6.2.4. Immunocytochemistry (ICC)

At 21 DIV, cells were removed from the incubator and the ICC protocol was conducted for dendritic spine analysis across the three SERT genotypes. Neurons were double-labelled with drebrin and microtubule-associated protein 2 (MAP2) antibodies to highlight dendritic processes (MAP2) and dendritic spine protrusions (drebrin) simultaneously. Moreover, 4′,6-diamidino-2-phenylindole (DAPI) was used as a nuclear counterstain. The triple labelling and dendritic spine analysis was based on previously established, published protocols [136, 141, 142].

First, half of the media was replaced with ice-cold 8% PFA containing 6% sucrose (4% PFA and 3% sucrose final concentration) to fix the cells onto the coverslips. Cells were fixed for 20 min at RT. The fixative was then removed, and the cells were washed 3 times with ice-cold 1x TBS for 5 min each. The TBS was then decanted, and the cells were incubated in permeabilization buffer containing 0.05% saponin for 20 min at RT. Cells were washed 3 times in 1x TBST for 5 min each, following which, were blocked for at least 1 hr in blocking buffer. The blocking buffer contained 0.3 M glycine to quench any residual aldehyde groups from the PFA fixation. Cells were then washed 3 times in 1x TBST for 5 min each.

After blocking, cells were double-labelled with anti-drebrin monoclonal and anti-MAP2 polyclonal antibodies (Table 6.2.2), diluted in blocking buffer, overnight at 4ºC. The next day, cells were washed in permeabilization buffer twice for 15 min each, then in blocking buffer for 30 min, both at RT. They were then incubated in Alexa Fluor™ 647 and Alexa Fluor™ 488 secondary antibodies diluted in blocking buffer for 2 hrs at RT (Table 6.2.2). The plates containing these cells were kept protected from light during the secondary antibody incubation and for all subsequent steps. Finally, the cells were washed in permeabilization buffer three times for 10 min each. Coverslips were then mounted onto LabServ frosted microscope slides (ThermoFisher Scientific, LBS2951RC; MA, USA)

containing ProLong™ Gold Antifade Reagent with DAPI (ThermoFisher Scientific, P36934; MA, USA) and were allowed to cure for at least 24 hrs before imaging. All incubations were conducted on an orbital shaker. Table 6.2.3 provides component and concentration information for all buffers and solutions used in the ICC experiments.

Table 6.2.2 Primary and secondary antibodies information used for immunocytochemistry dendritic spine analysis.

Primary Antibodies			
Marker (clone)	Antibody Raised in	Antibody Dilution	Manufacturer (Code)
Drebrin (M2F6)	Mouse	1:500	Invitrogen (MA1-20377)
MAP2	Chicken	1:5000	Abcam (ab5392)
Secondary Antibodies			
Secondary Antibody	Host x Raised Against	Antibody Dilution	Manufacturer (Code)
Alexa Fluor™ 647	Donkey x Mouse	1:1000	Invitrogen (A31571)
Alexa Fluor™ 488	Goat x Chicken	1:1000	Invitrogen (A11039)

Table 6.2.3 Buffer components and concentrations used for ICC dendritic spine analysis on primary neuronal cultures.

Fixative Solution			
Component	Initial Concentration	Mass/Volume (for 20 ml)	Final Concentration
PFA	8%	1.6 g	4%
Sucrose	6%	1.4 g	3%
Dulbecco's PBS	-	20ml	

** Add 1ml of fixative solution to cells containing 1ml of neurobasal media for final concentration of 4% PFA and 3% sucrose*

Permeabilization Buffer/Wash Buffer			
Component	Initial Concentration	Final Concentration	Volume (50 ml)
Saponin	1%	0.05%	2.5
TBST	-	1x	Up to 50 ml

Blocking Buffer			
Component	Initial Concentration	Final Concentration	Volume (50 ml)
BSA	5%	1%	10 ml
Saponin	1%	0.05%	5 ml
Glycine	1 M	0.3 M	15 ml
TBST	-	1x	Up to 50 ml

6.2.5. Dendritic Spine Analysis Methodology

Confocal images of primary cortical neuronal cultures co-labelled with MAP2 and drebrin were taken using a systematic random sampling approach on an Olympus FLUOVIEW FV3000 Confocal Laser Scanning Microscope (Olympus Corporation; Tokyo, Japan). Image acquisition and analysis was conducted on the Olympus FV31S-ST software (version 2.3). To establish an unbiased image acquisition approach, a 10x10 grid was created around the centre of the coverslip using the UPLXAPO 0.4NA 10x objective and the mapping feature on the FV31S-ST software. An image of each square in the grid was acquired, then each square was stitched together to create an entire sampling area (Figure 6.2.1). It was ensured that the 10x10 grid was large enough to capture most of the coverslip but also to avoid having multiple squares within the grid fall outside of the coverslip.

A random number between 1 and 10 was then generated for each coverslip, which was designated as the first square to be sampled on the first row of the 10x10 grid. Next, a second random number between 8 and 12 (where $8 \leq n \leq 12$, $n \neq 10$)[2] was generated. This number designated the sample pitch, such that every *n*th square was sampled from the starting square until the end of the grid was reached. An interval between 8 and 12 was chosen as this would allow for adequate random sampling of each coverslip and would avoid introducing an over- or under- sampling bias for cultured neurons of a single genotype.

Within each square, Z-stack images of neurons were captured using UPLXAPO 60x 1.42NA or UPLXAPO 100x 1.42NA oil objectives (step size = 0.41μm) at 640x640 or 800x800 pixel resolution. Only neurons adhering to predetermined criteria were used for dendritic spine density analysis. Criteria were as follows:

- Neurons must be DAPI and MAP2 positive.
- Neurons must have tertiary dendrites and be drebrin positive.
- Tertiary dendrites used for dendritic spine analysis must be at least 20-30 μm away from the cell nucleus.
- Dendritic pathways for each neuron should be discernible; neurons in highly-clustered areas should be avoided.

Once imaging was complete, dendritic spines along a 20 μm section of a tertiary dendrite for each neuron that adhered to these criteria were counted (one 20 μm length of dendrite per neuron). A representative image of this is displayed in Figure 6.2.2. Dendritic spines from at least three neurons per coverslip (or pup) were counted and averaged across genotype.

[2] *n* = sample pitch. Note that 10 was avoided as a sample pitch as this would mean only squares aligning in a single column were sampled, thereby not being representative of the entire 10x10 grid.

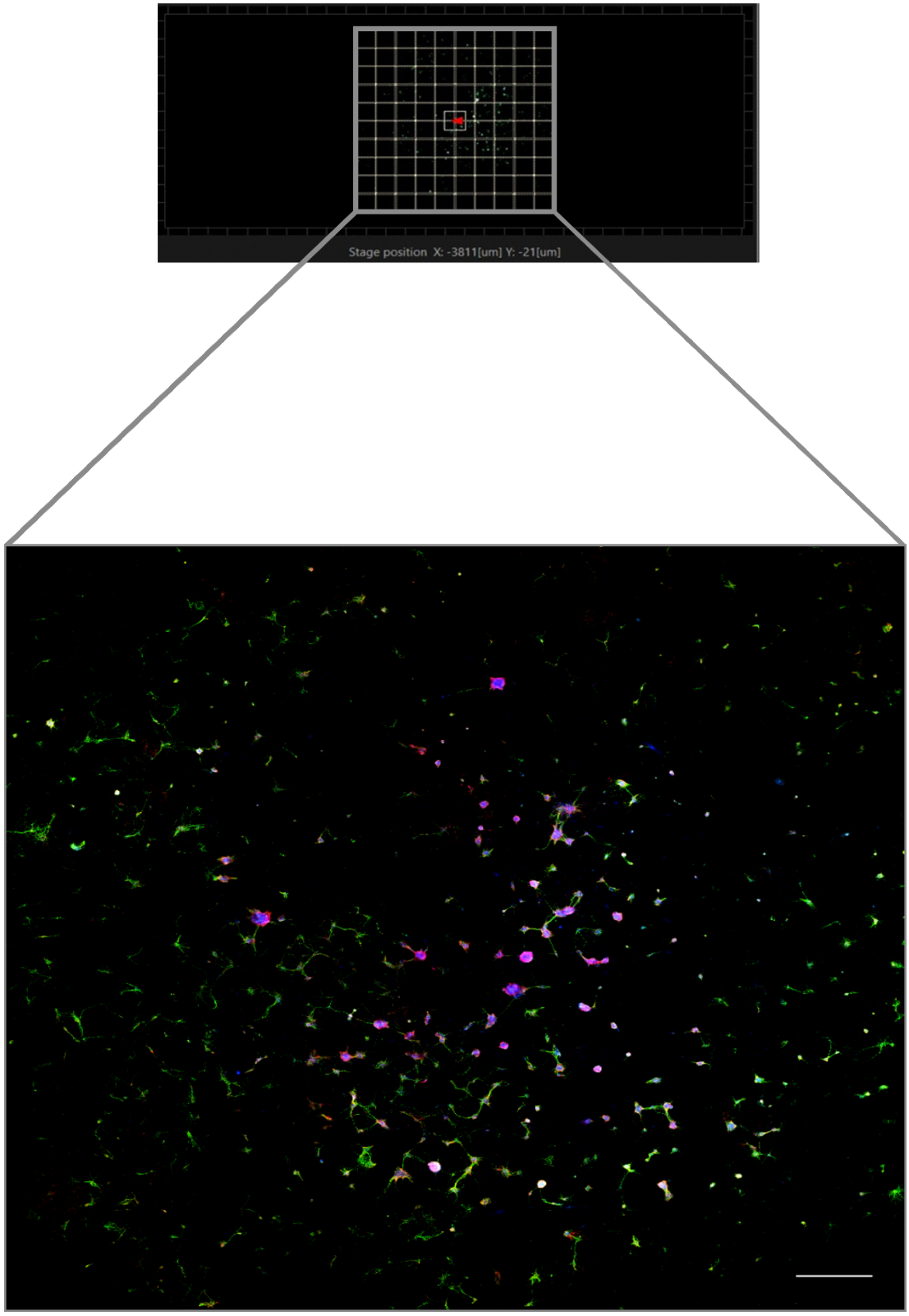

Figure 6.2.1 Method for systematic random sampling of neurons for dendritic spine analysis. Top: a 10x10 grid was produced around the centre of the coverslip using the 10x objective. Bottom: images of each square in the grid were stitched together to produce an image of the entire area for imaging and sampling. Scale bar = 1000 µm.

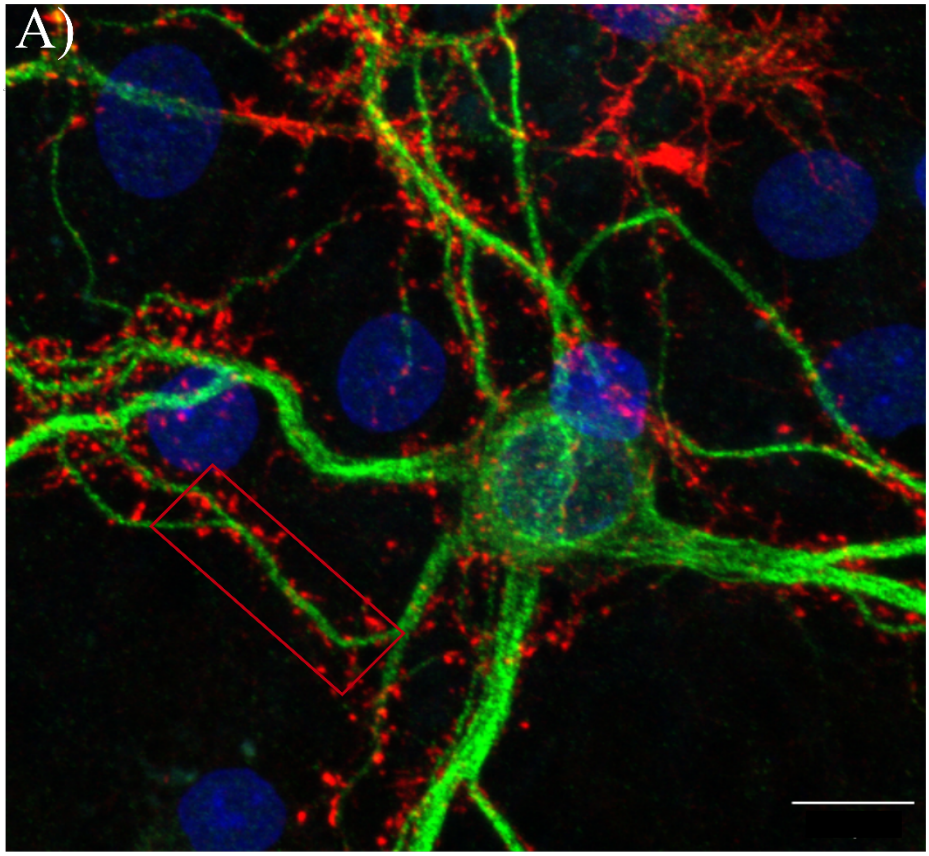

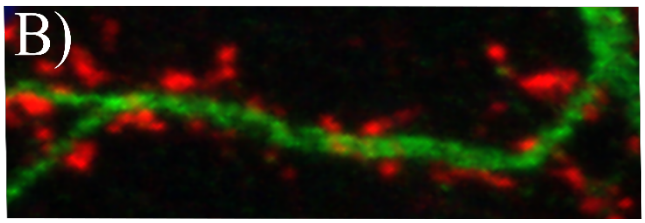

Figure 6.2.2 Method employed for dendritic spine density analysis for SERT WT, HET, and HOM cortical neurons. A) a neuron adhering to the imaging criteria and within a sample square was imaged. B) Magnified image of the rectangular area in A. Dendritic spines (as red protrusions) along a 20 µm section from a tertiary dendrite were counted. Scale bar = 10 µm.

Finally, to determine the dendritic spine density of SERT WT, HET and HOM cortical neurons, the dendritic spine counts for each neuron of each genotype was converted into a single dendritic spine density measurement, spines/20 µm, such that:

$$Dendritic\ Spine\ Density = \Sigma_{spines\ per\ 20\ \mu m\ dendrite}$$

Next, dendritic spine density of SERT HET and HOM neurons were calculated relative to the density of WT neurons. The average dendritic spine density for HET and HOM neurons was then calculated by converting these relative values into a percentage:

$$Density\ Relative\ to\ WT = \frac{Dendritic\ Spine\ Density_{HET/HOM}}{Dendritic\ Spine\ Density_{\bar{X}_{WT}}}$$

$$Percent\ Density\ to\ WT = \bar{X}_{Density\ Relative\ to\ WT} * 100$$

6.3. Results

Representative images of the DAPI, MAP2, and drebrin staining of neurons from across the three SERT genotypes are displayed in Figure 6.3.1. A one-way ANOVA was conducted to determine whether dendritic spine density in SERT HET and HOM neurons differed to the dendritic spine density of WT neurons, first using spines/20 µm, followed by the percent dendritic spine density relative to WT (Figure 6.3.2). For both spines/20 µm and percent density to WT, Levene's test of homogeneity was assumed across the three genotype groups (p = .127). The one-way ANOVA showed a significant difference in dendritic spine density across WT, HET, and HOM genotypes for both measures, $F(2, 85) = 61.94$, $p < .001$.

Follow-up Tukey post-hocs indicated that WT neurons (M = 13.86 spines/20 µm, SD = 3.42; M = 100%, SD = 0.24) significantly expressed an average 35% more dendritic spines than HET neurons (M = 9.07 spines/20 µm, SD = 3.17; M = 65.5%, SD = 0.23), $p < .001$. WT neurons also significantly expressed an average of 62% more dendritic spines than HOM neurons (M = 5.31 spines/20 µm, SD = 2.38; M = 38.3%, SD = 0.17), $p < .001$. Finally, neurons from HET animals expressed an average of 27% more dendritic spines than HOM animals, $p < .001$.

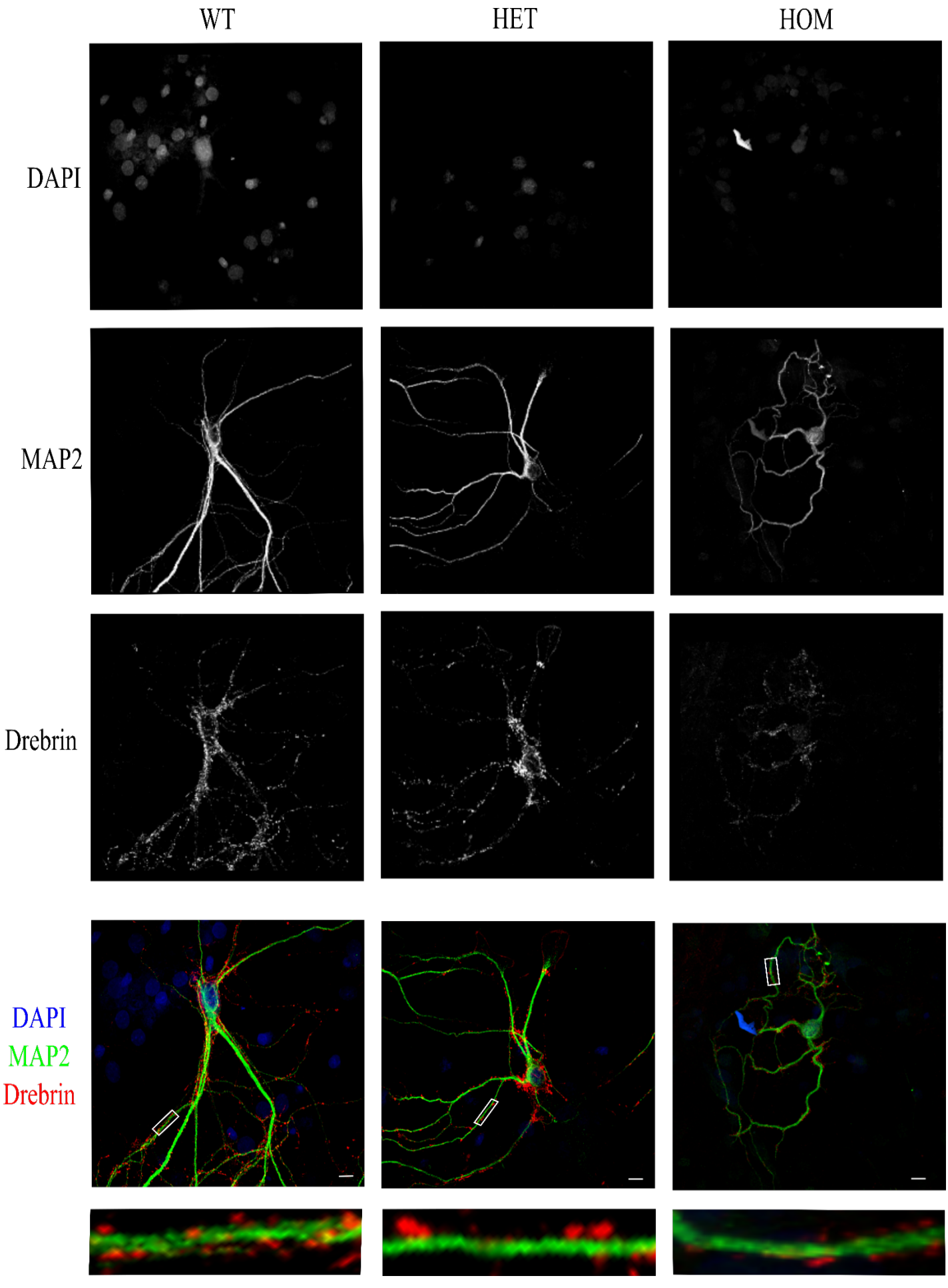
WT
HET
HOM
DAPI
MAP2
Drebrin
DAPI
MAP2
Drebrin

Figure 6.3.1 Representative images of cultured cortical neurons stained with MAP2 (green), drebrin (red), and DAPI (blue) across SERT genotypes. The boxed area in the colourised image corresponds to a 20 μm dendritic spine section used for dendritic spine analysis for each genotype, with a magnified image of this area shown underneath. Scale bar = 10 μm.

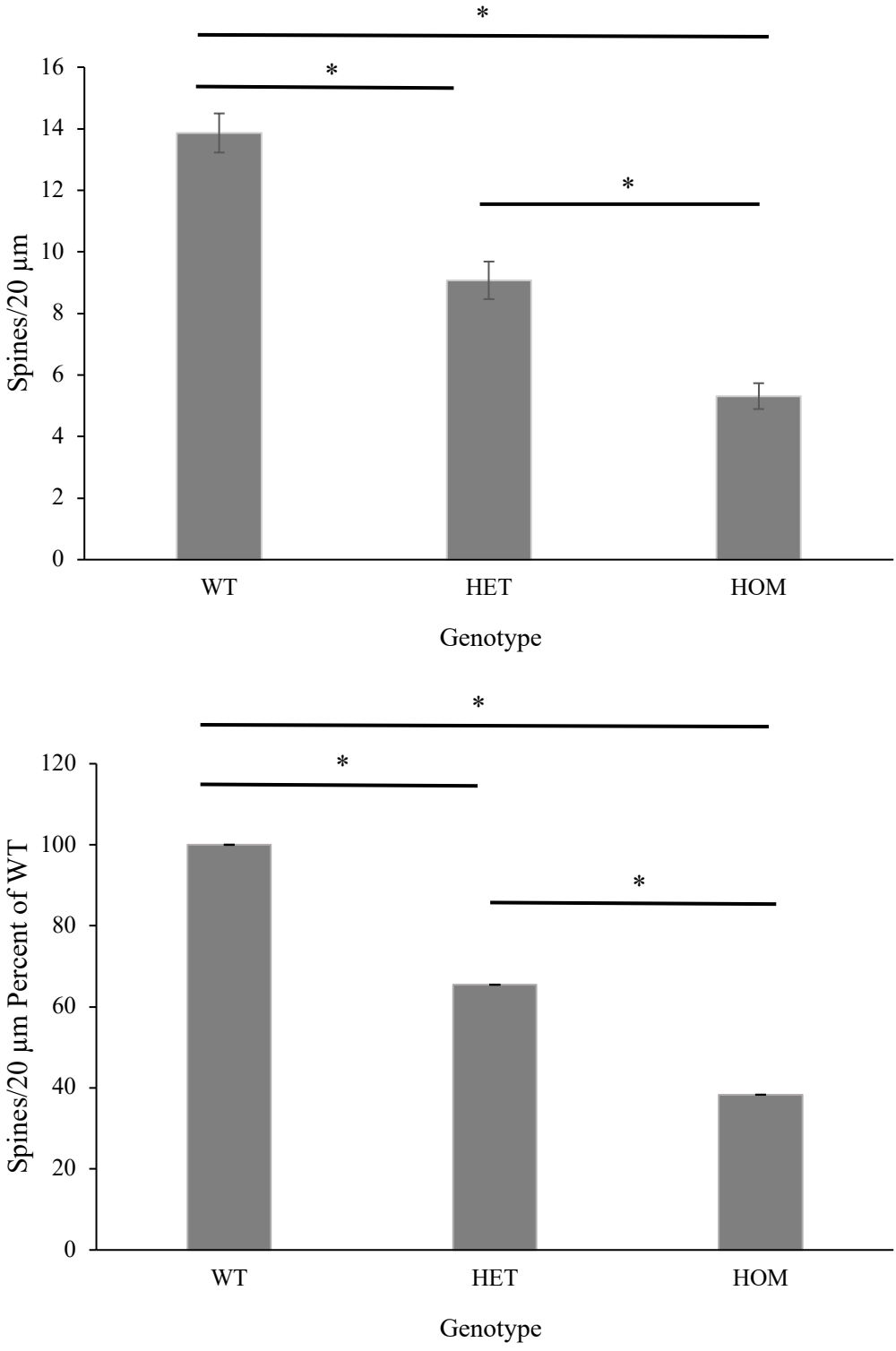

Figure 6.3.2 Average dendritic spine density across SERT WT, HET, and HOM neurons *in vitro*, counted from a total of 29 WT, 27 HET, and 32 HOM neurons (one 20 µm length of dendrite per neuron). Top: data presented as spines/20 µm. Bottom: data presented as percent density relative to WT. * $p < .001$. Error bars indicate ± SEM.

6.4. Discussion

The aim of this chapter was to culture primary cortical neurons from SERT WT, HET, and HOM PND0-1 pups and to use ICC to assess the dendritic spine density of neurons from across these SERT genotypes. It was hypothesised that SERT HET and HOM neurons would have reduced dendritic spine density in cultured cortical neurons compared to WT neurons, using MAP2 co-labelled with drebrin. This hypothesis was supported, as the results showed graded effects of SERT genetic reduction and deletion on dendritic spine density. Specifically, SERT reduction (HETs) resulted in the reduced expression of dendritic spines along tertiary dendrites compared to WT, and SERT deletion (HOMs) showed an even greater reduction in dendritic spine density compared to both HET and WT.

The graded reduction in dendritic spine density after SERT reduction and deletion suggests that SERT activity is required for spinogenesis and synaptogenesis at glutamatergic synapses. No studies have been conducted to determine the effects of genetic SERT deletion on dendritic spine formation and maturation *in vitro*. However, evidence using indirect methodologies, such as PSD95 and GluN1 protein and mRNA expression in tissue [119], do align with the results found in this experiment. Both PSD95 and GluN1 were reduced in the PFC of SERT HOMs during development and at adulthood, which provides indirect support for a reduction in dendritic spines in these animals. Whether this reduction is related to reduced density or morphology, or both, cannot be confirmed using these indirect measures. However, at least in an *in vitro* system using MAP2 and drebrin co-labelling, a comparatively more direct method, the results from the current experiment suggests that SERT HOM neurons display a reduction in dendritic spine density.

These results align with the finding that drebrin clustering was reduced after five min of 5-HT_{2A} agonism in WT hippocampal cultures at 21 DIV [138]. The 5-HT_{2A} receptor is also highly abundant in the cortex [143]. To speculate, it may be that the nine-fold increase in

extracellular 5-HT in SERT HOM cortical cultures may result in greater 5-HT_{2A} receptor activation. This activation would lead onto the reduction of dendritic spine densities in these HOM neurons as shown in this experiment, because the increase in extracellular 5-HT enhances the activation of postsynaptic 5-HT receptors, thereby resulting in overstimulation of these receptors [48].

To add to this, the reduced dendritic spine density found in 5-HT_7 KO cortical and striatal neurons compared to WT neurons [137], may also be converging on these mechanisms. For example, the KO of the 5-HT_7 receptor would allow for greater activation of other 5-HT receptors, such as the 5-HT_{2A} receptor, which would in turn result in the same reduction in drebrin clustering in dendritic spines observed after 5-HT_{2A} receptor agonism. The mechanisms with which changes to the 5-HT system *in vitro* can result in abnormal spinogenesis and changes to dendritic spine density can only be speculated here. Further *in vitro* experiments are required to elucidate the mechanisms with which serotonergic activity, and especially the SERT, influence dendritic spine density, and whether these mechanisms do converge on 5-HT_{2A} receptor activation as the converging evidence may suggest.

6.4.1. Concluding Remarks

Overall, the results from this ICC experiment showed that dendritic spine density of cortical neurons is directly associated with the severity of genetic SERT ablation *in vitro*. The reduced dendritic spine density along tertiary dendrites in SERT HET and HOM neurons, compared to WT, suggests that SERT activity is required for the development and genesis of synapses and dendritic spines. These results indicate that, at least in an *in vitro* mixed culture system, the SERT regulates glutamatergic excitatory transmission at the level of synaptogenesis and spinogenesis. Whether the mechanisms with which the SERT exerts this regulation is direct or indirect is yet to be determined, but the present results provide novel

insight into how SERT activity may influence dendritic spine formation and development *in vitro*.

CHAPTER 7. GENERAL DISCUSSION

7.1. Thesis Overview

7.1.1. Research Aims

The aim of this thesis was to determine the influence of genetic SERT deletion on drebrin A expression as a marker of dendritic spines in the frontal cortex of SERT KO rats. Given that this animal model has been used to understand the behavioural and molecular bases of various neuropsychiatric disorders, of which many display aberrations in synaptic plasticity, this thesis investigated the efficacy of the SERT KO model in mirroring these abnormalities at the synapse using both tissue-based and *in vitro* methodologies. Specifically, the experiments in this thesis explored the hypothesis that SERT KO animals would show reduced mRNA and protein expression for drebrin, PSD95 and SYP at PND14 and PND60, and would have reduced dendritic spine density in tertiary dendrites of cortical neurons *in vitro*, relative to WT animals.

7.1.2. Research Outcomes

Overall, the results indicated partial support for this hypothesis. The most salient findings suggested that mRNA expression of drebrin, PSD95 and SYP in the frontal cortex was reduced in SERT HET and HOM animals relative to WT, but only at PND14. This was mirrored at the functional level by the finding that HETs and HOMs expressed less than half the amount of presynaptic SYP protein expression relative to WT animals, also at PND14. Importantly, these observed reductions at both the mRNA and protein levels were absent by PND60, such that HETs and HOMs no longer differed from WTs at adulthood. Over time, it was evident that mRNA expression for drebrin, PSD95 and SYP, and protein expression for SYP, in SERT KO animals increased so that the observed reductions at PND14 were resolved by PND60. In addition, a comparatively more direct analysis of dendritic spine density in SERT

KO neurons, primary neuronal culture and ICC, showed that dendritic spine density was reduced in HET and HOM neurons compared to WT neurons. By using drebrin-labelled puncta to identify dendritic spines on MAP2-labelled dendrites, it was found that SERT HOM cortical neurons expressed almost two-thirds less dendritic spines compared to WT neurons. Finally, an RNAscope® protocol for the detection of drebrin mRNA *in situ* was established and optimised. Preliminary experiments using RNAscope® corroborated the reduced drebrin mRNA expression in SERT HET and HOM animals at PND14 identified using qPCR and indicated that drebrin mRNA transcription can occur at synapses, as well as in cell bodies, thereby offering interesting avenues for future research.

7.2. Relation of Thesis Outcomes to Literature

As stated previously, the reduction among drebrin, PSD95 and SYP at the mRNA and protein levels in HET and HOM animals occurring only at PND14 is indicative of a developmental delay in synaptogenesis among these animals, with findings from both the qPCR and western immunoblotting experiments suggesting that these abnormalities are resolved by adulthood. Indeed, Brivio and colleagues found similar synaptic marker aberrations in the PFC of HOM animals [119]. Specifically, they showed that PSD95 mRNA and protein expression in the PFC was reduced in HOM animals at PND21. GluN1 mRNA and protein expression was also reduced at this timepoint. Previous reports show that drebrin A is required for PSD95 accumulation in dendritic spines [102]. Moreover, the application of an NMDA antagonist in the cortex of WT mice increased the expression of the NMDA receptor 2A subunit, an effect not observed in DAKO mice [110]. Thus, the accumulation of NMDA receptors and PSD95 are both dependent on postsynaptic drebrin A expression. Considering the results by Brivio and colleagues, these findings would suggest that drebrin A mRNA and protein expression would also likely be reduced in the PFC of SERT HOM rats at PND21. In this way, the trend of a downregulation of drebrin and PSD95 mRNA at PND14 observed in

this thesis is consistent with these previous findings on the relationships between drebrin, PSD95 and NMDA receptor subunit expression. Moreover, this evidence suggests that synaptic organisation is closely regulated, such that abnormalities observed on the spine surface are indicative of abnormalities occurring at the submembranous regions, including the PSD and the actin cytoskeleton, and vice versa. Based on this close regulation of synaptic organisation, it is unsurprising that PSD95 and drebrin mRNA expression were found to be correlated at PND14 and PND60 in this thesis.

Interestingly, this thesis extends upon the results from Brivio and colleagues by showing that synaptic abnormalities during development in SERT HOM animals also exist at presynaptic terminals. Both mRNA and protein expression for SYP was reduced in the frontal cortex of HOMs, indicating aberrant neurotransmitter vesicular transport in these animals. These findings complement reports that SYP is affected by changes in 5-HT availability in adults. Tryptophan hydroxylase inhibition via para-chloroamphetamine has been shown to reduce SYP expression in areas including the hippocampus in adult rats [133]. Because tryptophan hydroxylase is an enzyme involved in the serotonergic synthesis pathway, inhibition of this enzyme reduces 5-HT synthesis and neurotransmission. Stimulation of the 5-HT_{1A} receptor led to a recovery of SYP expression in these brain regions, indicating that SYP expression is influenced by homeostatic changes to 5-HT neurotransmission at adulthood.

Intriguingly, the inverse relationship between 5-HT and SYP expression was found in this thesis. Whereas the inhibition of 5-HT synthesis and neurotransmission led to the reduction of SYP at adulthood [133], this same reduction in SYP is evident in SERT HOM animals during development, who exhibit a nine-fold increase in extracellular 5-HT [40]. These contrasting results may be due to differences in the timing of the manipulation of 5-HT neurotransmission [144]. For example, SSRI treatment during the pre-adolescent period in murine models impaired serotonergic activity in the raphe nuclei, the location of 5-HT cell bodies, which was

an effect that persisted into adulthood [145]. In SERT KO mice, developmental plasticity of the somatosensory cortex is also reduced during postnatal development, such that genetic deletion of the SERT results in the abnormal innervation and organisation of thalamocortical axons into the somatosensory cortex [146]. This same effect was found *in vivo* in PND2-5 pups after intraperitoneal administration of citalopram, an SSRI [147]. Moreover, in 5-HT_{1A} receptor KO mice, greater extracellular 5-HT via 5-HT_{1A} autoreceptor inhibition during development resulted in anxious and depressive phenotypes that lasted into adulthood [148]. An attempt at 5-HT_{1A} autoreceptor gene rescue in these animals could not resolve these depressive phenotypes during adulthood [144, 148]. As well, pharmacological blockade of the 5-HT_{1A} receptor during PND13-34, but not during adulthood, mimicked the effects of 5-HT_{1A} KO mice, thereby showing that many of these effects only occur when 5-HT homeostasis is disrupted during specific periods of development [148].

Overall, it is clear there are periods of development where homeostatic 5-HT activity and neurotransmission are critical [145, 149]. The disruption of this homeostatic activity during the pre-weaning phase, especially via higher extracellular serotonergic presence through genetic and pharmacological SERT or 5-HT_{1A} receptor inhibition, can have lasting consequences on both behaviour and the structural circuitry within the brain. Indeed, this notion that increased extracellular 5-HT during a critical window of development can result in abnormalities in brain connectivity and structure has been postulated previously [34]. Based on these findings, the reduction in SYP protein expression at PND14 in SERT HOM and HET animals is likely due to the increased extracellular presence of 5-HT in these animals above homeostatic levels. Because extracellular 5-HT homeostasis is regulated by the SERT [146], it is unsurprising that SERT deletion in HOM animals would disrupt serotonergic homeostasis and lead to abnormalities in the development of presynaptic terminals. The functional consequences of a reduction in SYP expression would result in reduced vesicular trafficking

and exocytosis in the frontal cortex, and therefore weaker synaptic connections. This would be in line with the abnormal axonal projections of thalamocortical neurons onto the somatosensory cortex found in SERT KO mice previously [146], suggesting that this reduction in SYP in SERT HOM rats may not be exclusive to the frontal cortex but extends to multiple brain regions.

The reduction in drebrin, PSD95 and SYP mRNA and protein expression in SERT KO animals during development is therefore consistent with these findings that changes to 5-HT neurotransmission during the critical postnatal period disrupts molecular and structural systems in the brains of these animals. Indeed, 5-HT is known to be a neuromodulator of varying processes in neuronal development, including neuronal migration and cellular architecture [34], highlighting the crucial role this neurotransmitter possesses during neurodevelopment. For example, embryonic blocking of 5-HT synthesis results in the inhibition of dendritic arborization of pyramidal neurons, leading onto abnormal pyramidal neuron development and maturation [150]. Moreover, elevated extracellular 5-HT *in vivo* has been shown to reduce the embryonic migration of interneurons in cortical slices, an effect mediated by the 5-HT_6 receptor [151], as well as reducing serotonergic neurite growth from the raphe nuclei to the mPFC [152]. This finding of abnormal interneuron migration in the cerebral cortex was also replicated in SERT KO mice [151], suggesting that excessive levels of extracellular 5-HT can influence cell migration in the cortex [34]. Related to this effect on neuronal morphology, SERT KO mice exhibit a thinner cortical layer IV at adulthood than control mice [153], indicating the extensive effects of genetic SERT deletion on cortical structure. Comparatively, at the human level, grey matter volumes are reduced in individuals who express the S allele of the 5-HTTLPR [154]. Overall, these findings support the notion that during neurodevelopment, serotonin is necessary for normal cellular organisation of the cerebral cortex [150]. Based on this evidence, genetic SERT deletion in the SERT KO rat model, and its resultant increase in extracellular 5-HT,

would impact on this typical organisation in the cerebral cortex, thereby leading onto the developmental reductions in the mRNA and protein levels of the synaptic markers observed in this thesis.

Given serotonin's involvement in both neuromodulation and the organisation of the cerebral cortex during development, it is unsurprising that this neurotransmitter system also modulates the excitatory glutamatergic system [144, 155]. Extracellular 5-HT shows preferential modulation towards activity of both excitatory and inhibitory synapses [144], and serotonergic modulation of the excitatory glutamatergic system in particular can occur at both pre- and post- synaptic sites [155]. At post-synaptic sites, 5-HT activity in the hippocampus blocks the activation of NMDA and AMPA receptors, and therefore suppresses LTP induction [156]. Given that LTP is associated with increased spine size [71], LTP suppression would affect the regulation of dendritic spine morphology, in turn impacting learning and memory systems. Stimulation of hippocampal 5-HT_1 receptors [157], and hippocampal and cortical 5-HT_6 receptors [158], have been shown to mediate these effects. Interestingly, these same receptor subtypes have been shown to mediate the effects of extracellular 5-HT on cortical development as stated previously.

In contrast, 5-HT_{2A} agonism in the hippocampus enhances presynaptic neurotransmission of glutamate onto the dorsolateral septal nucleus *in vivo* [159]. Related to this, *in vitro* agonism of the 5-HT_{2A} receptor for 15 min reduces F-actin and drebrin clustering in mature hippocampal neurons [138]. Given that glutamate-mediated overstimulation of the NMDA receptor can reduce dendritic spine size via LTD [77], these results may indicate a convergent mechanism of action for the 5-HT_{2A} receptor on influencing glutamatergic activity across both pre- and post- synaptic sites, an effect which may be enhanced after excessive 5-HT_{2A} activation.

Overall, these studies indicate that increased activation of postsynaptic 5-HT receptors can modulate glutamatergic neurotransmission, and that both activation and inhibition of these receptors can lead to reduced synaptic activity via changes to glutamatergic signalling. To speculate, the nine-fold increase in extracellular 5-HT in the SERT KO model, which would enhance serotonergic receptor activation [48], could be increasing glutamatergic neurotransmission via heightened serotonergic receptor activity, particularly the 5-HT_{2A} receptor. This excessive extracellular 5-HT could in turn influence the regulation of synaptic markers at both the mRNA and protein levels as observed in this thesis. If so, the influence of 5-HT_{2A} receptor activity on the glutamatergic system and on dendritic spine density may also expound, at least in part, the reduced spine density along SERT HOM tertiary dendrites found *in vitro* in this thesis.

Indeed, these speculated effects may only be evident during the critical postnatal window where excessive extracellular 5-HT also has major effects on cortical organisation and connectivity and where 5-HT receptors have not been downregulated yet despite excessive extracellular 5-HT presence. However, as observed in this thesis, the reduced mRNA expression of drebrin, PSD95 and SYP, and the reduced protein expression of SYP in SERT KO animals, at PND14 wanes by adulthood. The serotonin system is known to have two distinct roles in the CNS [8]. During development the serotonergic system acts as a neuromodulator and therefore influences other neurotransmitter systems, whereas once brain maturity has been reached, serotonin assumes the role of a neurotransmitter [8]. These two distinct roles may expound how alterations in synaptic markers found in this thesis in SERT KO animals is limited to the developmental period, at least in the frontal cortex. Perhaps an increase in extracellular 5-HT in the SERT KO model affects synaptic marker mRNA and protein expression insofar as the serotonin system acts as a neuromodulator on the

glutamatergic system, an effect which may be overridden once the 5-HT system assumes the role of a neurotransmitter.

Indeed, the downregulation of PSD95 and GluN1 mRNA and protein expression in the PFC of SERT HOMs compared to WT is also greater during development than at adulthood [119]. Not only this, but the reduced mRNA levels found during PND21 in these animals for PSD95 were abolished by PND100 [119]. Therefore, the emerging pattern from this thesis and from previous findings is that excessive extracellular 5-HT in SERT KO animals affects glutamatergic and dendritic spine marker expression more substantially during development than at adulthood, coinciding with serotonin's role as a neuromodulator of excitatory neurotransmission.

Interestingly, while serotonin's modulatory role in neuronal migration, wiring and cortical organisation ceases by adulthood [8], research suggests that even in adulthood, the 5-HT system is involved in adult neurogenesis [8, 160]. To speculate, it may be that the serotonin-mediated neurogenesis occurring as SERT KO animals reach adulthood, and the reduced activity of the serotonergic system as a neuromodulator, may be happening simultaneously. In this way, excessive extracellular 5-HT observed in SERT KO adults would no longer be impinging on glutamatergic synapses and on excitatory neurotransmission. As a result, the reduced mRNA expression of PSD95 and drebrin, and the mRNA and protein expression of SYP, among SERT KO animals would be absolved by adulthood. However, this theory is only speculative, and it is likely a simplified explanation of the mechanisms that may be occurring in the brains of these animals underlying the resolution of this developmentally-regulated synaptic dysfunction. Hence, future research is required to fully elucidate the mechanisms governing the resolution of synaptic marker dysfunction by the time adulthood is reached.

Another salient finding from this thesis was that *in vitro*, SERT HET neurons express one third less, and SERT HOM express nearly two thirds less, dendritic spines than WT cortical neurons. To our knowledge, this is the first instance in which primary cortical neurons from across the SERT genotypes have been cultured, and the first to show that HET and HOM neurons display a substantial reduction in dendritic spine density along tertiary dendrites. Previous reports show that at 21 DIV, dendritic spines along hippocampal neurons have reached maturity and peak density, but that spine density begins to decrease at 28 DIV [139]. Therefore, the primary cortical neurons in this thesis were fixed at 21 DIV to ensure that the dendritic spine analysis was conducted when spines have reached maturity. Moreover, neurons at 21 DIV are chronologically similar to PND21 neurons *in vivo* [139], and findings from mouse cultured cortical neurons show that the timing of synaptogenesis *in vitro* coincides with the timing as observed *in vivo* [161]. While comparisons between *in vitro* and *in vivo* experiments are encouraged because they provide a more holistic framework to understanding neuronal function and behaviour, there are substantial differences between the isolated *in vitro* environment and the *in situ* native brain state [162]. Neurons in culture are cultivated in an environment where the typical maturation and growth processes, as well as nutrient conditions, vary from those in the native state *in situ* [139]. It is also important to note that dendritic spines are more densely packed in the native environment than in culture [139]. For example, dendritic spines in hippocampal neurons at 21 DIV, where peak density has been reached, are only one third dense than those found using Golgi-Cox staining in the native brain state in adult hippocampal neurons [163]. One of the main reasons for these differences would be that the native brain state constitutes a complex, three-dimensional structure while the *in vitro* state is a two-dimensional artificial culture system.

Nonetheless, Belle and colleagues emphasise that despite the inherent differences between these two systems, similar patterns or trends of neural behaviour and response should

be expected [162]. From this perspective, the *in vivo* reduction of mRNA expression of drebrin, PSD95 and SYP, and reduction of SYP protein expression, in the frontal cortex at PND14 is akin to the reduced dendritic spine density of SERT KO neurons found *in vitro* at 21 DIV. Therefore, a reduction in SYP protein expression *in vivo* at PND14 is indicative of reduced synaptogenesis, which is mirrored by the reduced dendritic spine densities found *in vitro* along SERT HET and HOM dendrites at 21 DIV, and vice versa. While a directly proportional relationship between these two systems may not exist, it is clear by using both indirect (*in vivo*) and direct (*in vitro*) methodologies in this thesis, that SERT reduction and deletion results in developmentally-regulated changes to glutamatergic synapses and dendritic spines in the frontal cortex.

Taken together, the results from this thesis validate the use of this *in vitro* culture system to understand the molecular changes associated with genetic SERT deletion, given that the *in vitro* dendritic spine analysis aligns with findings suggested by the *in vivo* qPCR and western blot analyses. Therefore, future experiments can successfully employ primary cortical cultures of SERT KO to determine the consequences of genetic SERT ablation, and how this may be different between SERT reduction and deletion compared to SERT WT. Such investigations will be able to further characterise the molecular and cellular mechanisms underlying the phenotypical changes in this SERT KO model and elucidate the efficacy of this animal model in mimicking the cellular and molecular changes of various neuropsychiatric diseases.

7.3. Implications for Neuropsychiatric Disorders

7.3.1. Major Depressive Disorder

The findings from this thesis parallel the synaptic alterations observed in MDD, thereby providing further validation of the SERT KO model in mimicking the neurological effects underlying this disorder. As stated previously, BDNF expression in humans is reduced after

chronic and acute stress [52], and is also reduced in the SERT KO model in both HET and HOM adults [164]. Findings demonstrate that this same neurotrophic factor is important for the strengthening of synaptic connectivity, and has been shown to positively regulate the cytoskeletal architecture of dendritic spines of cortical and hippocampal neurons *in vitro* [165]. Moreover, BDNF expression is necessary for the maintenance of mature dendritic spines of excitatory synapses, with reduced BDNF expression resulting in reduced dendritic spine density [165].

Therefore, the reduction in spine density of cortical SERT HET and HOM neurons found in this thesis is consistent with this convergent evidence on the role of BDNF expression in MDD. In this way, if BDNF expression is reduced in both MDD, and the SERT KO model which mimics this disorder, dendritic spine density should also be reduced in SERT KO neurons. It is unsurprising, then, that therapeutic effects of antidepressant treatment are mediated by increases in BDNF expression, leading to enhanced hippocampal neurogenesis [13, 14]. As a result, antidepressant-mediated rescue of BDNF expression would promote the stability and maintenance of mature dendritic spines, thereby underlying the antidepressant effects of SSRIs and TCAs. An examination of BDNF expression across these SERT primary cortical cultures would be required to substantiate these ideas. Regardless, the results from this thesis provide further support and validation of the SERT KO model in mirroring the molecular mechanisms associated with MDD.

One of the main theories about the underlying causes of MDD is that early life stress combines with genetic susceptibility to increase the likelihood of developing MDD at adulthood [18]. Indeed, stress during the perinatal and postnatal periods can affect neuronal activity and function and impinge on mechanisms associated with synaptogenesis and spine formation [166]. Therefore, just as genetic SERT reduction or deletion alters glutamatergic activity and synaptic function during the pre-weaning phase as shown in this thesis, animal

models of early life stress also reduces spine stability [167], and glutamate homeostasis via increased glutamatergic activity [166], at adulthood. These similarities may be underlying the efficacy of SERT KO animals in modelling MDD phenotypes. What is interesting is that the abnormalities in the glutamatergic system in SERT KO rats observed at PND14 here were no longer observed by PND60. Given that this thesis showed reduced dendritic spine density in culture and SYP expression at PND14, among SERT HETs, it is tempting to speculate that MDD susceptibility at the human level may be mediated by instances of early life stress alongside abnormal alterations of glutamatergic homeostasis that develop during the peri- and post- natal periods among human carriers of the S allele. This theory would imply that the S allele is only involved indirectly in MDD susceptibility via its effects on glutamate homeostasis during development, which would partly explain why recent data do not support the direct involvement of the S allele on developing MDD in adult populations [19].

7.3.2. Autism Spectrum Disorder

As stated previously, human studies show that adults with ASD have increased dendritic spine densities on cortical pyramidal neurons [84]. However, this contradicts other reports among adolescents and toddlers with ASD that show reduced dendritic spine densities on cortical neurons [168]. As well, an increase in dendritic spine density may not necessarily indicate stronger synaptic strength, as these increased spines may be immature dendritic spines or filopodia. Therefore, the age of the ASD patients, as well as the morphology of the dendritic spines, must be considered when examining how dendritic spines are altered in ASD [169]. Nonetheless, the reduced spine densities in ASD toddlers and adolescents as previously reported [168], is consistent with the same reduction in SYP protein expression at PND14 and reduced densities along SERT HET and HOM cortical neurons *in vitro* found in this thesis. These commonalities once again reemphasise the importance of assessing the neurobiological changes in glutamatergic signalling and synaptic activity occurring during development, and

not only during adulthood. Therefore, developmental studies must be utilised to further establish the validity of the SERT KO model in mirroring the behavioural and neurobiological phenotypes associated with ASD.

As mentioned previously, there is a dearth of studies identifying any commonalities between neurobiological changes in the SERT KO model to those found in humans with ASD, even though the SERT KO model adequately mirrors the behavioural phenotypes associated with ASD (Section 1.2.2). Nonetheless, a plethora of synaptic genes responsible for proteins associated with trans-synaptic signalling, spine scaffolding, and cytoskeletal remodelling, have been implicated in ASD [85]. Given the heterogeneity of this disorder, understanding the associated synaptic abnormalities among ASD patients can be complex. Therefore, this thesis highlights that *in vitro* SERT KO cultures can provide an initial and less-complex system to unravel the potential mechanisms associated with synaptic abnormalities in ASD at all levels of the synapse, from across the synaptic cleft to within the cytoskeleton in dendritic spines. This initial assessment can then be consolidated *in vivo* either using the SERT KO animal model, or human patients. Thus, the establishment of an *in vitro* system of the SERT KO model will therefore offer new avenues to examine whether neurological changes after SERT reduction and deletion parallel the neurological changes implicated in ASD pathology.

7.3.3. Substance Abuse Disorder

Reduced SERT activity is known to enhance the rewarding properties and subjective experience associated with drugs such as cocaine [58, 59], and MDMA [62], using both CPP and self-administration paradigms. As well, the glutamatergic system is altered after exposure to drugs of abuse [170, 171]. The primary target of cocaine is the DAT, and SERT KO animals are postulated to find MDMA more reinforcing due to MDMA in this model only acting on the DAT [62]. In theory, the stimulation of the DAT after exposure to these drugs in the SERT KO

model would enhance dopamine D_1 receptor activation, which has been shown to increase AMPA and NMDA receptor activity [171], and by extension positively regulate synaptic plasticity by increasing dendritic spine density and size at a higher rate than SERT WT animals. As well, blockage of the AMPA receptor attenuates the reinforcing properties of both cocaine and MDMA, and even ethanol [171, 172], indicating that the glutamate system mediates the reinforcement of these drugs.

However, the findings from this thesis and elsewhere [119] do not align with this theory. The reduced synaptic marker and dendritic spine expression in the frontal cortex of SERT KO animals would suggest that it would be more difficult for these animals to find these drugs of abuse rewarding compared to WT animals, at least during development, which is not the case. It may be that glutamatergic dysregulation during development would not be influencing these KO animals' susceptibility towards the rewarding properties of drugs of abuse such as MDMA at a greater level than WT animals at adulthood, or vice versa. Given that self-administration and CPP are primarily studied in adulthood, it would be interesting to determine whether SERT KO animals show different levels of reinforcement towards drugs of abuse when they are exposed to these drugs during development, where synaptic alterations in the frontal cortex are more prominent.

Drugs of abuse have varying pharmacodynamic profiles, with different drugs resulting in either increases or decreases in glutamatergic neurotransmission and activity [171]. Consequently, alterations in spine density are also dependent on drug type [88, 89]. Given the heterogenous effects of drug exposure on glutamatergic activity, the SERT KO model may not be a valid model to mirror the effects of all drugs of abuse. More work is required to determine the accuracy with which the SERT KO model mirrors both the behavioural and neurobiological changes associated with different drugs of abuse. Moreover, the recovery of synaptic aberrations at adulthood poses new hypotheses about why drugs of abuse are more reinforcing

in the SERT KO model in adulthood. These hypotheses include the possibility that developmentally-limited aberrations to synaptic activity in the SERT KO model, combined with exposure to drugs of abuse at this time, may confer greater risk for behaviours associated with drug abuse at adulthood, given that early adolescent exposure to drugs at the human level strongly predicts SUD development at adulthood [173]. Therefore, understanding the mechanisms underlying SUD susceptibility may elucidate how glutamatergic activity and synaptic dysfunction across the lifespan is associated with greater drug-seeking and drug-reinforcing behaviours at adulthood.

7.4. Limitations

The results obtained in this thesis must be considered in light of experimental and methodological limitations. The primers for drebrin, PSD95, and *Hprt1* used in the qPCR experiment failed to reach the required amplification efficiency of 80-120%. Given that *Hprt1* was used as the reference gene, the trend towards reduced mRNA expression of drebrin, PSD95 and SYP at PND14 may not be an accurate representation of the effects occurring in SERT KO animals. Perhaps optimising the cycling conditions, particularly the annealing temperature, would have resulted in more efficient primer sets, and therefore more accurate measurements of synaptic marker mRNA expression.

An alternative approach would have been to substantiate the results from the qPCR experiments using RNAscope®, which was successfully optimised in this thesis. Therefore, it is promising that both qPCR, and the preliminary assessment of drebrin mRNA using RNAscope®, showed similar levels of drebrin mRNA expression with reduced expression in SERT HET and HOM compared to WT. While the RNAscope® experiment was preliminary, the similarities between these two distinct measures of mRNA expression gives credence to the qPCR data generated, despite the somewhat weak primer efficiencies obtained.

It is unfortunate that timing constraints hindered the establishment of a semi-quantitative analysis for RNAscope® to assess the relative expression of mRNA puncta across the different genotypes and ages. Such a method would have validated the results obtained in the preliminary assessment of drebrin mRNA across SERT genotypes at the two timepoints and validated the results from the qPCR experiments. Moreover, it would have allowed for an investigation on whether the effects are restricted to the frontal cortex or are found widely throughout multiple brain regions. Therefore, to further optimise the RNAscope® protocol here, a semi-quantitative measure must be established, particularly given that others have successfully employed such methods to assess RNAscope® mRNA puncta in brain and non-brain tissue using well-known quantification software such as ImageJ [134, 174, 175].

In addition, this thesis only focused on synaptic alterations occurring in the frontal cortex. MDD, ASD, and SUDs are disparate neuropsychiatric disorders, each having distinct neurological pathways involved in their respective aetiologies. Therefore, given that these disorders all affect higher order functions found in the frontal cortex [63, 84, 91], it seemed appropriate to focus on this brain region alone. However, MDD is also associated with dysregulation of the synapse in the hippocampus and amygdala [15, 81], ASD with this dysregulation in the parietal and temporal lobes, and cerebellum [84, 176], and SUDs with synaptic dysregulation also occurring in the NAcc [89]. Moreover, evidence shows there can be differential regulation of synapses across these brain regions within these disorders [15], highlighting that what was observed in the frontal cortex in this thesis may not be observed in other brain regions involved in these disorders and the SERT KO model. Therefore, this thesis only provides a limited picture of the synaptic abnormalities that may be involved in the SERT KO model and in the mechanisms that may be underlying MDD, ASD, and SUD pathophysiology.

7.5. Future Directions

This thesis provides a preliminary understanding of how glutamatergic neurotransmission and synaptic plasticity may be affected by genetic SERT reduction and deletion during development. Given that drebrin A begins to accumulate at PND14, and should be fully abundant by PND60 [96], only these two timepoints were studied. However, a more substantial examination of these aberrations in the glutamatergic system in SERT KO animals across development is warranted, which can be fulfilled by assessing synaptic marker mRNA and protein expression at multiple timepoints. These markers could be assessed at PND0, 7, 14, 21, 40, 60, and 100, to test the hypothesis from this thesis that the younger the SERT KO animal, the greater the reductions in synaptic markers. While such an experiment is complicated by the fact that drebrin A is not present at PND0-7 [96], markers such as SYP and PSD95 are just as efficacious to further validate the hypothesis that synaptogenesis is stunted in SERT HET and HOM animals and that these aberrations are absolved by adulthood, especially given the strong correlations found between these markers at both mRNA and protein levels. In addition, a cross-region analysis could shed light on whether this developmentally-regulated delay in synaptogenesis in SERT KO is consistent in multiple regions associated with neuropsychiatric disease pathology. Such an analysis could utilise the optimisation of RNAscope® to assess the mRNA expression of synaptic genes across these regions within the same brain and tissue section. For example, coronal or sagittal sections can be used to compare mRNA puncta expression in the cortex to subcortical regions such as the hippocampus, amygdala, and NAcc, which are involved in the pathology of MDD, ASD and SUDs.

Moreover, subsequent work of the SERT KO *in vitro* culture system is important to further characterise this system. For example, it would be prudent to assess whether the mechanisms involved in antidepressant effects can also be modelled in this *in vitro* culture

system. Given that BDNF seems required for antidepressant effects via hippocampal neurogenesis [14], experiments could be conducted on cultured hippocampal SERT KO neurons to determine whether BDNF exposure induces a recovery of dendritic spine density in SERT KO neurons. Experiments such as these would further elucidate the nature of this culture system and validate its potential in mirroring the cellular and molecular mechanisms involved in neuropsychiatric disease.

As well, the mechanisms involved in the developmentally-regulated reduction of dendritic spine density in cortical neurons in SERT KO animals, identified both directly (*in vitro*) and indirectly (*in vivo*), remains to be fully elucidated. Such a gap could be addressed using the *in vitro* culture system of SERT KO neurons utilised in this thesis. As stated previously, multiple studies converge on the activation of the 5-HT_{2A} receptor in serotonergic involvement in regulating dendritic spine density. In addition, the increase in extracellular 5-HT in SERT KO aligns with this converging evidence. Therefore, a potential model of dendritic spine regulation after SERT KO is proposed (Figure 7.5.1). Future experiments should assess the validity of this model, for example, by exposing SERT KO neurons *in vitro* to 5-HT_{2A} receptor agonists and antagonists and determining whether dendritic spine density reductions in SERT KO neurons, as observed in this thesis, are potentiated or inhibited, respectively, using co-labelling of MAP2 and drebrin.

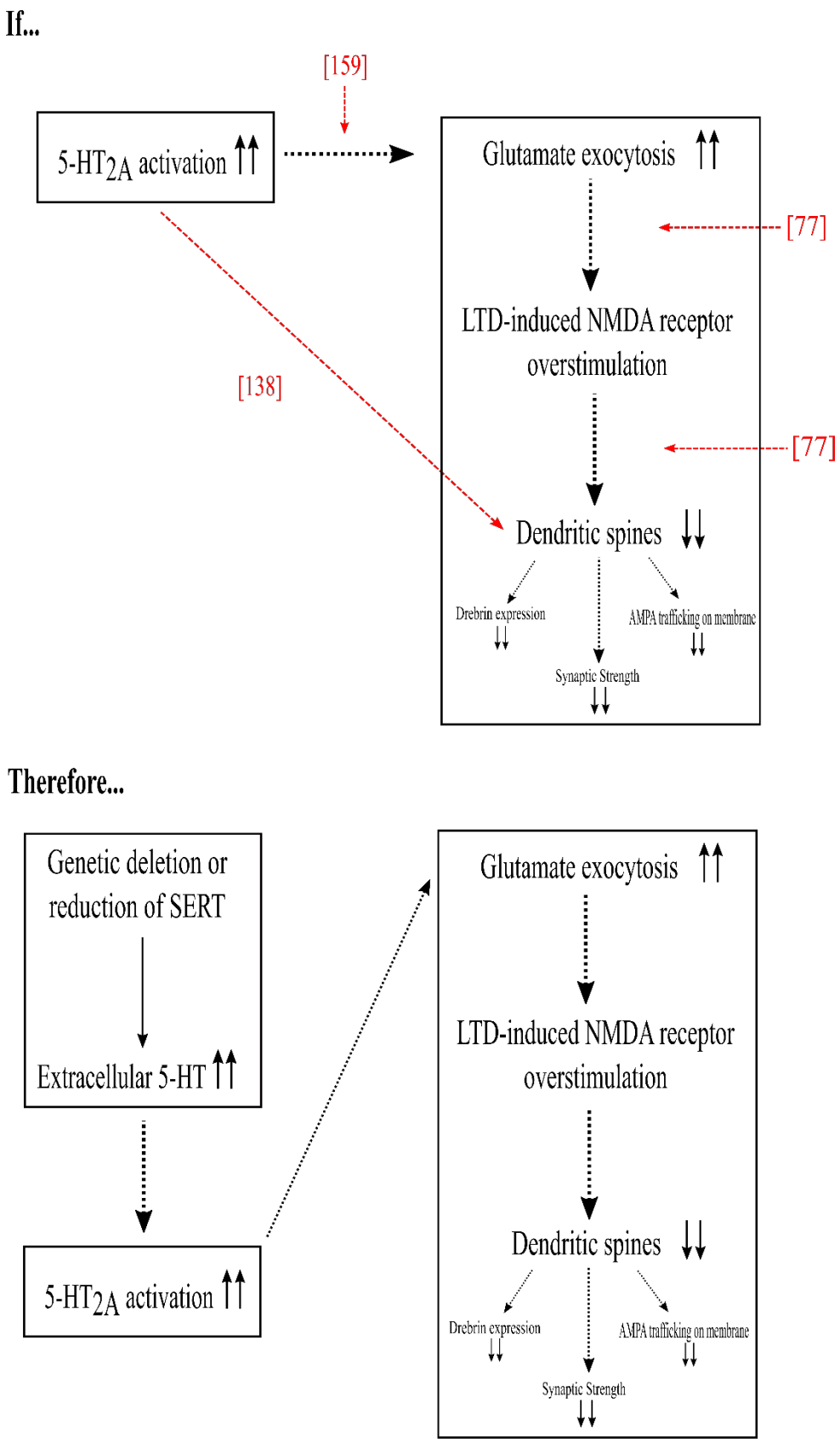

Figure 7.5.1 Proposed model of the mechanisms involved in SERT KO regulation of dendritic spine density at glutamatergic synapses. Red arrows highlight sources showing empirical evidence for the relationship between the linked molecular events.

7.6. Conclusions

This thesis aimed to assess whether genetic SERT reduction and deletion alters synaptic activity at glutamatergic synapses in the frontal cortex. The expression of an oft-neglected protein, drebrin A, which is crucial for regulating dendritic spine activity, was assessed alongside pre- and post- synaptic markers, synaptophysin and PSD95, across two timepoints. Altogether, results showed a developmentally-limited reduction in the mRNA expression of these genes in SERT KO animals, as well as the protein expression of synaptophysin, *in vivo*. These findings were also mirrored *in vitro* in primary cortical neurons. The results obtained from this thesis emphasise that a shift from focusing on molecular changes in the SERT KO at adulthood, to assessing molecular changes in this animal model during development, may be necessary. This refocusing aligns with the developmentally-limited ability of 5-HT to act as a neuromodulator on the glutamate system, which would have lasting consequences at adulthood. Given that the SERT KO models MDD, ASD, and SUDs, the findings in this thesis provide novel insight into how the S allele at the human level may contribute to the dysregulation of dendritic spines, and by extension, indirectly contribute to the synaptic dysregulation that have been implicated in the aetiology of these disorders.

APPENDICES

Appendix A. Sex Effects at Adulthood for qPCR

The data for each synaptic gene at adulthood was separated by sex to identify whether ΔΔCq values for drebrin, PSD95 and SYP differed among male and female SERT animals. For drebrin (Figure A.1), a 3 (genotype: WT, HET, HOM) x 2 (sex: male, female) factorial ANOVA showed no main effect of genotype ($F(2, 21) = 2.42$, $p = .113$, $\eta_p^2 = .188$, *ns*), sex ($F(1, 21) = 2.19$, $p = .154$, $\eta_p^2 = .094$, *ns*), nor a genotype * sex interaction ($F(2, 21) = 0.51$, $p = .605$, $\eta_p^2 = .047$, *ns*). No main effects or interactions were observed for PSD95 (genotype: $F(2, 21) = 2.55$, $p = .102$, $\eta_p^2 = .195$, *ns*; sex: $F(1, 21) = 0.79$, $p = .383$, $\eta_p^2 = .036$, *ns*; genotype * sex: $F(2, 21) = 0.27$, $p = .763$, $\eta_p^2 = .025$, *ns*), as shown in Figure A.2, nor for SYP (genotype: $F(2, 21) = 0.44$, $p = .652$, $\eta_p^2 = .040$, *ns*; sex: $F(1, 21) = 1.40$, $p = .250$, $\eta_p^2 = .063$, *ns*; genotype * sex: $F(2, 21) = 0.45$, $p = .616$, $\eta_p^2 = .045$, *ns*), as shown in Figure A.3. Therefore, no sex differences for the expression of drebrin, PSD95, and SYP at adulthood was observed. Based on these results, the planned comparison between PND14 and PND60 was conducted as stated in Chapter 3.

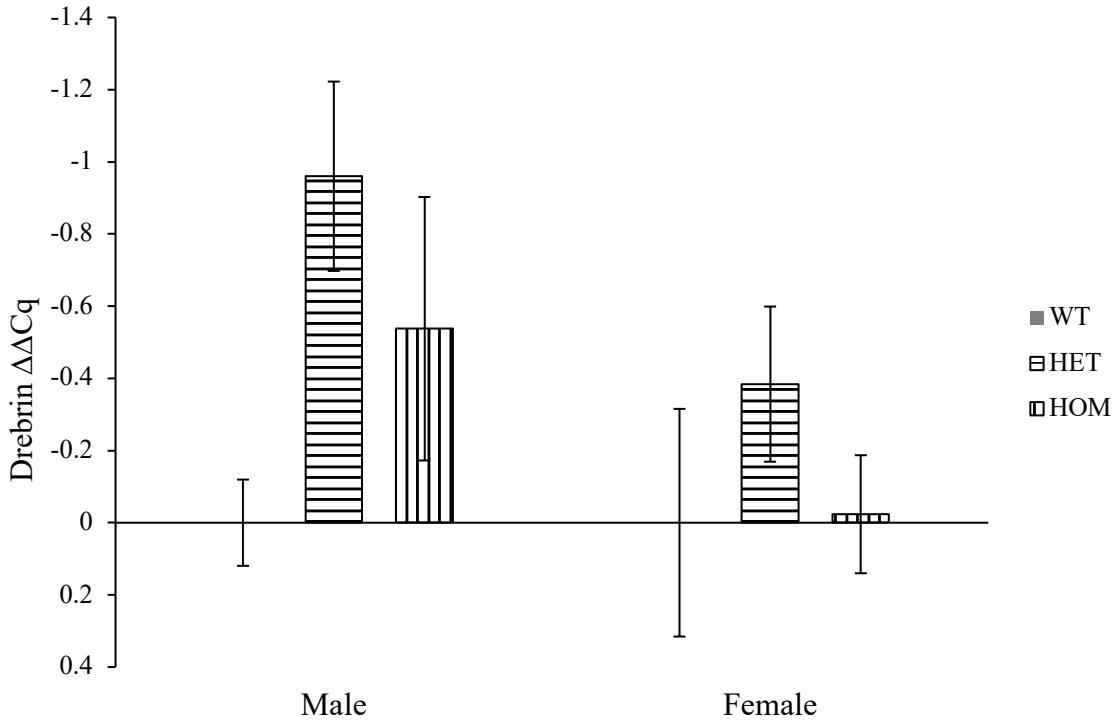

Figure A.1 Mean drebrin ΔΔCq values for adult SERT HET and HOM animals normalised against WT, separated by sex. Error bars indicate ± SEM. Y-axis is inverted for graphical presentation purposes.

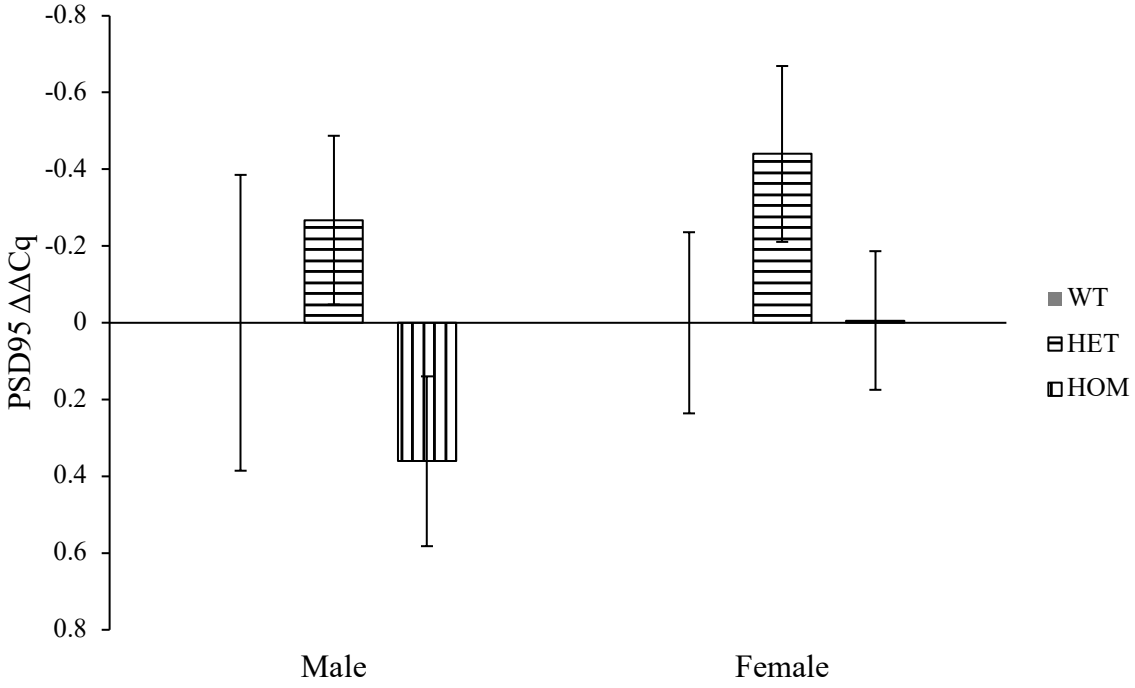

Figure A.2 Mean PSD95 ΔΔCq values for adult SERT HET and HOM animals normalised against WT, separated by sex. Error bars indicate ± SEM. Y-axis is inverted for graphical presentation purposes.

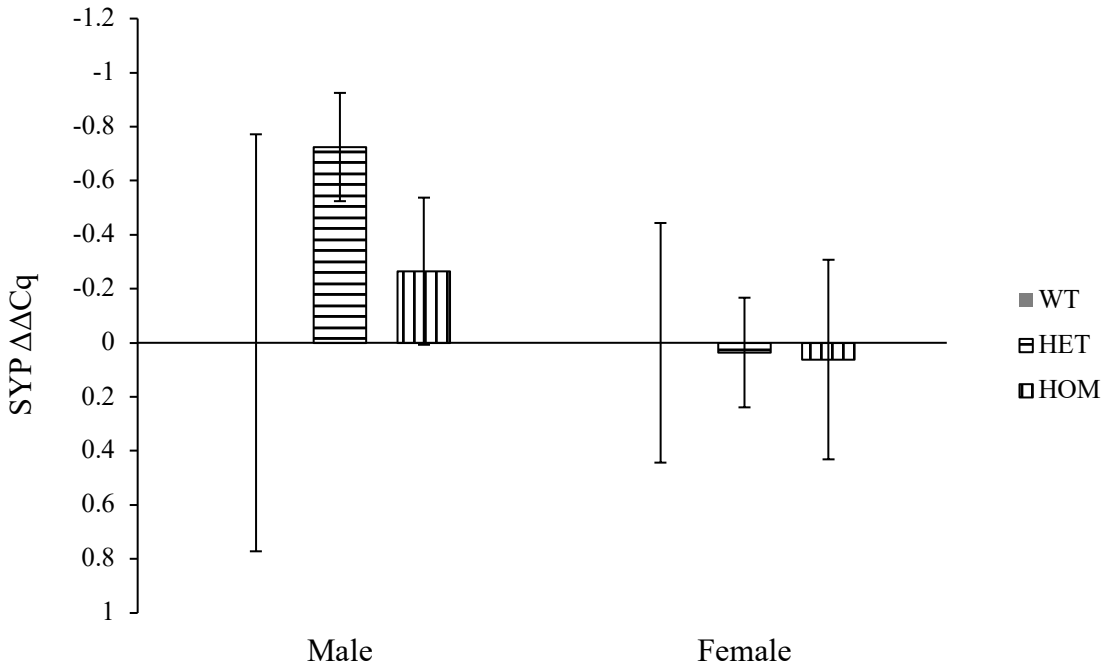

Figure A.3 Mean SYP ΔΔCq values for adult SERT HET and HOM animals normalised against WT, separated by sex. Error bars indicate ± SEM. Y-axis is inverted for graphical presentation purposes.

Appendix B. Q-Q Plots for SYP ΔΔCq Data

Because Levene's test of equality of variances for SYP ΔΔCq values was significant, and therefore the assumption of equal variances was violated, Q-Q plots were checked for approximate normality. Q-Q plots depict the observed standardised residuals against the expected standardised residuals. Data is normally distributed if these two values form a straight line. Visual observation suggests that this assumption of approximate normality is upheld, because both observed and expected standardised residuals form a straight line (Figure B.4).

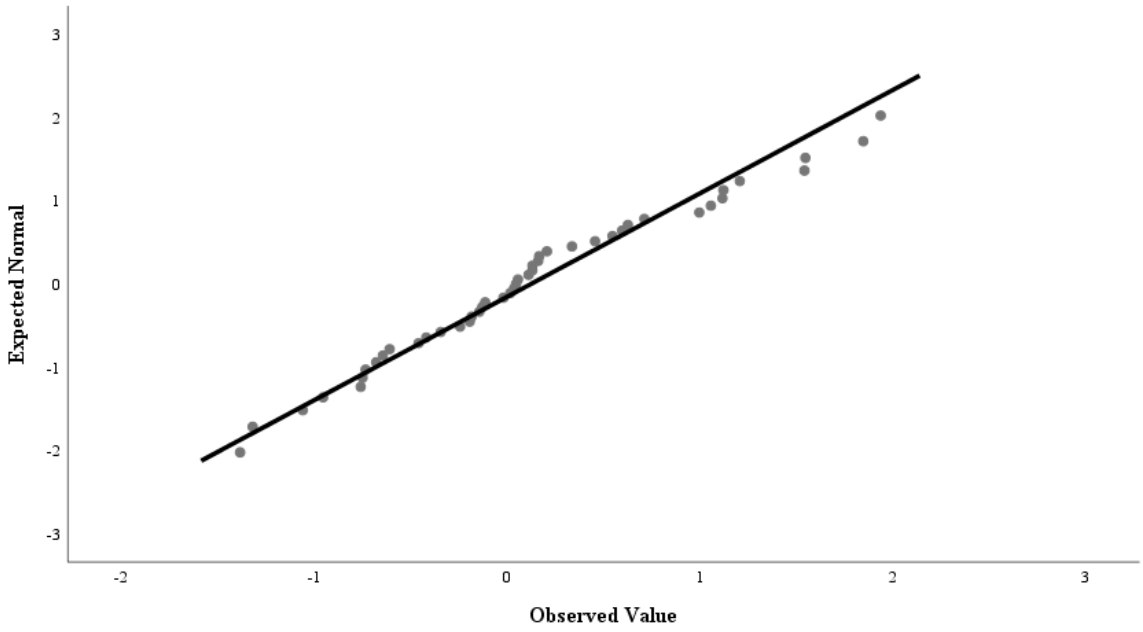

Figure B.4 Q-Q plots comparing observed standardised residuals against expected residuals for SYP ΔΔCq values. Visual inspection demonstrates that all variables are approximately normally distributed.

Appendix C. Sex Effects at Adulthood for Western Blot

As with the qPCR experiments, the data for each target protein at adulthood was separated by sex to identify whether sexually-mature male and female SERT animals differed in drebrin, PSD95, and SYP protein expression. A 3 (genotype: WT, HET, HOM) x 2 (sex: male, female) factorial ANOVA showed no main effect of sex ($F(1, 21) = 1.68$, $p = .209$, $\eta_p^2 = .074$, *ns*) or genotype ($F(2, 21) = 1.61$, $p = .223$, $\eta_p^2 = .133$, *ns*) for synaptophysin expression at adulthood (Figure C.5). Moreover, no interaction was observed ($F(2, 21) = .55$, $p = .586$, $\eta_p^2 = .050$, *ns*). For PSD95, main effects of sex ($F(1, 21) = .01$, $p = .938$, $\eta_p^2 = .000$, *ns*) and genotype ($F(2, 21) = .674$, $p = .520$, $\eta_p^2 = .060$, *ns*) were not observed (Figure C.6), along with no interaction ($F(2, 21) = .34$, $p = .719$, $\eta_p^2 = .031$, *ns*). Lastly, a main effect of sex for drebrin expression showed a trend towards significance, ($F(1, 21) = 3.54$, $p = .074$, $\eta_p^2 = .144$), as shown in Figure C.7. However, no main effect of genotype ($F(2, 21) = 1.15$, $p = .336$, $\eta_p^2 = .099$, *ns*), nor a sex * genotype interaction ($F(2, 21) = .85$, $p = .443$, $\eta_p^2 = .075$, *ns*), was observed. Tukey post-hoc analysis showed that the main effect of sex was driven by an increased drebrin expression among female HET ($M = 1.45$, $SD = 0.42$) animals compared to male HOM ($M = 0.83$, $SD = 0.40$) animals, which showed a weak trend towards significance ($p = .087$). Therefore, minimal sex differences for the drebrin, PSD95, and SYP protein expression at adulthood was observed. Based on these results, the planned comparison between PND14 and PND60 was conducted as stated in Chapter 4.

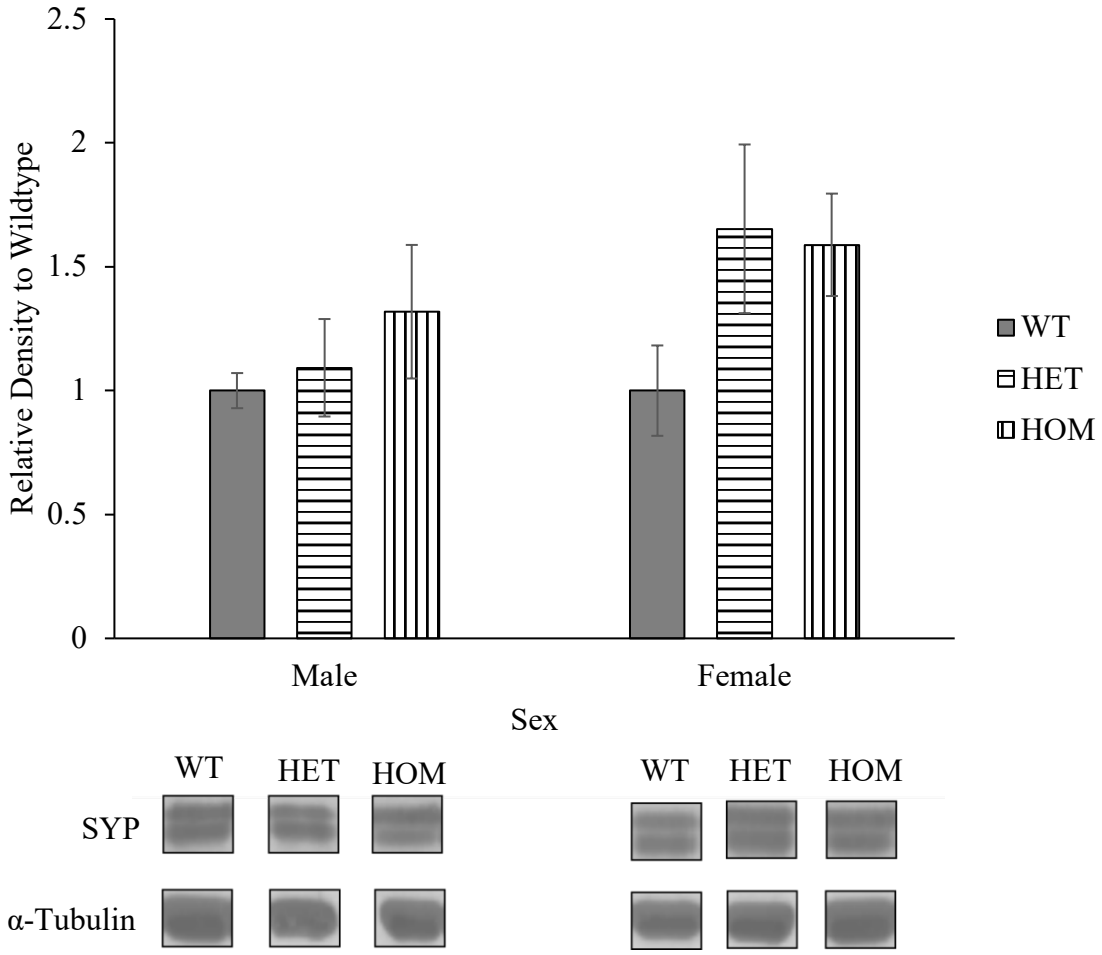

Figure C.5 Mean relative density of synaptophysin (SYP) expression in the frontal cortex of male and female SERT HET and HOM adults relative to WT control. Representative bands for each group for both synaptophysin and loading control (α-Tubulin) are also displayed. Error bars indicate ± SEM.

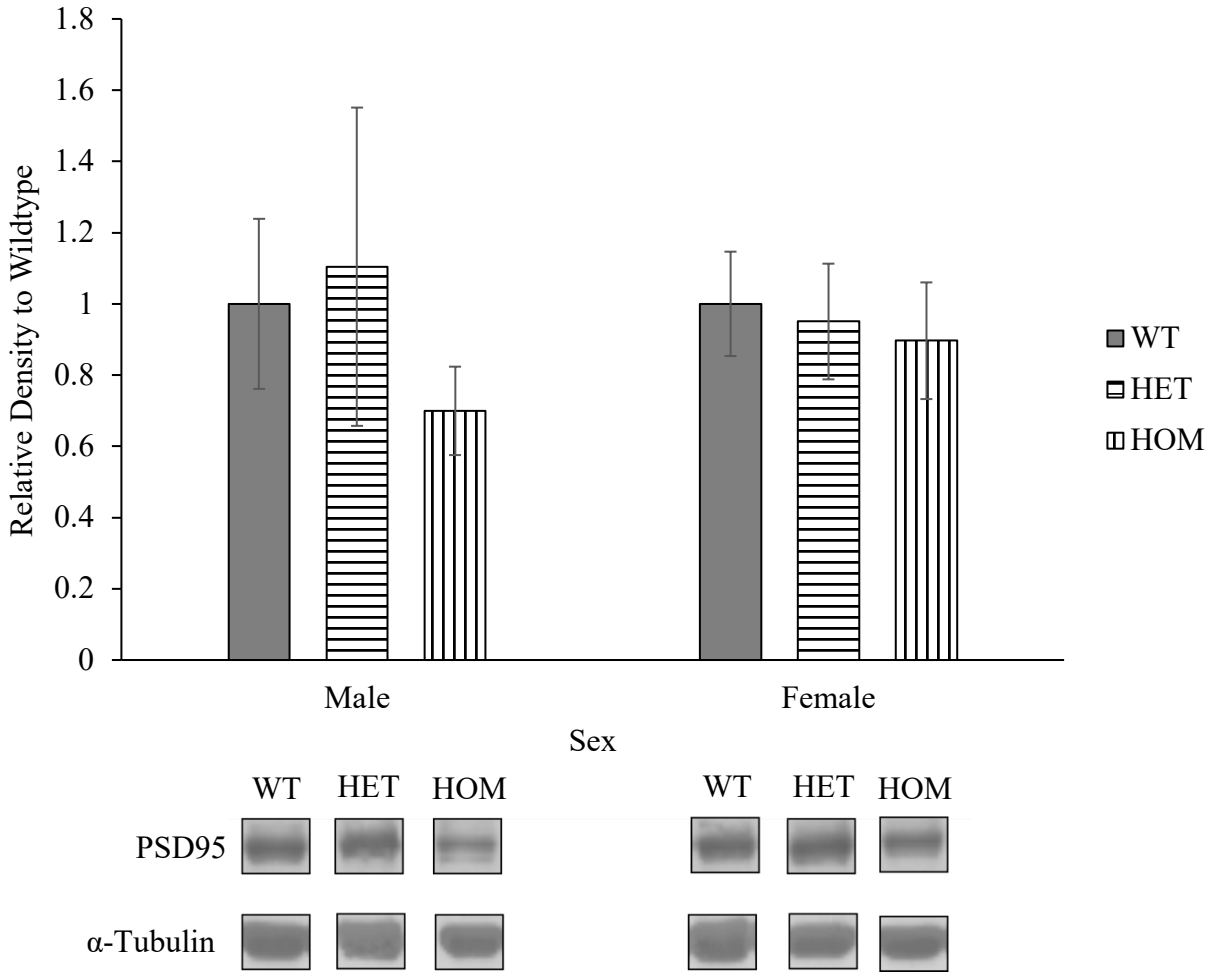

Figure C.6 Mean relative density of PSD95 expression in the frontal cortex of male and female SERT HET and HOM adults relative to WT control. Representative bands for each group for both PSD95 and loading control (α-Tubulin) are also displayed. Error bars indicate ± SEM.

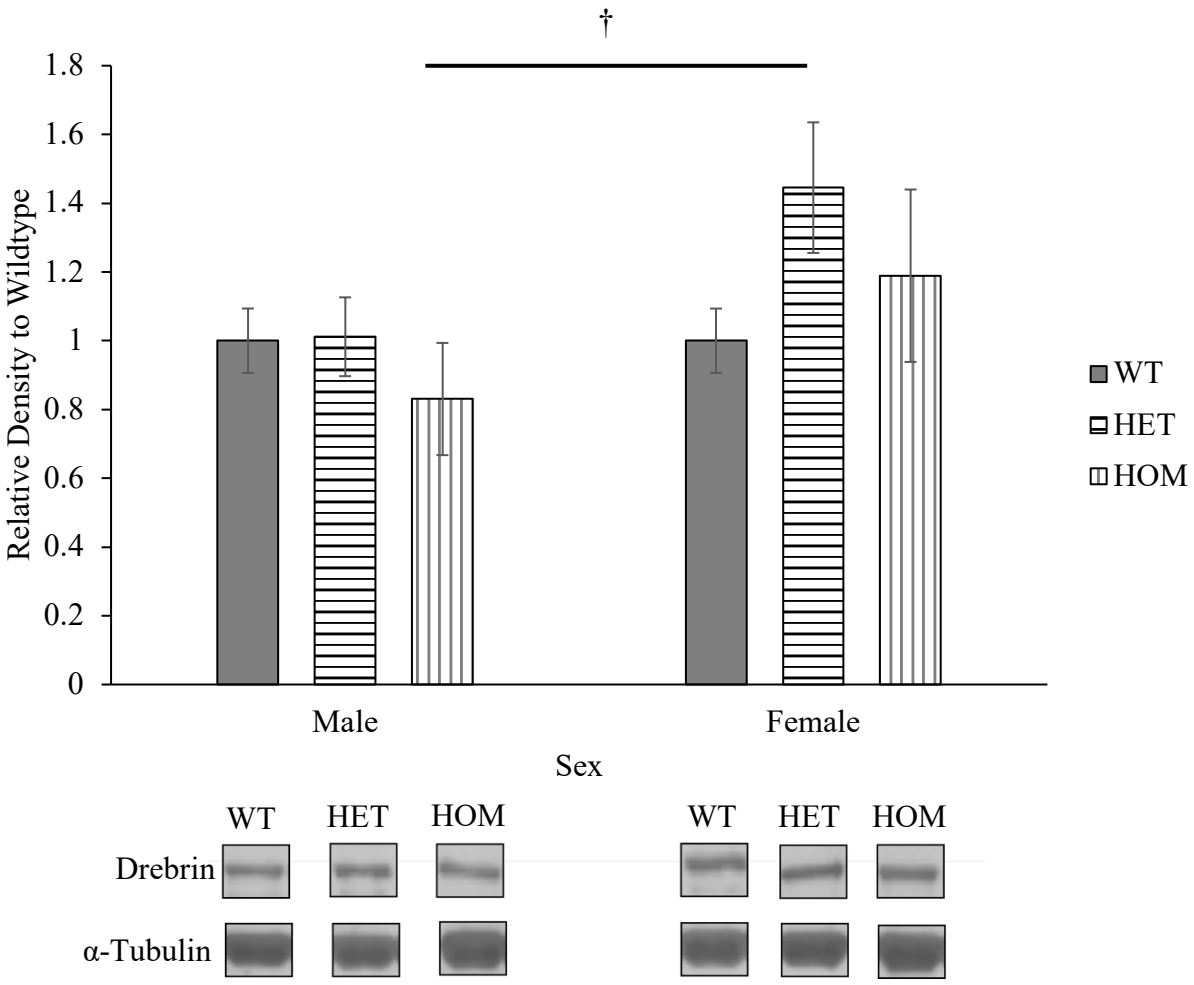

Figure C.7 Mean relative density of drebrin expression in the frontal cortex of male and female SERT HET and HOM adults relative to WT control. Representative bands for each group for both drebrin and loading control (α-Tubulin) are also displayed. † $p = .087$. Error bars indicate ± SEM.

Appendix D. Q-Q Plot for Western Blot Relative Density Data

For all relative density measures across synaptic proteins (drebrin, PSD95, and SYP) Levene's homogeneity test of variance was significant, indicating that the assumption of equality of variances across the six groups was violated. To continue using parametric testing for the statistical analysis, Q-Q plots for drebrin, PSD95 and SYP relative density values were generated. These plots indicated approximate normal distribution for all three variables, as shown in Figure D.8. The analysis was then continued using parametric testing (Chapter 4).

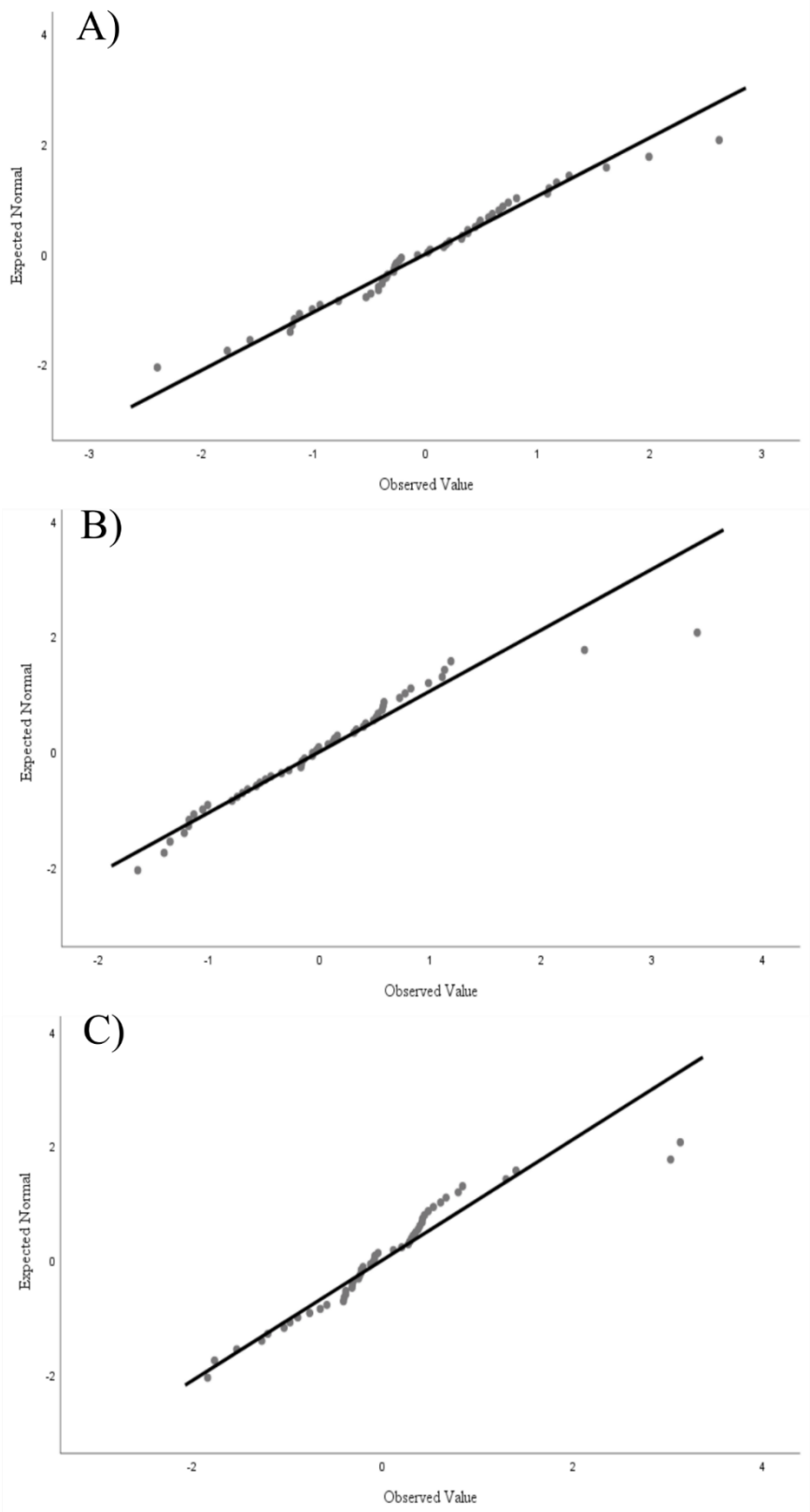

Figure D.8 Q-Q plots comparing observed standardised residuals against expected residuals for relative density to WT values for A) SYP, B) PSD95, and C) drebrin. Visual inspection demonstrates that all variables are approximately normally distributed.

Appendix E. Buffers and Concentrations

Buffers and solutions were prepared using ddH_2O and autoclaved to sterilise if necessary. The pH was also adjusted using an Orion™ digital pH meter (Model SA520), if required, using an appropriate acid or base.

Tris-Acetate-EDTA (TAE) Buffer

Tris Base	2 M
0.5 M Na_2EDTA, pH 8.0	50 mM
Glacial Acetic Acid	0.94 M

A 50x stock of TAE buffer was prepared. The components were combined, then the volume adjusted to 500 ml with ddH_2O. The buffer was then sterilised by autoclaving.

Xylene Cyanol Loading Dye, 6x

Tris, pH 7.8	50 mM
Xylene Cyanol FF	0.25%
Glycerol	30%

The components were combined and brought up to the desired volume with ddH_2O. The dye was then aliquoted into individual Eppendorf tubes and stored at 4ºC.

Radioimmunoprecipitation Assay (RIPA) Buffer, pH 7.5

Tris HCl, pH 8	50 mM
NaCl	150 mM
Triton X-100	0.1%

Sodium Deoxycholate	0.5%
SDS	0.1%

Salts and detergents were mixed with 800 ml ddH_2O. Once dissolved, Triton X-100 was added and the mixture stirred once more before adjusting the pH to 7.5 and adjusting up to 1 L. The buffer was aliquoted in 15 ml Falcon tubes then stored at -20ºC.

Tris-EDTA (TE) Buffer, pH 7.0

Tris base	50 mM
EDTA	5 mM

The components were combined, pH adjusted to 7.0 using NaOH pellets, then made up to the desired volume using ddH_2O. For use as a sample diluent for western blotting, SDS was also added to the buffer at a final concentration of 0.5% before adjusting the pH and filling up to the desired volume.

2x Laemmli Buffer (LB)

Tris HCl, pH 6.8	62.5 mM
Glycerol	25%
Bromophenol Blue	0.01%
SDS	2%

The components were added into a 50 ml Falcon tube, and the remaining volume made up with ddH_2O. Once combined, 0.95 ml aliquots were prepared, and the buffer stored at -20ºC. Finally, 50 µl of β-mercaptoethanol was added fresh and the buffer vortexed to mix before use.

Separating Gel, 10% (2 gels)

1.5 M Tris, pH 8.8	5 ml
SDS, 10%	200 µl
Acrylamide/Bis (29:1), 30%	6.66 ml
APS, 10%	100 µl
Tetramethylethylenediamine (TEMED)	10 µl

The components were added to a 50 ml Falcon tube containing 8 ml ddH_2O, stirred to mix then used immediately.

Stacking Gel, 4% (2 gels)

0.5 M Tris HCl, pH 6.8	2.5 ml
SDS, 10%	100 µl
Acrylamide/Bis (29:1), 30%	1.33 ml
APS, 10%	50 µl
TEMED	10 µl

The components were added to a 15 ml Falcon tube containing 6.1 ml ddH_2O, stirred to mix then used immediately.

SDS-PAGE Running Buffer

Tris Base	250 mM
Glycine	1.92 M
SDS	1%

SDS-PAGE running buffer was prepared as a 10x stock (500 ml). The components were combined and dissolved with ddH_2O at 70% of the final volume, then adjusted up to 500 ml.

Transfer Buffer

Tris Base	25 mM
Glycine	192 mM
SDS	1.3 mM
Methanol	20%

Transfer buffer solution was prepared for western blot experiments at a 1x concentration and at a volume of 2 L. Tris, glycine, and SDS were added and mixed with up to 1.6 L of ddH_2O. Once dissolved, 20% (400 ml) of methanol was added to the buffer, then mixed completely before use.

Tris Buffered Saline (TBS), pH 7.6

Tris Base	50 mM
NaCl	150 mM

TBS was prepared at 10x concentration (1 L). The components were combined, and the pH adjusted to 7.6 using concentrated hydrochloric acid. Once adjusted, ddH_2O was added to make up to the final desired volume.

TBST

To make 1x TBS with Tween-20 (TBST), Tween-20 was added to 1x solution of TBS at a final concentration of 0.1% (1 ml).

Diethyl pyrocarbonate (DEPC)-treated ddH_2O

To prepare RNAse-free ddH_2O for use in RNAscope®, 0.1 ml of DEPC was added to every 100 ml of ddH_2O. The mixture was stirred vigorously and incubated overnight. Finally, the ddH_2O was sterilised by autoclaving for 60 min before use. RNAscope® wash buffers were prepared with DEPC-treated ddH_2O by combining 50x RNAscope® wash buffer reagent (1x final concentration) with DEPC-treated ddH_2O.

References

[1] Insel, T. R., & Landis, S. C. (2013). Twenty-five years of progress: The view from NIMH and NINDS. *Neuron*, *80*(3), 561–567. https://doi.org/10.1016/j.neuron.2013.09.041

[2] Heinzen, E. L., Neale, B. M., Traynelis, S. F., Allen, A. S., & Goldstein, D. B. (2015). The Genetics of Neuropsychiatric Diseases: Looking In and Beyond the Exome. *Annual Review of Neuroscience*, *38*, 47–68. https://doi.org/10.1146/annurev-neuro-071714-034136

[3] Zhu, X., Need, A. C., Petrovski, S., & Goldstein, D. B. (2014). One gene, many neuropsychiatric disorders: Lessons from Mendelian diseases. In *Nature Neuroscience* (Vol. 17, Issue 6, pp. 773–781). https://doi.org/10.1038/nn.3713

[4] Uher, R., & Zwicker, A. (2017). Etiology in psychiatry: embracing the reality of poly-gene-environmental causation of mental illness. *World Psychiatry*, *16*(2), 121–129. https://doi.org/10.1002/wps.20436

[5] American Psychiatric Association. (2013). American Psychiatric Association: Diagnostic and Statistical Manual of Mental Disorders, Fifth Edition. Arlington, VA, American Psychiatric Association. In *Arlington*. https://doi.org/10.1176/appi.books.9780890425596.744053

[6] Ramos-Gorostiza, P., & Adán-Manes, J. (2013). The problem of psychopathology and phenomenology. What is viable and not viable in phenomenologieal psychiatry. In *Actas Espanolas de Psiquiatria* (Vol. 41, Issue 5, pp. 301–310).

[7] Manchia, M., Carpiniello, B., Valtorta, F., & Comai, S. (2017). Serotonin Dysfunction, Aggressive Behavior, and Mental Illness: Exploring the Link Using a Dimensional Approach. *ACS Chemical Neuroscience*, *8*(5), 961–972.

https://doi.org/10.1021/acschemneuro.6b00427

[8] Brummelte, S., Mc Glanaghy, E., Bonnin, A., & Oberlander, T. F. (2017). Developmental changes in serotonin signaling: Implications for early brain function, behavior and adaptation. *Neuroscience*, *342*, 212–231. https://doi.org/10.1016/j.neuroscience.2016.02.037

[9] Benninghoff, J., Van Der Ven, A., Schloesser, R. J., Moessner, R., Möller, H. J., & Rujescu, D. (2012). The complex role of the serotonin transporter in adult neurogenesis and neuroplasticity. A critical review. *World Journal of Biological Psychiatry*, *13*(4), 240–247. https://doi.org/10.3109/15622975.2011.640941

[10] Dean, J., & Keshavan, M. (2017). The neurobiology of depression: An integrated view. *Asian Journal of Psychiatry*, *27*, 101–111. https://doi.org/10.1016/j.ajp.2017.01.025

[11] Schloss, P., & Williams, D. C. (1998). The serotonin transporter: A primary target for antidepressant drugs. In *Journal of Psychopharmacology* (Vol. 12, Issue 2, pp. 115–121). https://doi.org/10.1177/026988119801200201

[12] Gillman, P. K. (2007). Tricyclic antidepressant pharmacology and therapeutic drug interactions updated. *British Journal of Pharmacology*, *151*(6), 737–748. https://doi.org/10.1038/sj.bjp.0707253

[13] Yohn, C. N., Gergues, M. M., & Samuels, B. A. (2017). The role of 5-HT receptors in depression. In *Molecular Brain* (Vol. 10, Issue 1). https://doi.org/10.1186/s13041-017-0306-y

[14] Chen, B., Dowlatshahi, D., MacQueen, G. M., Wang, J. F., & Young, L. T. (2001). Increased hippocampal BDNF immunoreactivity in subjects treated with antidepressant medication. *Biological Psychiatry*, *50*(4), 260–265. https://doi.org/10.1016/S0006-

3223(01)01083-6

[15] Nietzer, S. L., Bonn, M., Jansen, F., Heiming, R. S., Lewejohann, L., Sachser, N., Asan, E. S., … Schmitt, A. G. (2011). Serotonin transporter knockout and repeated social defeat stress: Impact on neuronal morphology and plasticity in limbic brain areas. *Behavioural Brain Research*, *220*(1), 52–54. https://doi.org/10.1016/j.bbr.2011.01.011

[16] Little, K. Y., McLaughlin, D. P., Zhang, L., Livermore, C. S., Dalack, G. W., McFinton, P. R., Delproposto, Z. S., … Cook, E. H. (1998). Cocaine, ethanol, and genotype effects on human midbrain serotonin transporter binding sites and mRNA levels. *American Journal of Psychiatry*, *155*(2), 207–213.

[17] Lesch, K. P., & Waider, J. (2012). Serotonin in the Modulation of Neural Plasticity and Networks: Implications for Neurodevelopmental Disorders. *Neuron*, *76*(1), 175–191. https://doi.org/10.1016/j.neuron.2012.09.013

[18] Caspi, A., Sugden, K., Moffitt, T. E., Taylor, A., Craig, I. W., Harrington, H. L., McClay, J., … Poulton, R. (2003). Influence of life stress on depression: Moderation by a polymorphism in the 5-HTT gene. *Science*, *301*(5631), 386–389. https://doi.org/10.1126/science.1083968

[19] Border, R., Johnson, E. C., Evans, L. M., Smolen, A., Berley, N., Sullivan, P. F., & Keller, M. C. (2019). No Support for Historical Candidate Gene or Candidate Gene-by-Interaction Hypotheses for Major Depression Across Multiple Large Samples. *American Journal of Psychiatry*, *May*, appi.ajp.2018.1. https://doi.org/10.1176/appi.ajp.2018.18070881

[20] Houwing, D. J., Buwalda, B., van der Zee, E. A., de Boer, S. F., & Olivier, J. D. A. (2017). The Serotonin Transporter and Early Life Stress: Translational Perspectives. *Frontiers in Cellular Neuroscience*, *11*. https://doi.org/10.3389/fncel.2017.00117

[21] Volkow, N. D., Michaelides, M., & Baler, R. (2019). The Neuroscience of Drug Reward and Addiction. *Physiological Reviews*, *99*(4), 2115–2140. https://doi.org/10.1152/physrev.00014.2018

[22] Müller, C. P., & Homberg, J. R. (2015). The role of serotonin in drug use and addiction. *Behavioural Brain Research*, *277*, 146–192. https://doi.org/10.1016/j.bbr.2014.04.007

[23] Gould, R. W., Gage, H. D., Banks, M. L., Blaylock, B. L., Czoty, P. W., & Nader, M. A. (2011). Differential effects of cocaine and MDMA self-administration on cortical serotonin transporter availability in monkeys. *Neuropharmacology*, *61*(1–2), 245–251. https://doi.org/10.1016/j.neuropharm.2011.04.007

[24] Semple, D. S., Ebmeir, K. P., Glabus, M. F., O'Carroll, R. E., & Johnstone, E. C. (1999). Reeduced in vivo binding to the serotonin transporter in the cerebral cortex of MDMA ("ecstasy") users. *The British Journal of Psychiatry*, *175*, 63–69. https://doi.org/https://doi.org/10.1192/bjp.175.1.63

[25] Morini, R., Mlinar, B., Baccini, G., & Corradetti, R. (2011). Enhanced hippocampal long-term potentiation following repeated MDMA treatment in Dark-Agouti rats. *European Neuropsychopharmacology*, *21*(1), 80–91. https://doi.org/10.1016/j.euroneuro.2010.07.007

[26] Zorick, T., Sugar, C. A., Hellemann, G., Shoptaw, S., & London, E. D. (2011). Poor response to sertraline in methamphetamine dependence is associated with sustained craving for methamphetamine. *Drug and Alcohol Dependence*, *118*(2–3), 500–503. https://doi.org/10.1016/j.drugalcdep.2011.04.015

[27] Naranjo, C. A., Poulos, C. X., Bremner, K. E., & Lanctot, K. L. (1994). Fluoxetine attenuates alcohol intake and desire to drink. *International Clinical Psychopharmacology*, *9*(3), 163–172. https://doi.org/10.1097/00004850-199409000-00004

[28] Enoch, M. A., Gorodetsky, E., Hodgkinson, C., Roy, A., & Goldman, D. (2011). Functional genetic variants that increase synaptic serotonin and 5-HT3 receptor sensitivity predict alcohol and drug dependence. *Molecular Psychiatry*, *16*(11), 1139–1146. https://doi.org/10.1038/mp.2010.94

[29] Tristán-Noguero, A., Fernàndez-Castillo, N., Roncero, C., Sánchez-Mora, C., Ramos-Quiroga, J. A., Daigre, C., Egido, Á., … Ribasés, M. (2013). Lack of association between the LPR and VNTR polymorphisms of the serotonin transporter gene and cocaine dependence in a Spanish sample. *Psychiatry Research*, *210*(3), 1287–1289. https://doi.org/10.1016/j.psychres.2013.09.004

[30] Johnson, B. A., Elkashef, A. M., Seneviratne, C., Ait-Daoud, N., Kahn, R. C., Li, S. H., Bloch, D. A., … Li, M. D. (2010). Association between genotype of the serotonin transporter-linked polymorphic region of the serotonin transporter gene and age of onset of methamphetamine use: A preliminary analysis. *Frontiers in Psychiatry*. https://doi.org/10.3389/fpsyt.2010.00145

[31] Gerra, G., Garofano, L., Santoro, G., Bosari, S., Pellegrini, C., Zaimovic, A., Moi, G., … Donnini, C. (2004). Association between low-activity serotonin transporter genotype and heroin dependence: Behavioral and personality correlates. *American Journal of Medical Genetics*, *126B*(1), 37–42. https://doi.org/10.1002/ajmg.b.20111

[32] Ohmoto, M., Hirakoshi, M., & Mitsumoto, Y. (2013). Effects of moderating factors including serotonin transporter polymorphisms on smoking behavior: A systematic review and meta-analysis update. *Nicotine and Tobacco Research*, *15*(2), 572–582. https://doi.org/10.1093/ntr/nts149

[33] Brune, C. W., Kim, S. J., Salt, J., Leventhal, B. L., Lord, C., & Cook, E. H. (2006). 5-HTTLPR genotype-specific phenotype in children and adolescents with autism. *American*

Journal of Psychiatry, *163*(12), 2148–2156. https://doi.org/10.1176/ajp.2006.163.12.2148

[34] Daubert, E. A., & Condron, B. G. (2010). Serotonin: A regulator of neuronal morphology and circuitry. *Trends in Neurosciences*, *33*(9), 424–434. https://doi.org/10.1016/j.tins.2010.05.005

[35] Gebril, O., Khalil, R., & Meguid, N. (2015). A study of blood serotonin and serotonin transporter promoter variant (5-HTTLPR) polymorphism in Egyptian autistic children. *Advanced Biomedical Research*, *4:94*. https://doi.org/10.4103/2277-9175.156658

[36] Croonenberghs, J., Spaas, K., Wauters, A., Verkerk, R., Scharpe, S., Deboutte, D., & Maes, M. (2008). Faulty serotonin – DHEA interactions in autism: results of the 5-hydroxytryptophan challenge test. *Neuroendocrinology Letters*, *29*(3), 385–390.

[37] Holmes, A. (2008). Genetic variation in cortico-amygdala serotonin function and risk for stress-related disease. *Neuroscience and Biobehavioral Reviews*, *32*(7), 1293–1314. https://doi.org/10.1016/j.neubiorev.2008.03.006

[38] Jaiswal, P., Guhathakurta, S., Singh, A. S., Verma, D., Pandey, M., Varghese, M., Sinha, S., … Rajamma, U. (2015). SLC6A4 markers modulate platelet 5-HT level and specific behaviors of autism: A study from an Indian population. *Progress in Neuro-Psychopharmacology and Biological Psychiatry*, *56*, 196–206. https://doi.org/10.1016/j.pnpbp.2014.09.004

[39] Huang, C. H., & Santangelo, S. L. (2008). Autism and serotonin transporter gene polymorphisms: A systematic review and meta-analysis. *American Journal of Medical Genetics, Part B: Neuropsychiatric Genetics*, *147*(6), 903–913. https://doi.org/10.1002/ajmg.b.30720

[40] Homberg, J. R., Olivier, J. D. A., Smits, B. M. G., Mul, J. D., Mudde, J., Verheul, M., Nieuwenhuizen, O. F. M., … Cuppen, E. (2007). Characterization of the serotonin transporter knockout rat: A selective change in the functioning of the serotonergic system. *Neuroscience*, *146*(4), 1662–1676. https://doi.org/10.1016/j.neuroscience.2007.03.030

[41] Bengel, D., Murphy, D. L., Andrews, A. M., Wichems, C. H., Feltner, D., Heils, A., Mössner, R., … Lesch, K.-P. (1998). Altered Brain Serotonin Homeostasis and Locomotor Insensitivity to 3,4-Methylenedioxymethamphetamine ("Ecstasy") in Serotonin Transporter-Deficient Mice. *Molecular Pharmacology*, *53*(4), 649–655. https://doi.org/10.1124/mol.53.4.649

[42] Fabre, V., Beaufour, C., Evrard, A., Rioux, A., Hanoun, N., Lesch, K. P., Murphy, D. L., … Martres, M. P. (2000). Altered expression and functions of serotonin 5-HT(1A) and 5-HT(1B) receptors in knock-out mice lacking the 5-HT transporter. *European Journal of Neuroscience*, *12*(7), 2299–2310. https://doi.org/10.1046/j.1460-9568.2000.00126.x

[43] Fox, M. A., Jensen, C. L., French, H. T., Stein, A. R., Huang, S. J., Tolliver, T. J., & Murphy, D. L. (2008). Neurochemical, behavioral, and physiological effects of pharmacologically enhanced serotonin levels in serotonin transporter (SERT)-deficient mice. *Psychopharmacology*, *201*(2), 203–218. https://doi.org/10.1007/s00213-008-1268-7

[44] Houwing, D. J., Ramsteijn, A. S., Riemersma, I. W., & Olivier, J. D. A. (2019). Maternal separation induces anhedonia in female heterozygous serotonin transporter knockout rats. *Behavioural Brain Research*, *356*(August 2018), 204–207. https://doi.org/10.1016/j.bbr.2018.08.031

[45] Lesch, K. P., Benjamin, J., Bengel, D., Petri, S., Muller, C. R., Heils, A., Greenberg, B. D., … Murphy, D. L. (1996). Association of anxiety-related traits with a polymorphism

in the serotonin transporter gene regulatory region. *Science*, *274*(5292), 1527–1531. https://doi.org/10.1126/science.274.5292.1527

[46] Holmes, A., Li, Q., Murphy, D. L., Gold, E., & Crawley, J. N. (2003). Abnormal anxiety-related behavior in serotonin transporter null mutant mice: The influence of genetic background. *Genes, Brain and Behavior*, *2*, 365–380. https://doi.org/10.1046/j.1601-1848.2003.00050.x

[47] Alexandre, C., Popa, D., Fabre, V., Bouali, S., Patrice, V., Lesch, K., Hamon, M., & Adrien, J. (2006). Early Life Blockade of 5-Hydroxytryptamine 1A Receptors Normalizes Sleep and Depression-Like Behavior in Adult Knock-Out Mice Lacking the Serotonin Transporter. *Journal of Neuroscience*, *26*(20), 5554–5564. https://doi.org/10.1523/jneurosci.5156-05.2006

[48] Olivier, J. D. A., Van Der Hart, M. G. C., Van Swelm, R. P. L., Dederen, P. J., Homberg, J. R., Cremers, T., Deen, P. M. T., … Ellenbroek, B. A. (2008). A study in male and female 5-HT transporter knockout rats: An animal model for anxiety and depression disorders. *Neuroscience*, *152*(3), 573–584. https://doi.org/10.1016/j.neuroscience.2007.12.032

[49] Tjurmina, O. A., Armando, I., Saavedra, J. M., Goldstein, D. S., & Murphy, D. L. (2002). Exaggerated adrenomedullary response to immobilization in mice with targeted disruption of the serotonin transporter gene. *Endocrinology*, *143*(12), 4520–4526. https://doi.org/10.1210/en.2002-220416

[50] Kendler, K. S., Kuhn, J. W., Vittum, J., Prescott, C. A., & Riley, B. (2005). The interaction of stressful life events and a serotonin transporter polymorphism in the prediction of episodes of major depression: A replication. *Archives of General Psychiatry*, *62*(5), 529–535. https://doi.org/10.1001/archpsyc.62.5.529

[51] Jiang, X., Wang, J., Luo, T., & Li, Q. (2009). Impaired hypothalamic-pituitary-adrenal axis and its feedback regulation in serotonin transporter knockout mice. *Psychoneuroendocrinology*, *34*(3), 317–331. https://doi.org/10.1016/j.psyneuen.2008.09.011

[52] Murakami, S., Imbe, H., Morikawa, Y., Kubo, C., & Senba, E. (2005). Chronic stress, as well as acute stress, reduces BDNF mRNA expression in the rat hippocampus but less robustly. *Neuroscience Research*, *53*(2), 129–139. https://doi.org/10.1016/j.neures.2005.06.008

[53] Molteni, R., Cattaneo, A., Calabrese, F., Macchi, F., Olivier, J. D. A., Racagni, G., Ellenbroek, B. A., … Riva, M. A. (2010). Reduced function of the serotonin transporter is associated with decreased expression of BDNF in rodents as well as in humans. *Neurobiology of Disease*, *37*(3), 747–755. https://doi.org/10.1016/j.nbd.2009.12.014

[54] Calabrese, F., Van Der Doelen, R. H. A., Guidotti, G., Racagni, G., Kozicz, T., Homberg, J. R., & Riva, M. A. (2015). Exposure to early life stress regulates Bdnf expression in SERT mutant rats in an anatomically selective fashion. *Journal of Neurochemistry*, *132*(1), 146–154. https://doi.org/10.1111/jnc.12846

[55] Tanaka, M., Sato, A., Kasai, S., Hagino, Y., Kotajima-Murakami, H., Kashii, H., Takamatsu, Y., … Ikeda, K. (2018). Brain hyperserotonemia causes autism-relevant social deficits in mice. *Molecular Autism*, *9*(1). https://doi.org/10.1186/s13229-018-0243-3

[56] Kalueff, A. V., Olivier, J. D. A., Nonkes, L. J. P., & Homberg, J. R. (2010). Conserved role for the serotonin transporter gene in rat and mouse neurobehavioral endophenotypes. *Neuroscience and Biobehavioral Reviews*, *34*(3), 373–386. https://doi.org/10.1016/j.neubiorev.2009.08.003

[57] Moy, S. S., Nadler, J. J., Young, N. B., Nonneman, R. J., Grossman, A. W., Murphy, D. L., D'Ercole, A. J., … Lauder, J. M. (2009). Social approach in genetically engineered mouse lines relevant to autism. *Genes, Brain and Behavior*, *8*(2), 129–142. https://doi.org/10.1111/j.1601-183X.2008.00452.x

[58] Caffino, L., Verheij, M. M. M., Que, L., Guo, C., Homberg, J. R., & Fumagalli, F. (2018). Increased cocaine self-administration in rats lacking the serotonin transporter: a role for glutamatergic signaling in the habenula. *Addiction Biology*, *24*(6), 1167–1178. https://doi.org/10.1111/adb.12673

[59] Homberg, Judith R., De Boer, S. F., Raasø, H. S., Olivier, J. D. A., Verheul, M., Ronken, E., Cools, A. R., … Cuppen, E. (2008). Adaptations in pre- and postsynaptic 5-HT1A receptor function and cocaine supersensitivity in serotonin transporter knockout rats. *Psychopharmacology*, *200*(3), 367–380. https://doi.org/10.1007/s00213-008-1212-x

[60] Sora, I., Wichems, C., Takahashi, N., Li, X.-F., Zeng, Z., Revay, R., Lesch, K.-P., … Uhl, G. R. (2002). Cocaine reward models: Conditioned place preference can be established in dopamine- and in serotonin-transporter knockout mice. *Proceedings of the National Academy of Sciences*, *95*(13), 7699–7704. https://doi.org/10.1073/pnas.95.13.7699

[61] Trigo, J. M., Renoir, T., Lanfumey, L., Hamon, M., Lesch, K. P., Robledo, P., & Maldonado, R. (2007). 3,4-Methylenedioxymethamphetamine Self-Administration is Abolished in Serotonin Transporter Knockout Mice. *Biological Psychiatry*, *62*(6), 669–679. https://doi.org/10.1016/j.biopsych.2006.11.005

[62] Oakly, A. C., Brox, B. W., Schenk, S., & Ellenbroek, B. A. (2014). A genetic deletion of the serotonin transporter greatly enhances the reinforcing properties of MDMA in rats. *Molecular Psychiatry*, *19*(5), 534–535. https://doi.org/10.1038/mp.2013.75

[63] Maiti, P., Manna, J., Ilavazhagan, G., Rossignol, J., & Dunbar, G. L. (2015). Molecular

regulation of dendritic spine dynamics and their potential impact on synaptic plasticity and neurological diseases. *Neuroscience and Biobehavioral Reviews*, *59*(101), 208–237. https://doi.org/10.1016/j.neubiorev.2015.09.020

[64] Sekino, Y., Kojima, N., & Shirao, T. (2007). Role of actin cytoskeleton in dendritic spine morphogenesis. *Neurochemistry International*, *51*(2-4 SPEC. ISS.), 92–104. https://doi.org/10.1016/j.neuint.2007.04.029

[65] Bosch, M., Castro, J., Saneyoshi, T., Matsuno, H., Sur, M., & Hayashi, Y. (2014). Structural and molecular remodeling of dendritic spine substructures during long-term potentiation. *Neuron*, *82*(2), 444–459. https://doi.org/10.1016/j.neuron.2014.03.021

[66] Murakoshi, H., & Yasuda, R. (2012). Postsynaptic signaling during plasticity of dendritic spines. *Trends in Neurosciences*, *35*(2), 135–143. https://doi.org/10.1016/j.tins.2011.12.002

[67] Borovac, J., Bosch, M., & Okamoto, K. (2018). Regulation of actin dynamics during structural plasticity of dendritic spines: Signaling messengers and actin-binding proteins. *Molecular and Cellular Neuroscience*, *91*(July), 122–130. https://doi.org/10.1016/j.mcn.2018.07.001

[68] Takumi, Y., Ramírez-León, V., Laake, P., Rinvik, E., & Ottersen, O. P. (1999). Different modes of expression of AMPA and NMDA receptors in hippocampal synapses. *Nature Neuroscience*, *2*(7), 618–624. https://doi.org/10.1038/10172

[69] Sekino, Y., Koganezawa, N., Mizui, T., & Shirao, T. (2017). Role of Drebrin in Synaptic Plasticity. In T. Shirao & Y. Sekino (Eds.), *Drebrin: From Structure and Function to Physiological and Pathological Roles* (pp. 183–202). Springer Tokyo. https://doi.org/10.1007/978-4-431-56550-5

[70] Meyer, D., Bonhoeffer, T., & Scheuss, V. (2014). Balance and stability of synaptic structures during synaptic plasticity. *Neuron*, *82*(2), 430–443. https://doi.org/10.1016/j.neuron.2014.02.031

[71] Nakahata, Y., & Yasuda, R. (2018). Plasticity of spine structure: Local signaling, translation and cytoskeletal reorganization. *Frontiers in Synaptic Neuroscience*, *10*(AUG), 1–13. https://doi.org/10.3389/fnsyn.2018.00029

[72] Takahashi, H., & Naito, Y. (2017). Drebrin and Spine Formation. In T. Shirao & Y. Sekino (Eds.), *Drebrin: From Structure and Function to Physiological and Pathological Roles* (pp. 157–182). Springer Tokyo. https://doi.org/10.1007/978-4-431-56550-5

[73] Buard, I., Coultrap, S. J., Freund, R. K., Lee, Y.-S., Dell'Acqua, M. L., Silva, A. J., & Bayer, K. U. (2010). CaMKII "Autonomy" Is Required for Initiating But Not for Maintaining Neuronal Long-Term Information Storage. *Journal of Neuroscience*, *30*(24), 8214–8220. https://doi.org/10.1523/jneurosci.1469-10.2010

[74] Lisman, J., Yasuda, R., & Raghavachari, S. (2012). Mechanisms of CaMKII action in long-term potentiation. *Nature Reviews Neuroscience*, *13*(3), 169–182. https://doi.org/10.1038/nrn3192

[75] Arber, S., Barbayannis, F. A., Hanser, H., Schnelder, C., Stanyon, C. A., Bernards, O., & Caroni, P. (1998). Regulation of actin dynamics through phosphorylation of cofilin by LIM- kinase. *Nature*, *393*, 805–809. https://doi.org/10.1038/31729

[76] Baumgärtel, K., & Mansuy, I. M. (2012). Neural functions of calcineurin in synaptic plasticity and memory. *Learning and Memory*, *19*(9), 375–384. https://doi.org/10.1101/lm.027201.112

[77] Henson, M. A., Tucker, C. J., Zhao, M., & Dudek, S. M. (2017). Long-term depression-

associated signaling is required for an in vitro model of NMDA receptor-dependent synapse pruning. *Neurobiology of Learning and Memory*, *138*, 39–53. https://doi.org/10.1016/j.nlm.2016.10.013

[78] Zhou, Q., Homma, K. J., & Poo, M. M. (2004). Shrinkage of dendritic spines associated with long-term depression of hippocampal synapses. *Neuron*, *44*(5), 749–757. https://doi.org/10.1016/j.neuron.2004.11.011

[79] Rush, T., Martinez-Hernandez, J., Dollmeyer, M., Frandemiche, M. L., Borel, E., Boisseau, S., Jacquier-Sarlin, M., & Buisson, A. (2018). Synaptotoxicity in Alzheimer's Disease Involved a Dysregulation of Actin Cytoskeleton Dynamics through Cofilin 1 Phosphorylation. *The Journal of Neuroscience*, *38*(48), 10349–10361. https://doi.org/10.1523/jneurosci.1409-18.2018

[80] Qiao, H., Li, M. X., Xu, C., Chen, H. Bin, An, S. C., & Ma, X. M. (2016). Dendritic Spines in Depression: What We Learned from Animal Models. *Neural Plasticity*, *2016*, 20–24. https://doi.org/10.1155/2016/8056370

[81] Morais, M., Santos, P. A. R., Mateus-Pinheiro, A., Patrício, P., Pinto, L., Sousa, N., Pedroso, P., … Bessa, J. M. (2014). The effects of chronic stress on hippocampal adult neurogenesis and dendritic plasticity are reversed by selective MAO-A inhibition. *Journal of Psychopharmacology*, *28*(12), 1178–1183. https://doi.org/10.1177/0269881114553646

[82] Bischofberger, J., von Wolff, G., Seifert, G., Nissen, C., Scholliers, J., Clark, K., Vo Van, T., … Biber, K. (2017). Antidepressants Rescue Stress-Induced Disruption of Synaptic Plasticity via Serotonin Transporter–Independent Inhibition of L-Type Calcium Channels. *Biological Psychiatry*, *84*(1), 55–64. https://doi.org/10.1016/j.biopsych.2017.10.008

[83] Holmes, S. E., Scheinost, D., Finnema, S. J., Naganawa, M., Davis, M. T., DellaGioia, N., Nabulsi, N., … Esterlis, I. (2019). Lower synaptic density is associated with depression

severity and network alterations. *Nature Communications*, *10*(1), 1–10. https://doi.org/10.1038/s41467-019-09562-7

[84] Hutsler, J. J., & Zhang, H. (2010). Increased dendritic spine densities on cortical projection neurons in autism spectrum disorders. *Brain Research*, *1309*, 83–94. https://doi.org/10.1016/j.brainres.2009.09.120

[85] Joensuu, M., Lanoue, V., & Hotulainen, P. (2018). Dendritic spine actin cytoskeleton in autism spectrum disorder. *Progress in Neuro-Psychopharmacology and Biological Psychiatry*, *84*(August 2017), 362–381. https://doi.org/10.1016/j.pnpbp.2017.08.023

[86] Reichova, A., Zatkova, M., Bacova, Z., & Bakos, J. (2018). Abnormalities in interactions of Rho GTPases with scaffolding proteins contribute to neurodevelopmental disorders. *Journal of Neuroscience Research*, *96*(5), 781–788. https://doi.org/10.1002/jnr.24200

[87] Lai, K. O., & Ip, N. Y. (2013). Structural plasticity of dendritic spines: The underlying mechanisms and its dysregulation in brain disorders. *Biochimica et Biophysica Acta - Molecular Basis of Disease*, *1832*(12), 2257–2263. https://doi.org/10.1016/j.bbadis.2013.08.012

[88] DePoy, L. M., & Gourley, S. L. (2015). Synaptic Cytoskeletal Plasticity in the Prefrontal Cortex Following Psychostimulant Exposure. *Traffic*, *16*(9), 919–940. https://doi.org/10.1111/tra.12295

[89] Robinson, T. E., & Kolb, B. (2004). Structural plasticity associated with exposure to drugs of abuse. *Neuropharmacology*, *47*(SUPPL. 1), 33–46. https://doi.org/10.1016/j.neuropharm.2004.06.025

[90] Spiga, S., Mulas, G., Piras, F., & Diana, M. (2014). The “addicted” spine. *Frontiers in Neuroanatomy*, *8*(OCT), 1–7. https://doi.org/10.3389/fnana.2014.00110

[91] Esparza, M. A., Bollati, F., Garcia-Keller, C., Virgolini, M. B., Lopez, L. M., Brusco, A., Shen, H. W., … Cancela, L. M. (2012). Stress-induced sensitization to cocaine: Actin cytoskeleton remodeling within mesocorticolimbic nuclei. *European Journal of Neuroscience*, *36*(8), 3103–3117. https://doi.org/10.1111/j.1460-9568.2012.08239.x

[92] Caffino, L., Giannotti, G., Malpighi, C., Racagni, G., & Fumagalli, F. (2015). Short-term withdrawal from developmental exposure to cocaine activates the glucocorticoid receptor and alters spine dynamics. *European Neuropsychopharmacology*, *25*(10), 1832–1841. https://doi.org/10.1016/j.euroneuro.2015.05.002

[93] Shibasaki, M., Mizuno, K., Kurokawa, K., Suzuki, T., & Ohkuma, S. (2011). Role of actin depolymerizing factor in the development of methamphetamine-induced place preference in mice. *European Journal of Pharmacology*, *671*(1–3), 70–78. https://doi.org/10.1016/j.ejphar.2011.09.176

[94] Takashima, Y., Fannon, M. K. J., Galinato, M. H., Steiner, N. L., An, M., Zemljic-Harpf, A. E., Somkuwar, S. S., … Mandyam, C. D. (2018). Neuroadaptations in the dentate gyrus following contextual cued reinstatement of methamphetamine seeking. *Brain Structure and Function*, *233*(5), 2197–2211. https://doi.org/10.1007/s00429-018-1615-3

[95] Koganezawa, N., Hanamura, K., Sekino, Y., & Shirao, T. (2017). The role of drebrin in dendritic spines. *Molecular and Cellular Neuroscience*, *84*, 85–92. https://doi.org/10.1016/j.mcn.2017.01.004

[96] Hayashi, K., Ishikawa, R., Ye, L.-H., He, X.-L., Takata, K., Kohama, K., & Shirao, T. (1996). Modulatory role of drebrin on the cytoskeleton within dendritic spines in the rat cerebral cortex. *The Journal of Neuroscience : The Official Journal of the Society for Neuroscience*, *16*(22), 7161–7170.

[97] Shirao, T., & Sekino, Y. (2017). General Introduction to Drebrin. In T. Shirao & Y. Sekino

(Eds.), *Drebrin: From Structure and Function to Physiological and Pathological Roles* (pp. 3–22). Springer Tokyo. https://doi.org/10.1007/978-4-431-56550-5

[98] Kojima, N., Shirao, T., & Obata, K. (1993). Molecular cloning of a developmentally regulated brain protein, chicken drebrin A and its expression by alternative splicing of the drebrin gene. *Molecular Brain Research*. https://doi.org/10.1016/0169-328X(93)90154-H

[99] Ivanov, A., Esclapez, M., & Ferhat, L. (2009). Role of drebrin A in dendritic spine plasticity and synaptic function. *Communicative and Integrative Biology*, *2*(3), 268–270. https://doi.org/10.4161/cib.2.3.8166

[100] Aoki, C., Sekino, Y., Hanamura, K., Fujisawa, S., Mahadomrongkul, V., Ren, Y., & Shirao, T. (2005). Drebrin A is a postsynaptic protein that localizes in vivo to the submembranous surface of dendritic sites forming excitatory synapses. *Journal of Comparative Neurology*, *483*(4), 383–402. https://doi.org/10.1002/cne.20449

[101] Hayashi, K., & Shirao, T. (1999). Change in the shape of dendritic spines caused by overexpression of drebrin in cultured cortical neurons. *Journal of Neuroscience*, *19*(10), 3918–3925. https://doi.org/https://doi.org/10.1523/JNEUROSCI.19-10-03918.1999

[102] Takahashi, H., Sekino, Y., Tanaka, S., Mizui, T., Kishi, S., & Shirao, T. (2003). Drebrin-Dependent Actin Clustering in Dendritic Filopodia Governs Synaptic Targeting of Postsynaptic Density-95 and Dendritic Spine Morphogenesis. *The Journal of Neuroscience*, *23*(16), 6586–6595. https://doi.org/10.1523/jneurosci.23-16-06586.2003

[103] Takahashi, H., Mizui, T., & Shirao, T. (2006). Down-regulation of drebrin A expression suppresses synaptic targeting of NMDA receptors in developing hippocampal neurones. *Journal of Neurochemistry*, *97 Suppl 1*, 110–115. https://doi.org/10.1111/j.1471-4159.2005.03536.x

[104] Kobayashi, C., Aoki, C., Kojima, N., Yamazaki, H., & Shirao, T. (2007). Drebrin A content correlates with spine head size in the adult mouse cerebral cortex. *Journal of Comparative Neurology*, *503*(5), 618–626. https://doi.org/10.1002/cne.21408

[105] Takahashi, H., Yamazaki, H., Hanamura, K., Sekino, Y., & Shirao, T. (2009). Activity of the AMPA receptor regulates drebrin stabilization in dendritic spine morphogenesis. *Journal of Cell Science*, *122*(8), 1211–1219. https://doi.org/10.1242/jcs.043729

[106] Sekino, Y., Tanaka, S., Hanamura, K., Yamazaki, H., Sasagawa, Y., Xue, Y., Hayashi, K., & Shirao, T. (2005). Activation of N-methyl-d-aspartate receptor induces a shift of drebrin distribution: Disappearance from dendritic spines and appearance in dendritic shafts. *Molecular and Cellular Neuroscience*, *31*(3), 493–504. https://doi.org/10.1016/j.mcn.2005.11.003

[107] Mizui, T., Sekino, Y., Yamazaki, H., Ishizuka, Y., Takahashi, H., Kojima, N., Kojima, M., & Shirao, T. (2014). Myosin II ATPase activity mediates the long-term potentiation-induced exodus of stable F-actin bound by drebrin a from dendritic spines. *Cellular and Molecular Life Sciences*, *9*(16), 3053–3073. https://doi.org/10.1007/s00018-016-2214-1

[108] Fukazawa, Y., Saitoh, Y., Ozawa, F., Ohta, Y., Mizuno, K., & Inokuchi, K. (2003). Hippocampal LTP is accompanied by enhanced F-actin content within the dendritic spine that is essential for late LTP maintenance in vivo. *Neuron*, *38*(3), 447–460. https://doi.org/10.1016/S0896-6273(03)00206-X

[109] Yasuda, H., Kojima, N., Hanamura, K., Yamazaki, H., Sakimura, K., & Shirao, T. (2018). Drebrin Isoforms Critically Regulate NMDAR- and mGluR-Dependent LTD Induction. *Frontiers in Cellular Neuroscience*, *12*(October), 1–10. https://doi.org/10.3389/fncel.2018.00330

[110] Aoki, C., Kojima, N., Sabaliauskas, N., Shah, L., Ahmed, T. H., Oakford, J., Ahmed, T.,

… Shirao, T. (2009). Drebrin a knockout eliminates the rapid form of homeostatic synaptic plasticity at excitatory synapses of intact adult cerebral cortex. *Journal of Comparative Neurology*, *517*(1), 105–121. https://doi.org/10.1002/cne.22137

[111] Kojima, N., Yasuda, H., Hanamura, K., Ishizuka, Y., Sekino, Y., & Shirao, T. (2016). Drebrin A regulates hippocampal LTP and hippocampus-dependent fear learning in adult mice. *Neuroscience*, *324*, 218–226. https://doi.org/10.1016/j.neuroscience.2016.03.015

[112] Kobayashi, R., Sekino, Y., Shirao, T., Tanaka, S., Ogura, T., Inada, K., & Saji, M. (2004). Antisense knockdown of drebrin A, a dendritic spine protein, causes stronger preference, impaired pre-pulse inhibition, and an increased sensitivity to psychostimulant. *Neuroscience Research*, *49*(2), 205–217. https://doi.org/10.1016/j.neures.2004.02.014

[113] Shim, K. S., & Lubec, G. (2002). Drebrin, a dendritic spine protein, is manifold decreased in brains of patients with Alzheimer's disease and Down syndrome. *Neuroscience Letters*, *324*(3), 209–212. https://doi.org/10.1016/S0304-3940(02)00210-0

[114] Harigaya, Y., Shoji, M., Shirao, T., & Hirai, S. (1996). Disappearance of actin-binding protein, drebrin, from hippocampal synapses in Alzheimer's disease. *Journal of Neuroscience Research*, *43*(1), 87–92. https://doi.org/10.1002/jnr.490430111

[115] Hatanpaa, K., Issacs, K. R., Shirao, T., Brady, D. R., & Rapoport, S. I. (1999). Loss of Protein Regulating Synaptic Plasticity in Normal Aging of the Human Brain and in Alzheimer Disease. *Journal of Neuropathology and Experimental Neurology*, *58*(6), 637–643. https://doi.org/10.1192/bjp.111.479.1009-a

[116] Julien, C., Tremblay, C., Bendjelloul, F., Phivilay, A., Couloumbe, M.-A., Édmond, V., & Calon, F. (2008). Decreased drebrin mRNA expression in Alzheimer disease: Correlation with tau pathology. *Journal of Neuroscience Research*, *86*(10), 2292–2302. https://doi.org/10.1002/jnr.21667

[117] Counts, S. E., He, B., Nadeem, M., Wuu, J., Scheff, S. W., & Mufson, E. J. (2012). Hippocampal drebrin loss in mild cognitive impairment. *Neurodegenerative Diseases*, *10*(1–4), 216–219. https://doi.org/10.1159/000333122

[118] Counts, S. E., Nadeem, M., Lad, S. P., Wuu, J., & Mufson, E. J. (2006). Differential expression of synaptic proteins in the frontal and temporal cortex of elderly subjects with mild cognitive impairment. *Journal of Neuropathology and Experimental Neurology*, *65*(6), 592–601. https://doi.org/10.1097/00005072-200606000-00007

[119] Brivio, P., Homberg, J. R., Riva, M. A., & Calabrese, F. (2019). Alterations of Glutamatergic Markers in the Prefrontal Cortex of Serotonin Transporter Knockout Rats: A Developmental Timeline. *Cellular and Molecular Neurobiology*, *36*(5), 715–720. https://doi.org/10.1007/s10571-019-00673-9

[120] Longordo, F., Fan, J., Steimer, T., Kopp, C., & Lüthi, A. (2011). Do mice habituate to "gentle handling"? A comparison of resting behavior, corticosterone levels and synaptic function in handled and undisturbed C57BL/6J mice. *Sleep*, *34*(5), 679–681. https://doi.org/10.1093/sleep/34.5.679

[121] Schapiro, S., & Vukovich, K. R. (1970). Early experience effects upon cortical dendrites: A proposed model for development. *Science*, *167*(3916), 292–294. https://doi.org/10.1126/science.167.3916.292

[122] Bustin, S. A., Benes, V., Garson, J. A., Hellemans, J., Huggett, J., Kubista, M., Mueller, R., … Wittwer, C. T. (2009). The MIQE guidelines: Minimum information for publication of quantitative real-time PCR experiments. *Clinical Chemistry*, *55*(4), 611–622. https://doi.org/10.1373/clinchem.2008.112797

[123] Veselenak, R. L., Miller, A. L., Milligan, G. N., Bourne, N., & Pyles, R. B. (2014). Development and Utilization of a Custom PCR Array Workflow: Analysis of Gene

Expression in Mycoplasma genitalium and Guinea Pig (Cavia porcellus). *Molecular Biotechnology*, *57*, 172–183. https://doi.org/10.1007/s12033-014-9813-6

[124] Huggett, J., Dheda, K., Bustin, S., & Zumla, A. (2005). Real-time RT-PCR normalisation; strategies and considerations. *Genes and Immunity*, *6*(4), 279–284. https://doi.org/10.1038/sj.gene.6364190

[125] Rao, X., Huang, X., Zhou, Z., & Lin, X. (2013). An improvement of the 2ˆ(-delta delta CT) method for quantitative real-time polymerase chain reaction data analysis. *Biostatistics, Bioinformatics and Biomathematics*, *3*(3), 71–85.

[126] Evans, A. M. (1986). Age at Puberty and First Litter Size in Early and Late Paired Rats. *Biology of Reproduction*, *32*(2), 322–326. https://doi.org/10.1095/biolreprod34.2.322

[127] Robb, G. W., Amann, R. P., & Killian, G. J. (1978). Daily sperm production and epididymal sperm reserves of pubertal and adult rats. *Journal of Reproduction and Fertility*, *54*(1), 103–107. https://doi.org/10.1530/jrf.0.0540103

[128] Campion, S. N., Carvallo, F. R., Chapin, R. E., Nowland, W. S., Beauchamp, D., Jamon, R., Koitz, R., … Hurtt, M. E. (2013). Comparative assessment of the timing of sexual maturation in male Wistar Han and Sprague-Dawley rats. *Reproductive Toxicology*, *38*, 16–24. https://doi.org/10.1016/j.reprotox.2013.02.003

[129] Clayton, J. A. (2016). Studying both sexes: A guiding principle for biomedicine. *FASEB Journal*, *30*(2), 519–524. https://doi.org/10.1096/fj.15-279554

[130] Becker, J. B., Prendergast, B. J., & Liang, J. W. (2016). Female rats are not more variable than male rats: A meta-analysis of neuroscience studies. *Biology of Sex Differences*, *7:34*. https://doi.org/10.1186/s13293-016-0087-5

[131] Beery, A. K. (2018). Inclusion of females does not increase variability in rodent research

studies. *Current Opinion in Behavioral Sciences*, *23*, 143–149. https://doi.org/10.1016/j.cobeha.2018.06.016

[132] Bauernfeind, A. L., & Babbitt, C. C. (2017). The predictive nature of transcript expression levels on protein expression in adult human brain. *BMC Genomics*, *18:322*. https://doi.org/10.1186/s12864-017-3674-x

[133] Azmitia, E. C., Rubinstein, V. J., Strafaci, J. A., Rios, J. C., & Whitaker-Azmitia, P. M. (1995). 5-HT1A agonist and dexamethasone reversal of para-chloroamphetamine induced loss of MAP-2 and synaptophysin immunoreactivity in adult rat brain. *Brain Research*, *677*(2), 181–192. https://doi.org/10.1016/0006-8993(95)00051-Q

[134] Grabinski, T. M., Kneynsberg, A., Manfredsson, F. P., & Kanaan, N. M. (2015). A method for combining rnascope in situ hybridization with immunohistochemistry in thick free-floating brain sections and primary neuronal cultures. *PLoS ONE*, *10*(3). https://doi.org/10.1371/journal.pone.0120120

[135] Wang, F., Flanagan, J., Su, N., Wang, L. C., Bui, S., Nielson, A., Wu, X., … Luo, Y. (2012). RNAscope: A novel in situ RNA analysis platform for formalin-fixed, paraffin-embedded tissues. *Journal of Molecular Diagnostics*, *14*(1), 22–29. https://doi.org/10.1016/j.jmoldx.2011.08.002

[136] Nwabuisi-Heath, E., LaDu, M. J., & Yu, C. (2012). Simultaneous analysis of dendritic spine density, morphology and excitatory glutamate receptors during neuron maturation in vitro by quantitative immunocytochemistry. *Journal of Neuroscience Methods*, *207*(2), 137–147. https://doi.org/10.1016/j.jneumeth.2012.04.003

[137] Speranza, L., Labus, J., Volpicelli, F., Guseva, D., Lacivita, E., Leopoldo, M., Bellenchi, G. C., … Ponimaskin, E. (2017). Serotonin 5-HT7 receptor increases the density of dendritic spines and facilitates synaptogenesis in forebrain neurons. *Journal of*

Neurochemistry, *141*(5), 647–661. https://doi.org/10.1111/jnc.13962

[138] Roppongi, R. T., Kojima, N., Hanamura, K., Yamazaki, H., & Shirao, T. (2013). Selective reduction of drebrin and actin in dendritic spines of hippocampal neurons by activation of 5-HT2A receptors. *Neuroscience Letters*, *547*, 76–81. https://doi.org/10.1016/j.neulet.2013.04.061

[139] Papa, M., Bundman, M. C., Greenberger, V., & Segal, M. (1995). Morphological analysis of dendritic spine development in primary cultures of hippocampal neurons. *Journal of Neuroscience*, *15*(1), 1–11.

[140] Beaudoin, G. M. J., Lee, S. H., Singh, D., Yuan, Y., Ng, Y. G., Reichardt, L. F., & Arikkath, J. (2012). Culturing pyramidal neurons from the early postnatal mouse hippocampus and cortex. *Nature Protocols*, *7*(9), 1741–1754. https://doi.org/10.1038/nprot.2012.099

[141] Hanamura, K., Koganezawa, N., Kamiyama, K., Tanaka, N., Oka, T., Yamamura, M., Sekino, Y., & Shirao, T. (2018). High-content imaging analysis for detecting the loss of drebrin clusters along dendrites in cultured hippocampal neurons. *Journal of Pharmacological and Toxicological Methods*, *99*. https://doi.org/10.1016/j.vascn.2019.106607

[142] Mitsuoka, T., Hanamura, K., Koganezawa, N., Kikura-Hanajiri, R., Sekino, Y., & Shirao, T. (2018). Assessment of NMDA receptor inhibition of phencyclidine analogues using a high-throughput drebrin immunocytochemical assay. *Journal of Pharmacological and Toxicological Methods*, *99*. https://doi.org/10.1016/j.vascn.2019.106583

[143] Weisstaub, N. V., Zhou, M., Lira, A., Lambe, E., González-Maeso, J., Hornung, J. P., Sibille, E., … Gingrich, J. A. (2006). Cortical 5-HT2A receptor signaling modulates anxiety-like behaviors in mice. *Science*, *313*(5786), 536–540.

https://doi.org/10.1126/science.1123432

[144] Vahid-Ansari, F., Zhang, M., Zahrai, A., & Albert, P. R. (2019). Overcoming resistance to selective serotonin reuptake inhibitors: Targeting serotonin, serotonin-1A receptors and adult neuroplasticity. *Frontiers in Neuroscience*. https://doi.org/10.3389/fnins.2019.00404

[145] Teissier, A., Soiza-Reilly, M., & Gaspar, P. (2017). Refining the role of 5-HT in postnatal development of brain circuits. *Frontiers in Cellular Neuroscience*. https://doi.org/10.3389/fncel.2017.00139

[146] Miceli, S., Schubert, D., Negwer, M., Homberg, J., van Eijs, F., Kalkhoven, C., & van Lierop, I. (2013). High serotonin levels during brain development alter the structural input-output connectivity of neural networks in the rat somatosensory layer IV. *Frontiers in Cellular Neuroscience*, *7*(June), 1–15. https://doi.org/10.3389/fncel.2013.00088

[147] Akhmetshina, D., Zakharov, A., Vinokurova, D., Nasretdinov, A., Valeeva, G., & Khazipov, R. (2016). The serotonin reuptake inhibitor citalopram suppresses activity in the neonatal rat barrel cortex in vivo. *Brain Research Bulletin*, *124*, 48–54. https://doi.org/10.1016/j.brainresbull.2016.03.011

[148] Iacono, L. Lo, & Gross, C. (2008). α-Ca2+/calmodulin-dependent protein kinase II contributes to the developmental programming of anxiety in serotonin receptor 1A knock-out mice. *Journal of Neuroscience*, *28*(24), 6250–6257. https://doi.org/10.1523/JNEUROSCI.5219-07.2008

[149] Volpicelli, F., Speranza, L., di Porzio, U., Crispino, M., & Perrone-Capano, C. (2014). The serotonin receptor 7 and the structural plasticity of brain circuits. *Frontiers in Behavioral Neuroscience*. https://doi.org/10.3389/fnbeh.2014.00318

[150] Vitalis, T., Cases, O., Passemard, S., Callebert, J., & Parnavelas, J. G. (2007). Embryonic depletion of serotonin affects cortical development. *European Journal of Neuroscience*, *26*, 331–344. https://doi.org/10.1111/j.1460-9568.2007.05661.x

[151] Riccio, O., Potter, G., Walzer, C., Vallet, P., Szabó, G., Vutskits, L., Kiss, J. Z., & Dayer, A. G. (2009). Excess of serotonin affects embryonic interneuron migration through activation of the serotonin receptor 6. *Molecular Psychiatry*, *14*(3), 280–290. https://doi.org/10.1038/mp.2008.89

[152] Witteveen, J. S., Middelman, A., van Hulten, J. A., Martens, G. J. M., Homberg, J. R., & Kolk, S. M. (2013). Lack of serotonin reuptake during brain development alters rostral raphe-prefrontal network formation. *Frontiers in Cellular Neuroscience*, *7: 143*. https://doi.org/10.3389/fncel.2013.00143

[153] Altamura, C., Dell'Acqua, M. L., Moessner, R., Murphy, D. L., Lesch, K. P., & Persico, A. M. (2007). Altered neocortical cell density and layer thickness in serotonin transporter knockout mice: A quantitation study. *Cerebral Cortex*, *17*(6), 1394–1401. https://doi.org/10.1093/cercor/bhl051

[154] Frodl, T., Koutsouleris, N., Bottlender, R., Born, C., Jäger, M., Mörgenthaler, M., Scheuerecker, J., … Meisenzahl, E. M. (2008). Reduced gray matter brain volumes are associated with variants of the serotonin transporter gene in major depression. *Molecular Psychiatry*, *13*(12), 1093–1101. https://doi.org/10.1038/mp.2008.62

[155] Ciranna, L. (2006). Serotonin as a Modulator of Glutamate- and GABA-Mediated Neurotransmission: Implications in Physiological Functions and in Pathology. *Current Neuropharmacology*, *4*(2), 101–114. https://doi.org/10.2174/157015906776359540

[156] Staubli, U., & Otaky, N. (1994). Serotonin controls the magnitude of LTP induced by theta bursts via an action on NMDA-receptor-mediated responses. *Brain Research*,

643(1–2), 10–16. https://doi.org/10.1016/0006-8993(94)90003-5

[157] Schmitz, D., Empson, R. M., & Heinemann, U. (1995). Serotonin and 8-OH-DPAT reduce excitatory transmission in rat hippocampal area CA1 via reduction in presumed presynaptic Ca2+ entry. *Brain Research*, *701*(1–2), 249–254. https://doi.org/10.1016/0006-8993(95)01005-5

[158] Dawson, L. A., Nguyen, H. Q., & Li, P. (2001). The 5-HT6 receptor antagonist SB-271046 selectively enhances excitatory neurotransmission in the rat frontal cortex and hippocampus. *Neuropsychopharmacology*, *25*(5), 662–668. https://doi.org/10.1016/S0893-133X(01)00265-2

[159] Hasuo, H., Matsuoka, T., & Akasu, T. (2002). Activation of presynaptic 5-hydroxytryptamine 2A receptors facilitates excitatory synaptic transmission via protein kinase C in the dorsolateral septal nucleus. *Journal of Neuroscience*, *22*(17), 7509–7517. https://doi.org/10.1523/jneurosci.22-17-07509.2002

[160] Mahar, I., Bambico, F. R., Mechawar, N., & Nobrega, J. N. (2014). Stress, serotonin, and hippocampal neurogenesis in relation to depression and antidepressant effects. *Neuroscience and Biobehavioral Reviews*, *38*, 173–192. https://doi.org/10.1016/j.neubiorev.2013.11.009

[161] Lesuisse, C., & Martin, L. J. (2002). Long-term culture of mouse cortical neurons as a model for neuronal development, aging, and death. *Journal of Neurobiology*, *51*(1), 9–23. https://doi.org/10.1002/neu.10037

[162] Belle, A. M., Enright, H. A., Sales, A. P., Kulp, K., Osburn, J., Kuhn, E. A., Fischer, N. O., & Wheeler, E. K. (2018). Evaluation of in vitro neuronal platforms as surrogates for in vivo whole brain systems. *Scientific Reports*, *8:10820*. https://doi.org/10.1038/s41598-018-28950-5

[163] Woolley, C. S., Gould, E., Frankfurt, M., & McEwen, B. S. (1990). Naturally occurring fluctuation in dendritic spine density on adult hippocampal pyramidal neurons. *Journal of Neuroscience*, *10*(12), 4035–4039. https://doi.org/10.1523/jneurosci.10-12-04035.1990

[164] Calabrese, F., Guidotti, G., Middelman, A., Racagni, G., Homberg, J., & Riva, M. A. (2013). Lack of serotonin transporter alters BDNF expression in the rat brain during early postnatal development. *Molecular Neurobiology*, *48*(1), 244–256. https://doi.org/10.1007/s12035-013-8449-z

[165] Kellner, Y., Gödecke, N., Dierkes, T., Thieme, N., Zagrebelsky, M., & Korte, M. (2014). The BDNF effects on dendritic spines of mature hippocampal neurons depend on neuronal activity. *Frontiers in Synaptic Neuroscience*, *6:5*. https://doi.org/10.3389/fnsyn.2014.00005

[166] Toya, S., Takatsuru, Y., Kokubo, M., Amano, I., Shimokawa, N., & Koibuchi, N. (2014). Early-life-stress affects the homeostasis of glutamatergic synapses. *European Journal of Neuroscience*, *40*(11), 3627–3634. https://doi.org/10.1111/ejn.12728

[167] Takatsuru, Y., Yoshitomo, M., Nemoto, T., Eto, K., & Nabekura, J. (2009). Maternal separation decreases the stability of mushroom spines in adult mice somatosensory cortex. *Brain Research*, *1294*, 45–51. https://doi.org/10.1016/j.brainres.2009.07.092

[168] Williams, R. S., Hauser, S. L., Purpura, D. P., DeLong, G. R., & Swisher, C. N. (1980). Autism and Mental Retardation: Neuropathologic Studies Performed in Four Retarded Persons with Autistic Behavior. *Archives of Neurology*, *37*(12), 749–753. https://doi.org/10.1001/archneur.1980.00500610029003

[169] Martínez-Cerdeño, V. (2017). Dendrite and spine modifications in autism and related neurodevelopmental disorders in patients and animal models. *Developmental Neurobiology*, *77*(4), 393–404. https://doi.org/10.1002/dneu.22417

[170] Tzschentke, T. M., & Schmidt, W. J. (2003). Glutamatergic mechanisms in addiction. *Molecular Psychiatry*, *8*, 373–382. https://doi.org/10.1038/sj.mp.4001269

[171] D'Souza, M. S. (2015). Glutamatergic transmission in drug reward: Implications for drug addiction. *Frontiers in Neuroscience*, *9:404*. https://doi.org/10.3389/fnins.2015.00404

[172] García-Pardo, M. P., Miñarro, J., & Aguilar, M. A. (2018). Role of AMPA glutamate receptors in the conditioned rewarding effects of MDMA in mice. *Behavioural Brain Research*, *347*, 57–60. https://doi.org/10.1016/j.bbr.2018.03.010

[173] Jordan, C. J., & Andersen, S. L. (2017). Sensitive periods of substance abuse: Early risk for the transition to dependence. *Developmental Cognitive Neuroscience*, *25*, 29–44. https://doi.org/10.1016/j.dcn.2016.10.004

[174] Jolly, S., Lang, V., Koelzer, V. H., Sala Frigerio, C., Magno, L., Salinas, P. C., Whiting, P., & Palomer, E. (2019). Single-Cell Quantification of mRNA Expression in The Human Brain. *Scientific Reports*. https://doi.org/10.1038/s41598-019-48787-w

[175] Dean, J. G., Liu, T., Huff, S., Sheler, B., Barker, S. A., Strassman, R. J., Wang, M. M., & Borjigin, J. (2019). Biosynthesis and Extracellular Concentrations of N,N-dimethyltryptamine (DMT) in Mammalian Brain. *Scientific Reports*, *9:9333*. https://doi.org/10.1038/s41598-019-45812-w

[176] Fatemi, S. H., Aldinger, K. A., Ashwood, P., Bauman, M. L., Blaha, C. D., Blatt, G. J., Chauhan, A., … Welsh, J. P. (2012). Consensus paper: Pathological role of the cerebellum in Autism. *Cerebellum*, *11*(3), 777–807. https://doi.org/10.1007/s12311-012-0355-9